Title

STUDY OF THE IMPEDANCE BEHAVIOR OF SURFACE LAYERS FORMED ON LITHIUM ELECTRODES IN A PROPYLENE CARBONATE ELECTROLYTE

Authors

Thevenin, J.G.
Muller, R.H.

Publication Date

1986

LBL-20660
UC-25

Lawrence Berkeley Laboratory
UNIVERSITY OF CALIFORNIA

Materials & Molecular Research Division

STUDY OF THE IMPEDANCE BEHAVIOR OF SURFACE LAYERS FORMED ON LITHIUM ELECTRODES IN A PROPYLENE CARBONATE ELECTROLYTE

J.G. Thevenin and R.H. Muller

January 1986

Prepared for the U.S. Department of Energy under Contract DE-AC03-76SF00098

DISCLAIMER

LBL-20660

STUDY OF THE IMPEDANCE BEHAVIOR OF SURFACE LAYERS FORMED ON LITHIUM ELECTRODES IN A PROPYLENE CARBONATE ELECTROLYTE

J.G. Thevenin and R.H. Muller

Materials and Molecular Research Division
Lawrence Berkeley Laboratory
Berkeley, CA 94720

January 1986

TABLE OF CONTENTS

Abstract

Different models of homogeneous and heterogeneous interphases have been investigated for the interpretation of impedance measurements of surface layers formed on lithium electrodes in an organic electrolyte. These models are based on the assumption that the surface layer consists of organic and inorganic compounds with the properties of solid and polymer electrolytes. The models discussed are compact, porous and multilayer systems. The analysis of the models is derived from a study of the equivalent circuits and the corresponding impedance diagrams for the different interphase models. This analysis leads to the determination of impedance parameters for the evaluation of the thickness of surface layers. The impedance measurements for lithium in propylene carbonate lithium perchlorate solution can be fitted by two interphase models. (1) The surface layer can be assumed to consist of two sublayers of different permittivities and conductivities according to the Compact-Stratified Layer (CSL) Model. (2) The surface layer can also be assumed to consist of a mixture of solid and polymer electrolytes according to the Solid-Polymer Interphase (SPI) Model. The thickness of surface layers deduced from the impedance data appears in agreement with the thicknesses which have been obtained by ellipsometric measurements in previous work.

1. INTRODUCTION

The thermodynamic instability of lithium in contact with most nonaqueous battery electrolytes leads to the formation of layers on electrode surfaces that can result in an unexpected electrochemical behavior of the lithium electrode.[1,2]

Propylene carbonate-based electrolytes have been studied extensively. The morphological characteristics of the surface layer have been studied by scanning electron microscopy,[3,4] transmission electron microscopy,[7] ellipsometry,[8] and x-ray diffraction.[9] The kinetic properties of the layer have been studied by means of stationary polarization,[10,11] cyclic voltammetry,[12] potentiostatic and galvanostatic pulse techniques,[13] and electrode-impedance spectroscopy.[14]

For the purpose of simplification, the most important results obtained from the research listed above are the following:

1. The composition of the surface layer is determined by the products of the reactions between lithium and the solvent, the salt, and their impurities.
2. The surface layer can be an ionic conductor and an electronic insulator, and it acts as an interphase between the lithium electrode and the organic electrolyte. The properties of such a surface layer can be those of a solid electrolyte[13] and/or a porous insulating membrane.[14]

Even in the well-known propylene carbonate-based electrolytes, the composition and structure of the surface layer is not quite understood and generally assumed to be a mixture of organic and inorganic compounds. Consequently, the electrochemical properties of the surface layer can be completely misunderstood when using simple interphase models.

In the present report, a survey is given of different models of homogeneous and heterogeneous interphases which have been proposed for the analysis of the surface layers. Electrode-impedance spectroscopy, which is a convenient method to study the electrochemical properties of the film-covered lithium electrode, is used to determine the parameters of the surface layer. The experimental study has been carried out with the surface layers formed on the lithium electrode in a molar solution of lithium perchlorate in propylene carbonate.

2. LITERATURE REVIEW

2.1 Composition of the Surface Layer

Propylene carbonate (PC) has become one of the most commonly used solvents for lithium secondary battery research because of the successful cathodic deposition of lithium from various salts.[15] However, even for the often used molar solution of lithium perchlorate in propylene carbonate ($PC/LiClO_4$), the exact composition and structure of the surface layer formed on the lithium electrode remains poorly understood.[16]

Day and Sullivan[17] have provided evidence that PC is electrochemically decomposed at a potential of 0.6 V versus Li on a graphite electrode to form propylene gas and the graphite electrode to form propylene gas and the carbonate ion. Dousek, Jansta, and Riha[18] have shown that Li in lithium amalgam Li(Hg) decomposed PC according to the same reaction to give lithium carbonate (Li_2CO_3) and propylene gas (CH_3-CH=CH_2) as the main component of the gaseous phase, which was analyzed as: 93.7% propylene, 1.5% butane, 1.2% CO_2, 1% methane, 1% ethane, 0.8% propane, and 0.8% ethylene.

The fact that no massive PC decomposition with gas evolution was observed on elemental Li has been explained by Dey[1] on the basis that the surface of metallic Li in contact with PC is immediately insulated or passivated by a surface layer formed by microcrystals of Li_2CO_3 produced by the chemical reaction. Most authors have accepted this assumption and have also assumed the existence of LiOH and/or Li_2O due to the decomposition of the residual water of the electrolyte.[19,20]

For an electrolyte using unpurified propylene carbonate, Garreau, et

al. have found, using transmission electron microscopy[21] and photoelectron spectroscopy,[22] that the surface layer consists of a polymeric membrane with inserted lithium chloride and carbonate microcrystals. The polymeric membrane is assumed to result from the polymerization of propylene in the presence of the organic impurities in the electrolyte. The existence of lithium chloride microcrystals in the surface layer had been attributed to a possible decomposition of lithium perchlorate in the presence of lithium.

Recently, Nazri and Muller[23,24] have used different techniques, such as in-situ x-ray diffraction, photoelectron spectroscopy, IR spectroscopy, and mass spectroscopy, to study the surface layer formed in purified propylene carbonate. They have confirmed the presence of polymeric compounds in the surface layer as well as the presence of inorganic compounds such as lithium chloride, lithium carbonate, and lithium oxide.

Although the mechanisms of polymerization of PC and decomposition of $LiClO_4$ remain not well elucidated, it is obvious that the surface layer formed in the PC/$LiClO_4$ electrolyte cannot be represented by a single organic or inorganic compound. In fact, the surface layer has a complex composition, including all the reaction products of the solvent and solute, water, and organic impurities of the electrolyte.

2.2 Properties of the Surface Layer

Different studies of the electrochemical behavior of lithium electrodes in propylene carbonate-based electrolytes have demonstrated that the surface layer is an ionic conductor and an electronic insulator

acting as an interphase between the electrode and the electrolyte.[16,19] In order to determine the thickness of the surface layer in-situ electrochemically, it is necessary to make an assumption about its main composition in order to use an appropriate interphase model. Two different simplifying assumptions have been made in the literature to study the kinetic properties of such a surface layer. The first assumption is that the surface layer is an inorganic compound that acts as a solid electrolyte; in this case, the surface layer can be studied by means of the Solid Electrolyte Interphase model. The second assumption is that the surface layer is an organic compound that is a porous polymeric material; this assumption allows the surface layer to be studied by the Porous Polymer Interphase model.

2.2.1 The Solid-Electrolyte Interphase (SEI) Model

The so-called SEI model has been presented by Peled,[25,26] who assumed that the surface layer can be considered a solid electrolyte that acts as an interphase between the electrode and the electrolyte. (See Appendix III)

Geronov, Schwager, and Muller[6,13] used the galvanostatic pulse technique to study the conduction process in the surface layer formed in propylene carbonate- based electrolytes. The most likely composition of the surface layer was assumed to be Li_2CO_3 and/or Li_2O, according to the residual water content of the electrolyte (between 20 and 1000 ppm). Their study showed a decrease in the geometric capacitance from 1.5 to 0.2 $\mu F/cm^2$ during the increase of the polarization resistance from 20 to 650 Ωcm^2. For a relative permittivity of 5 (lithium carbonate), the

determination of the geometric capacitance led to a change in the thickness of the surface layer from $1x10^{-7}$ to $1.5x10^{-6}$ cm during the first week of immersion in the electrolyte. The thickness apparently remained unchanged during the next week. During the growth of the surface layer, the determination of the polarization resistance led to an estimate of the conductivity of the solid interphase of from 2.5 to $3.5 \times 10^{-9}\ \Omega^{-1}\ cm^{-1}$.

The same authors have also studied the surface layer by ellipsometry.[8] The thickness of the surface layer calculated from ellipsometer measurements increased linearly to $1.5x10^{-5}$ cm during two weeks of immersion in the electrolyte. The factor-of-10 difference between the optical and electrochemical thicknesses was attributed to the sensitivity of the respective methods used to detect the main regions of the surface layer: a compact region facing the electrode and a porous region facing the electrolyte. Capacitance measurements were able to detect only the thin compact region of the surface layer, while ellipsometer measurements were primarily affected by the thick porous region.

2.2.2 The Porous-Insulating Membrane (PIM) Model

This model was presented initially without a name by Thevenin,[31] who assumed that the surface layer can be considered as a porous polymeric membrane filled by the electrolyte. (See Appendix IV) [The term PEI (Polymer Electrolyte Interphase), which was introduced in a recent paper,[32] is not well chosen, because the surface layer studied in this model cannot be considered as a classical polymer electrolyte.] (See

Appendix V)

Garreau and Thevenin[14,33] have used electrode-impedance spectroscopy to study the charge transfer and diffusion processes involved in the surface layer formed in an organic electrolyte using unpurified propylene carbonate with 10 ppm of residual water. The analysis of the electrode-impedance diagrams after 24 hours of immersion showed a decrease in the interfacial capacitance from 28 to 5.5 $\mu F/cm^2$ associated with an increase in the charge-transfer resistance from 13 to 19 Ωcm^2. At the same time, an increase in the diffusion resistance from 8 to 20 Ωcm^2 was observed, while the Drossbach-Schultz frequency decreased from 0.4 to less than 0.02 Hz for a Warburg constant increasing from 2 to 8 $\Omega cm^2/sec^{1/2}$. Taking into account a standard value of 35 $\mu F/cm^2$ for the double-layer capacitance, which can be determined for a lithium-aluminum electrode in the same organic electrolyte,[34] the ratio $(1-\Theta)$ related to the active area of the electrode surface decreased from 0.8 to 0.1 during the formation of the surface layer. The growth of the surface layer over 24 hours led to an increase in thickness from $2x10^{-5}$ to more than $4x10^{-4}$ cm and an increase of diffusion coefficient from $4x10^{-10}$ to more than $3x10^{-8}$ cm^2/sec. The growth rate of the surface layer was nearly independent of the ion concentration in the 0.1 to 1 M/1 range of lithium perchlorate.

The same authors have also studied the surface layer by scanning electron microscopy.[33,35] The observation of a cross section of the surface layer dessicated under vacuum shows a plastic material with a thickness of about 10^{-4} cm, in good agreement with the thickness deduced from the impedance measurements at different immersion times.

Nevertheless, the diffusion coefficient of the lithium ion in the surface layer is several orders of magnitude lower than the expected one in the organic electrolyte.

3. THEORETICAL

3.1 Analysis of Electrode Impedance

The impedance of the metal/surface-layer/solution system, as shown in Fig. 3-1, can be defined as the sum of three impedances:

$$Z_T = Z_{M/L} + Z_L + Z_{L/S} + R_\Omega$$

where $Z_{M/L}$ is the impedance of the metal/surface-layer interface, Z_L is the intrinsic impedance of the surface layer, $Z_{L/S}$ is the impedance of the surface-layer/solution interface, and R_Ω is the solution resistance.

When the atoms in the electrode and the cations in the surface layer are of the same metal, a totally nonblocking situation occurs; this situation involves infinitely rapid discharge of the mobile charged species on the electrode. Thus, the double-layer capacitance at the metal/surface-layer interface is zero. Accordingly, for a lithium electrode facing a lithium ionic conductor, the impedance $Z_{M/L}$ is zero under these conditions.

The impedance Z is represented by the equivalent circuit of the surface layer. This circuit takes into account the different processes involved in the surface layer; their relative importances are determined both by the composition and structure of the surface layer. The

equivalent circuit can be defined a priori for various given compositions and structures of the surface layer. In fact, as shown in the rest of this section, the impedance Z_L can be defined only for surface layers having the properties of a solid electrolyte or a polymer electrolyte. Besides, the interpretation of the impedance can be derived only for planar compact and/or porous systems.

The impedance $Z_{L/S}$ can be represented by a pseudo-Randles equivalent circuit in which the Faradaic impedance is determined by the properties of the surface layer. Two main cases must be considered: the first one corresponds to a surface layer considered as an ionic and electronic conductor, while the second case corresponds to a surface layer considered as a pure ionic conductor (electronic insulator).

a) Case of a surface layer as an ionic and electronic conductor. Armstrong, et al.[27] have proposed a model of the surface-layer/solution interface to study the impedance of metals in the passive and transpassive regions. In order to deduce the interfacial impedance $Z_{L/S}$, they separated the surface monolayer facing the solution from the rest of the system. They then considered the rates of transfer and diffusion of the cations and anions to determine the components of the Faradaic impedance. Their model can be used for the surface layer formed in an organic electrolyte if such a surface layer is a partial electronic conductor, as shown in Appendices XIV and XV. But, in general, the total impedance must be represented by a complicated equivalent circuit that can lead to an impedance diagram which is useless for determining the thickness of the surface layer when the time constants of the processes

involved in the surface-layer and at the interface surface-layer/solution are not well separated.

b) Case of a surface-layer as a pure ionic conductor. This system appears to be much easier to study. There is no charge transfer process at the surface-layer/solution interface; the charge transfer resistance is infinite. Besides, the diffusion process in a highly concentrated electrolyte is negligible; the Warburg impedance is zero. Thus the Randles equivalent circuit is reduced to the solution resistance R_Ω in series with the double-layer capacitance C_{dl}. However, when the surface-layer has a high resistance and a low capacitance, the effect of the double-layer capacitance can be considered to be negligible. According to the above assumption, the total impedance can be rewritten as:

$$Z_T = Z_L + R_\Omega .$$

Thus, determining the equivalent circuit of the impedance Z_L in this case leads essentially to the study of the metal/surface-layer solution system. But even for a surface layer of known composition and structure it is possible to determine the thickness of the surface layer by impedance measurements only if the elementary processes can be clearly

identified on the impedance diagram and if the parameters of the parameters of the process are determined by another method.

3.2 Study of Interphase Models

3.2.1 Compact-layer Models

Two main compositions of the surface layer can be defined according to the morphological studies presented in the literature. The first composition corresponds to an inorganic layer with the properties of a solid electrolyte (the SEI model). The second composition corresponds to an organic and inorganic layer with the properties of a polymer electrolyte (the PEI model). The two models are analyzed in greater detail below.

3.2.1a The Solid-Electrolyte Interphase (SEI) Model

The surface-layer is considered as an interphase between the electrode and the electrolyte. This interphase has the properties of a solid electrolyte. As shown in Fig. 3-2, the equivalent circuit is defined by the bulk resistance R_b and the geometric capacitance C_g both of which are related to the conduction process in the solid electrolyte. The corresponding impedance diagram in the complex plane consists of a semicircle due to the R_b/C_g coupling over the whole frequency range. By analyzing this diagram one can determine the thickness of the surface-layer for a known permittivity or conductivity of the solid electrolyte. (See Appendix III)

3.2.1b The Polymer-Electrolyte Interphase (PEI) Model

The surface-layer is considered as an interphase between the electrode and the electrolyte. This interphase has the properties of a polymer electrolyte. As shown in Fig. 3-3, the equivalent circuit is determined by three types of impedances: (1) the conduction impedance defined by the bulk resistance R_b and the geometric capacitance C_g; (2) the charge transfer impedance represented by the charge transfer resistance R_{ct} and the double-layer capacitance C_{dl}; (3) the diffusion impedance Z_d defined by the Warburg or Drossbach-Schultz equation. (See Appendix II). The corresponding impedance diagram in the complex plane exhibits three features: (1) a semicircle in the high-frequency range, due to the R_b/C_g coupling; (2) a semicircle in the intermediate frequency range, due to the R_{ct}/C_{dl} coupling; and (3) a characteristic loop in the low-frequency range due to Z_d. By analyzing this diagram, especially the conduction and diffusion loops, one can determine the thickness of the surface-layer provided that either the conductivity or the permittivity is known. (See Appendix V)

3.2.2 Porous-Layer Models

The total impedance can be determined by a transmission-line model for which the finite thickness of the porous layer on the electrode is recognized. As the usual simplifying assumptions, the surface-layer is assumed to have straight parallel and cylindrical pores of uniform diameter and constant composition. Thus, the equivalent electrical circuit for a single pore is determined by four distinct impedances: (1) the liquid-phase impedance per unit pore length Z_l, related to the

properties of the organic electrolyte filling the pores; (2) the solid-phase impedance per unit length Z_s, determined by the properties of the solid part of the surface layer; (3) the impedance occurring on the pore base Z_b independent of the pore length, representing the impedance of the metal/liquid-phase interface; (4) the addmittance occurring on the pore wall per unit pore length $1/Z_p$, representing the admittance of the solid-phase/liquid-phase interface.

3.2.2a The Porous-Layer Interphase (PLI) Model

In the general case of this model, as shown in Fig. 3-4, the corresponding impedance diagram depends on the relative importance of the different impedances involved in the porous system. In principle, all the information can be derived by fitting the curve of the impedance diagram to the general equation of the total impedance. In practice, however, when one considers the large number of parameters involved in the equation, the curve-fitting technique is not efficient enough for an accurate determination of the layer thickness, even when the different impedances Z_l, Z_s, Z_b and Z_p are known as in the case of a planar system.

3.2.2b The Porous-Insulating Membrane (PIM) Model

A limiting case of a porous system is obtained when the surface layer is assumed to be formed by an insulating material such as a polymeric membrane. Thus, the impedances Z_s and Z_p are several orders of magnitude larger than the impedances Z_l and Z_b. Under these conditions, the equivalent circuit and impedance diagram related to the PIM model can be defined as shown in Fig. 3-5. The equivalent circuit of the active

surface area (1-Θ) is represented by the Randles circuit, while the equivalent circuit of the passive surface area (Θ) is represented by R_m and C_m, determined by the resistive and dielectric properties of the membrane. (See Appendix IV) The corresponding impedance diagram in the complex plane is made of two parts: (1) a semicircle in the high-frequency range, resulting from the coupling R_{ct}/C_{dl} related to the charge-transfer process on the active surface, and (2) a characteristic loop in the low-frequency range resulting from the diffusion process of the species through the pores. By analyzing this diagram, one can determine the thickness of the surface layer provided that the double-layer capacitance on the free metal surface is known.

3.2.3 Heterogeneous-layer Models

The surface layer that forms on the lithium electrode has a complex composition because of its mixture of organic and inorganic compounds. Thus, a heterogeneous structure of the surface layer can be assumed. A limiting case is to consider that the surface layer has the average properties of both solid and polymer electrolytes, which are mixed to form a continuous solid-polymer layer (the SPI) model). Other models are based on the assumption that the surface layer consists of two different compact or porous sublayers. A stratified structure can result from the presence of a solid electrolyte facing the liquid electrolyte (the CSL model). Another stratified structure can be defined by a compact solid electrolyte on the electrode surface and a porous insulating membrane facing the organic electrolyte (the PSL Model). All three of these models are analyzed in greater detail below.

3.2.3a The Solid-Polymer Interphase (SPI) Model

In this model the surface layer is assumed to consist of solid compounds inserted into polymeric compounds. As shown in Fig. 3-6, the pseudosublayers placed in parallel and/or in series lead to complicated equivalent circuits. Thus, the total equivalent circuit of the lithium covered by such a solid/polymer interphase can have characteristics similar to that of the PEI Model, but in the SPI case, the different time constants may not be well separated. The three loops mix to form a distorted loop, that can only suggest the existence of the different processes. Nevertheless, in Appendices VII, VIII, and IX, it is demonstrated that the impedance data can be analyzed with sufficient accuracy by using the Cole-Cole and Bode plots for depressed and overlapped semicircles. Assuming that the different processes can be separated by a geometric fitting between the experimental and computer-generated impedance diagrams, the main parameters of the surface layer can be evaluated, provided that either the permittivity or the conductivity is known. (See Appendix V)

3.2.3b The Compact-Stratified Layer (CSL) Model

In this model, the surface layer is assumed to be made of two sublayers, as shown in Fig. 3-7. The first sublayer is a solid electrolyte on the electrode surface, and the second sublayer is a polymer electrolyte in contact with the electrolytic solution. For this model, the equivalent circuit can be represented by two RC circuits placed in series when the dielectric and resistive properties of the sublayers are considered separately. But because the sublayers cannot be

simply separated by impedance measurements, the equivalent circuit of the surface layer can be considered as a unique R_iC_i circuit by taking into account the integral values of the resistance and capacitance of the surface layer. (See Appendix VI) The corresponding impedance diagram in the complex plane is a semicircle resulting from the R_i/C_i coupling over the whole frequency range. By analyzing this diagram, one can determine the total thickness of the surface layer, as well as the thickness of the two sublayers, provided that the two permittivities or conductivities are known.

A surface layer made of two sublayers of different kinds, for example a solid electrolyte and a polymer electrolyte, cannot be modeled because the equivalent circuits and corresponding impedance diagrams cannot be compared easily.

3.2.3c The Porous-Stratified Layer (PSL) Model

In this model, the surface layer is assumed to be made up of two sublayers, as shown in Fig. 3-8. The first sublayer is a compact solid electrolyte on the electrode surface, and the second sublayer is a porous insulating membrane. For this model, the equivalent circuit can be represented by the circuit of the SEI model placed in series with the circuit of the PIM Model. The corresponding impedance diagram in the complex plane consists of three loops, but only when the time constants of the processes are different. The first loop, in the high-frequency range, can be attributed to the conduction process in the SEI layer. The second loop, in the intermediate-frequency range can be due to the charge transfer process in the SEI and PIM layers. The third loop, in the low-frequency range, can be related to the diffusion process in the PIM layer.

By analyzing this impedance diagram, one can determine the thicknesses of the compact solid electrolyte and of the porous insulating membrane, using the SEI and PIM Models. (See Appendices III and IV). In general, the time constants of the different processes are not well separated, and in the high- and intermediate-frequency ranges, the conduction and charge-transfer loops mix to form a distorted loop. Under these conditions, it is impossible to determine the thicknesses of the sublayers.

FIGURE CAPTIONS

Fig. 3-1. Schematic view of the metal/surface-layer/solution system showing the corresponding impedance components.

Fig. 3-2. The Solid-Electrolyte Interphase (SEI) Model. (a) Schematic view; (b) Equivalent circuit; (c) Impedance diagram.

Fig. 3-3. The Polyer-Electrolyte Interphase (PEI) Model. (a) Schematic view; (b) Equivalent circuit; (c) Impedance diagram.

Fig. 3-4. The Porous-Layer Interphase (PLI) Model. (a) Schematic view; (b) Equivalent circuit; (c) Impedance diagram.

Fig. 3-5. The Porous-Insulating Membrane (PIM) Model. (a) Schematic view; (b) Equivalent circuit; (c) Impedance diagram.

Fig. 3-6. The Solid-Polymer Interphase (SPI) Model. (a) Schematic view; (b) Equivalent circuit; (c) Impedance diagram.

Fig. 3-7. The Compact-Stratified Layer (CSL) Model. (a) Schematic view; (b) Equivalent circuit; (c) Impedance diagram.

Fig. 3-8. The Porous-Stratified Layer (PSL) Model. (a) Schematic view; (b) Equivalent circuit; (c) Impedance diagram.

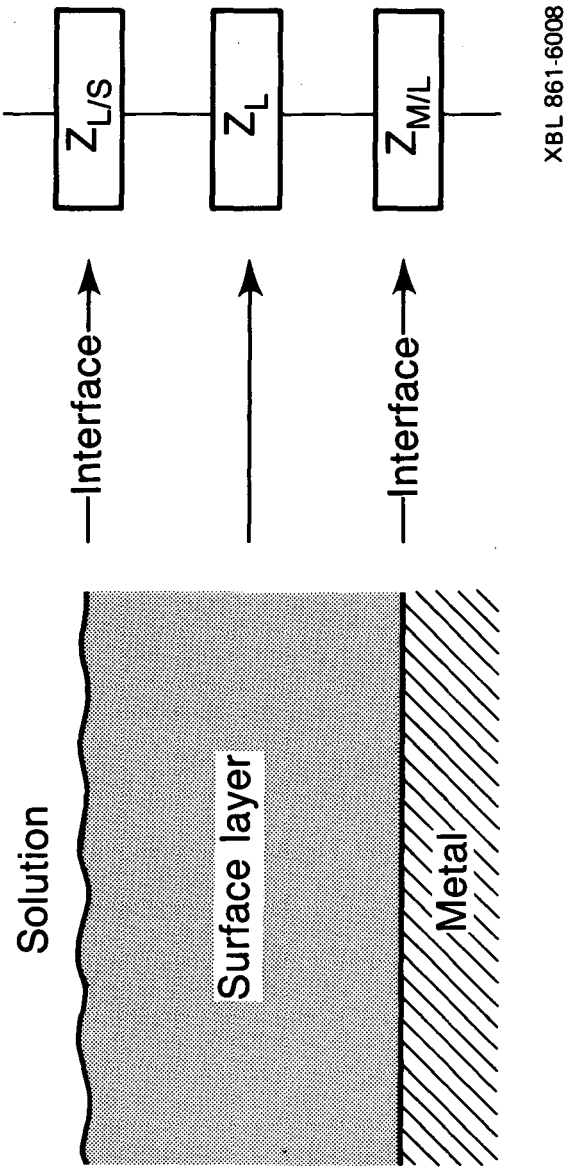
$Z_{L/S}$
Z_L
$Z_{M/L}$
XBL 861-6008
Interface
Interface
Solution
Surface layer
Metal

Fig. 3-1

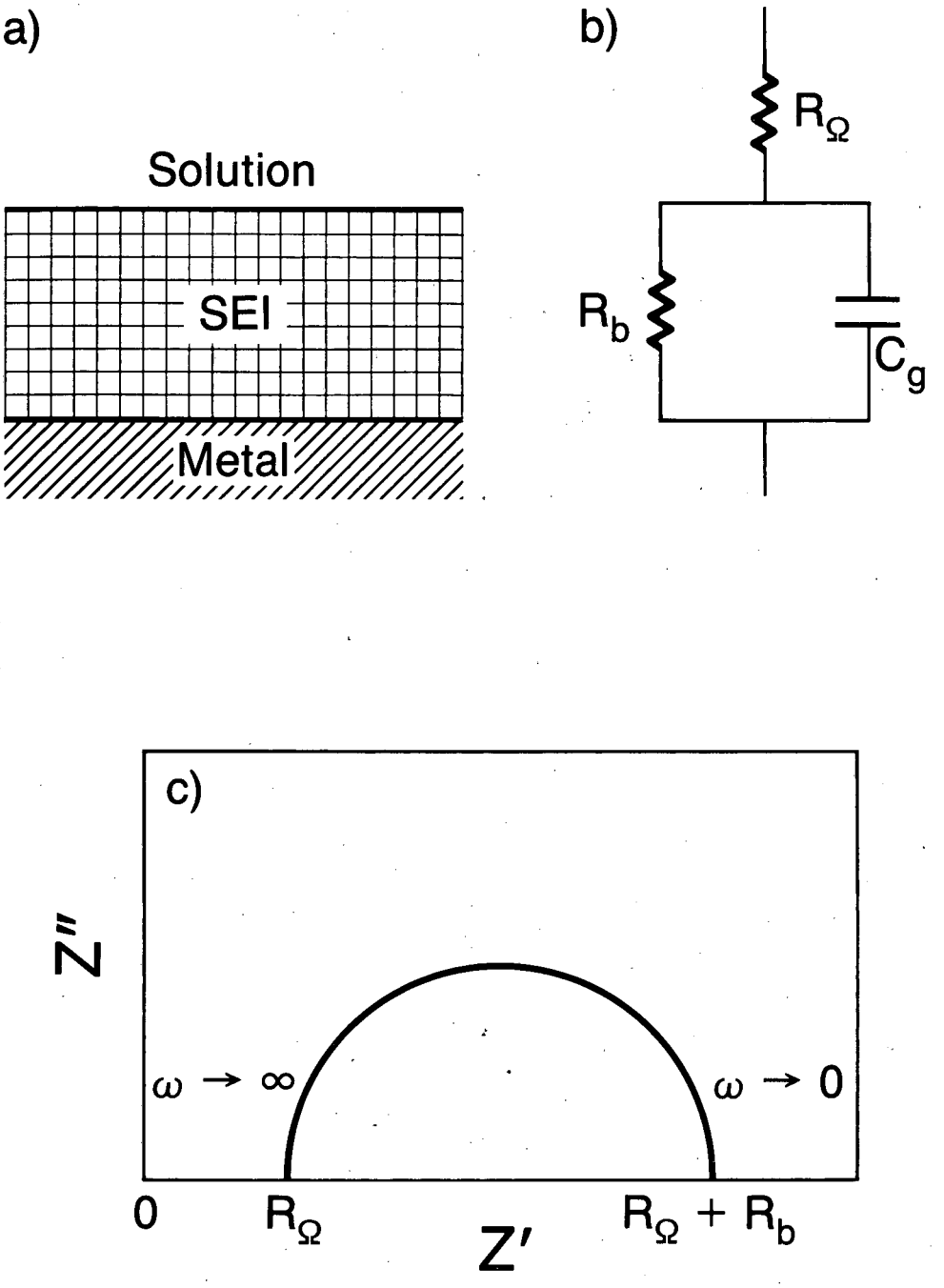

XBL 861-6029

Fig. 3-2

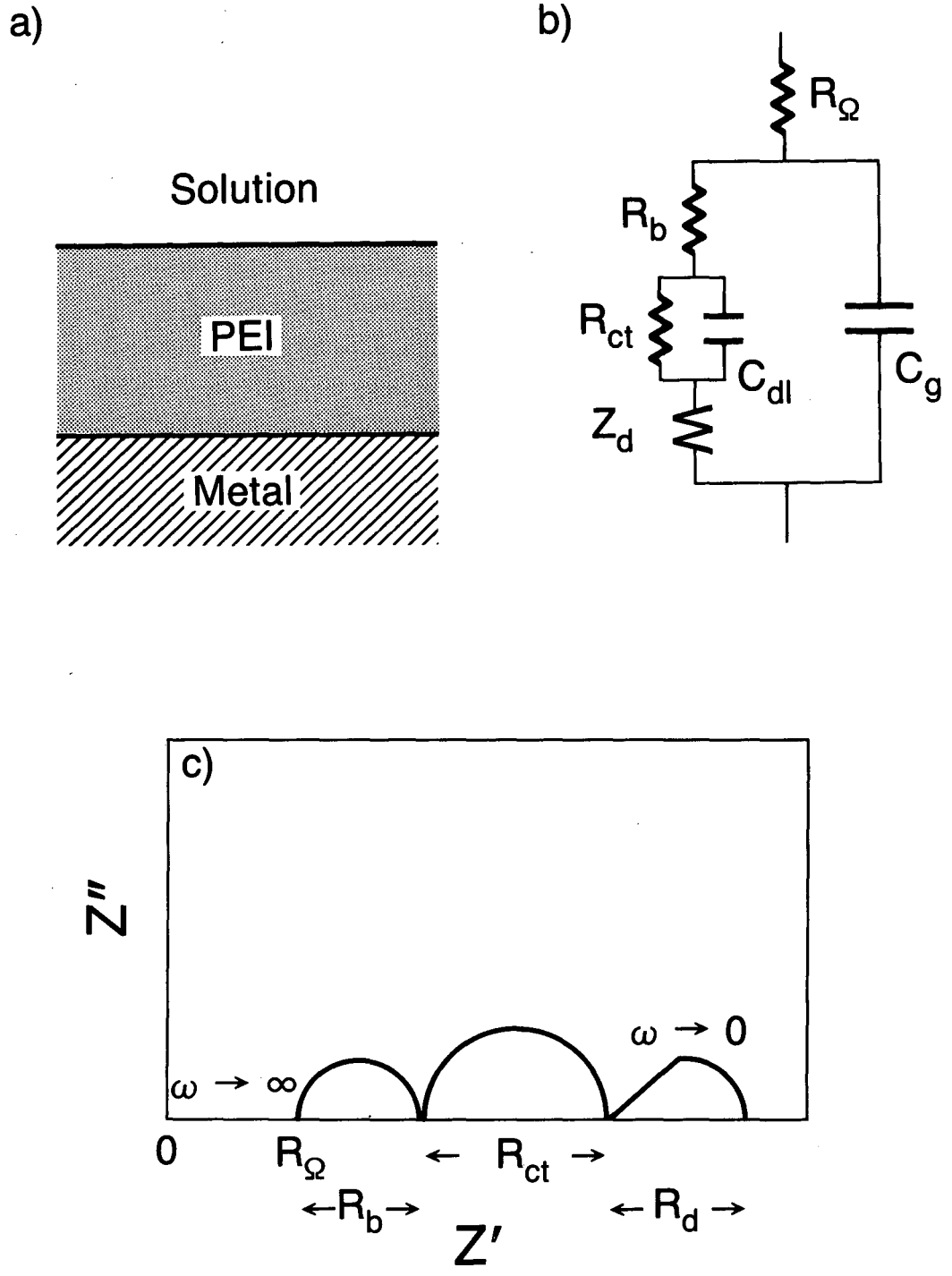

XBL 861-6038

Fig. 3-3

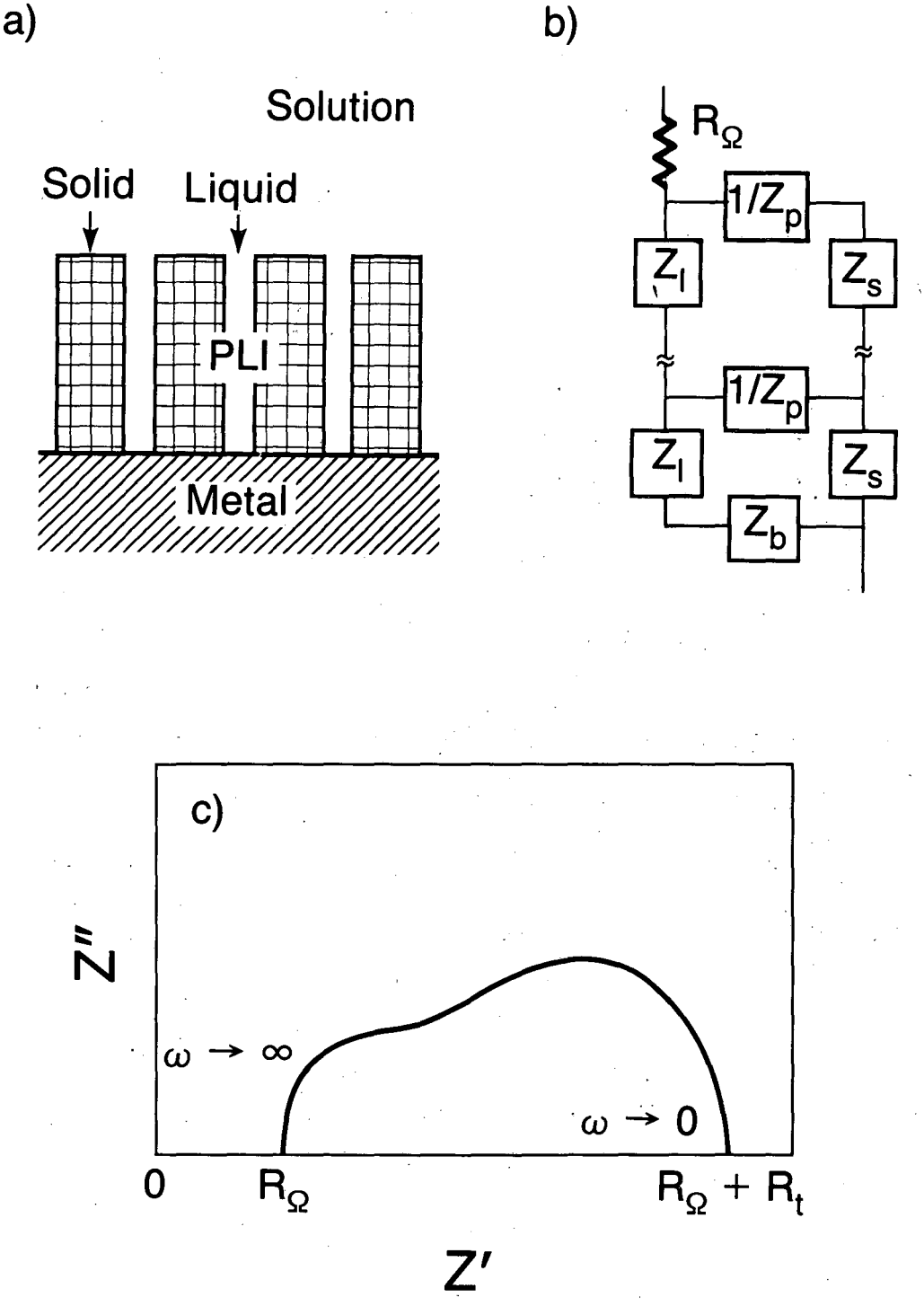

XBL 861-6031

Fig. 3-4

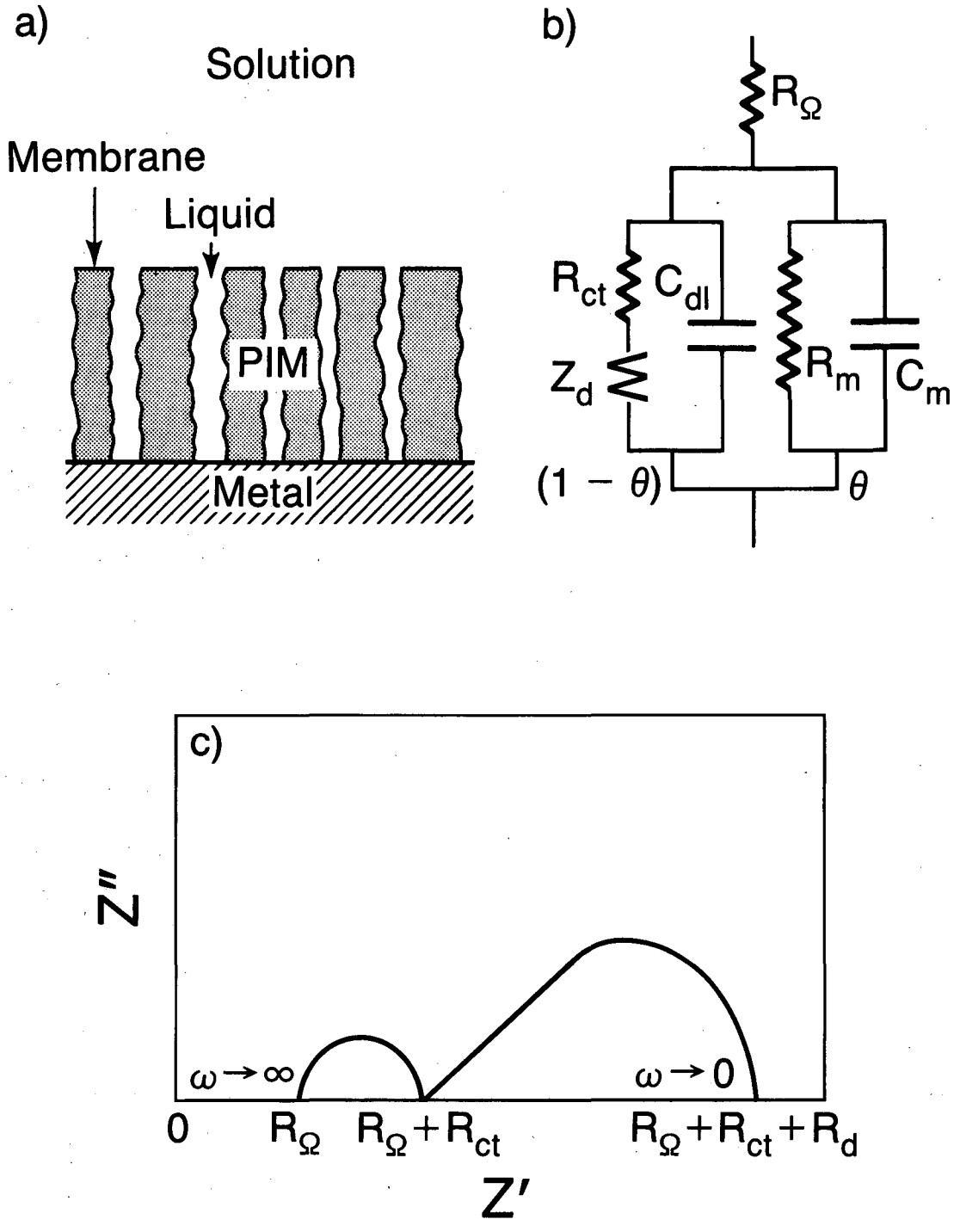

XBL 861-6036

Fig. 3-5

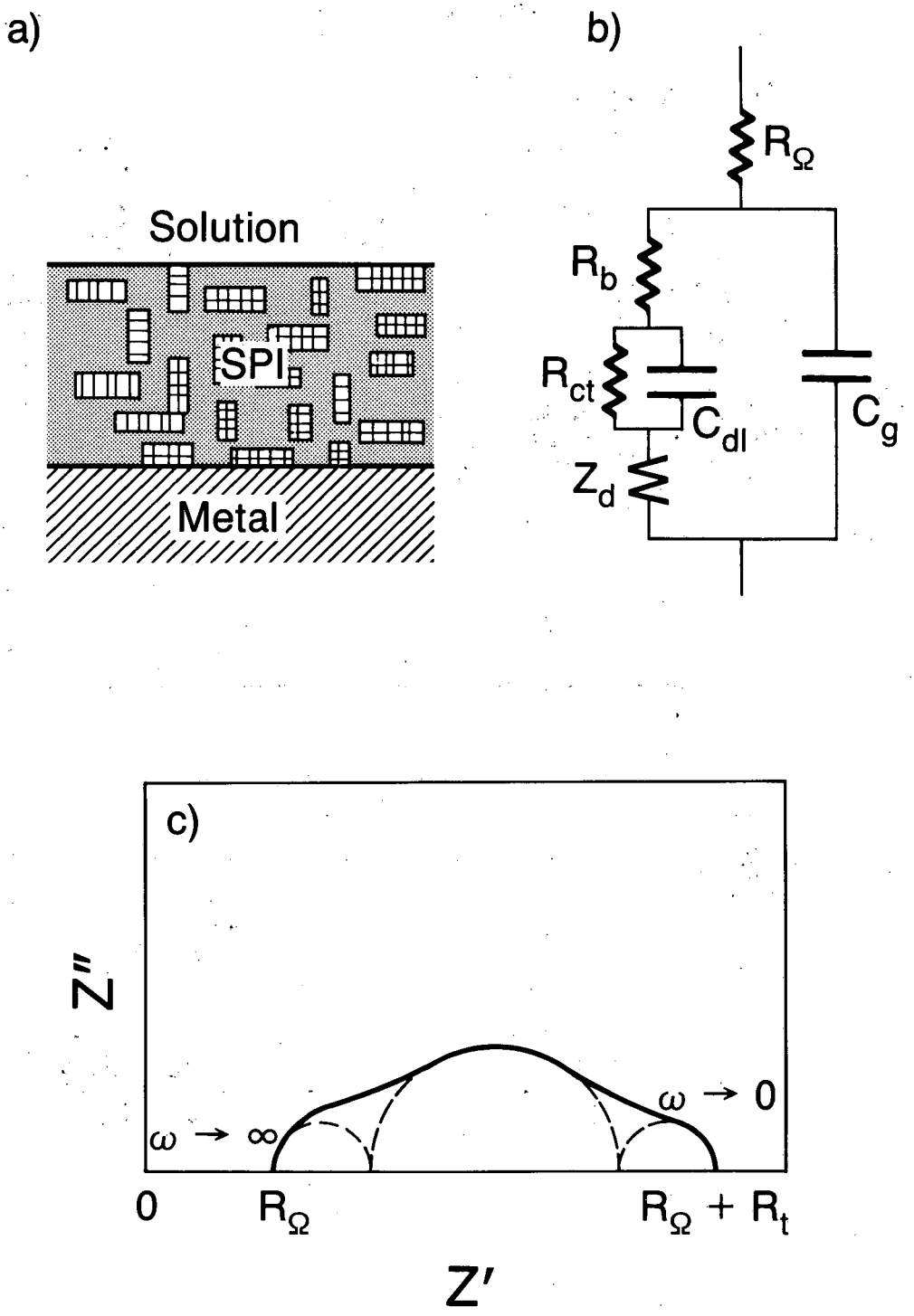
a)
Solution
SPI
Metal
b)
R_Ω
R_b
R_{ct}
C_{dl}
C_g
Z_d
c)
Z″
$\omega \to \infty$
$\omega \to 0$
0
R_Ω
$R_\Omega + R_t$
Z′
XBL 861-6035

Fig. 3-6

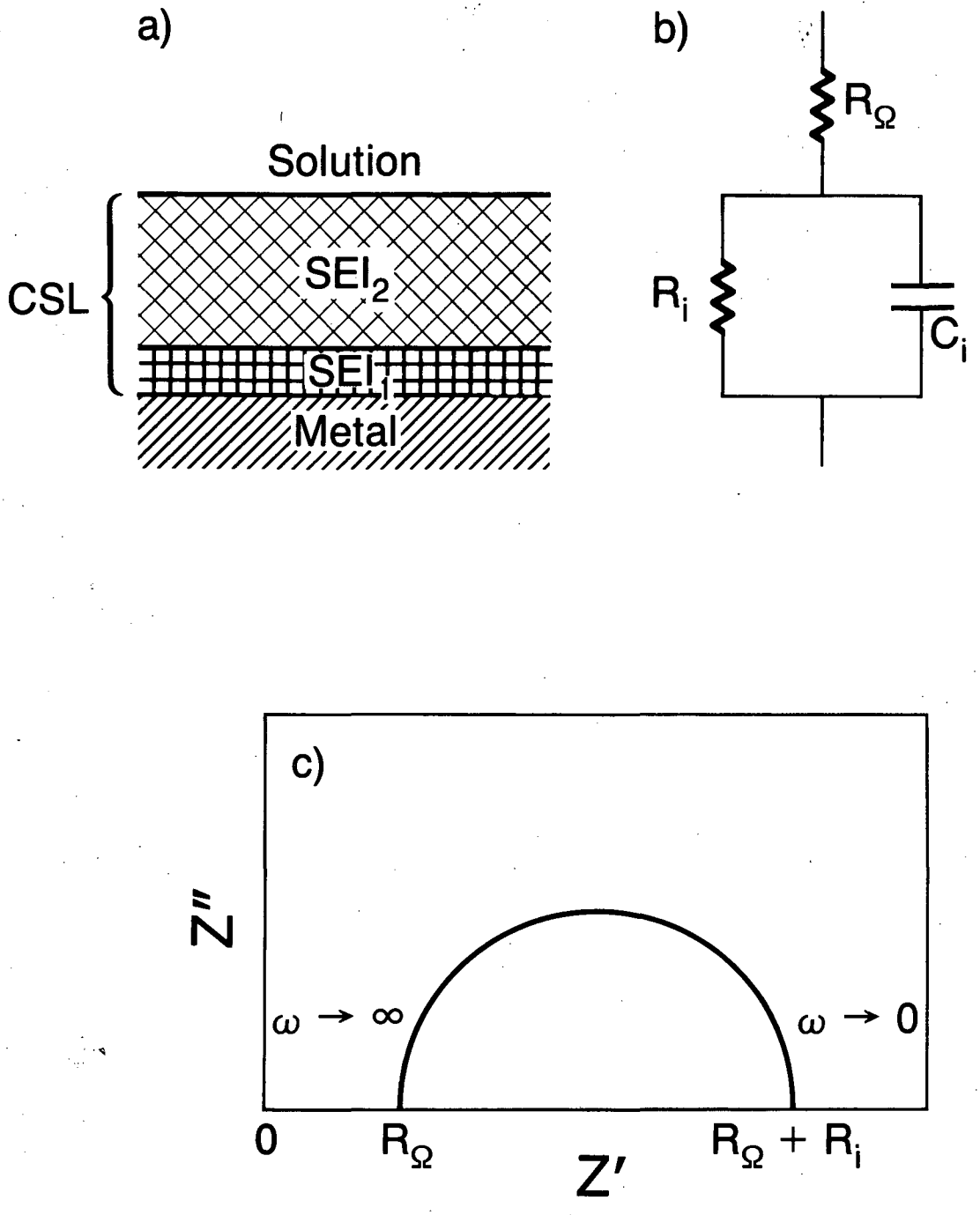

XBL 861-6027

Fig. 3-7

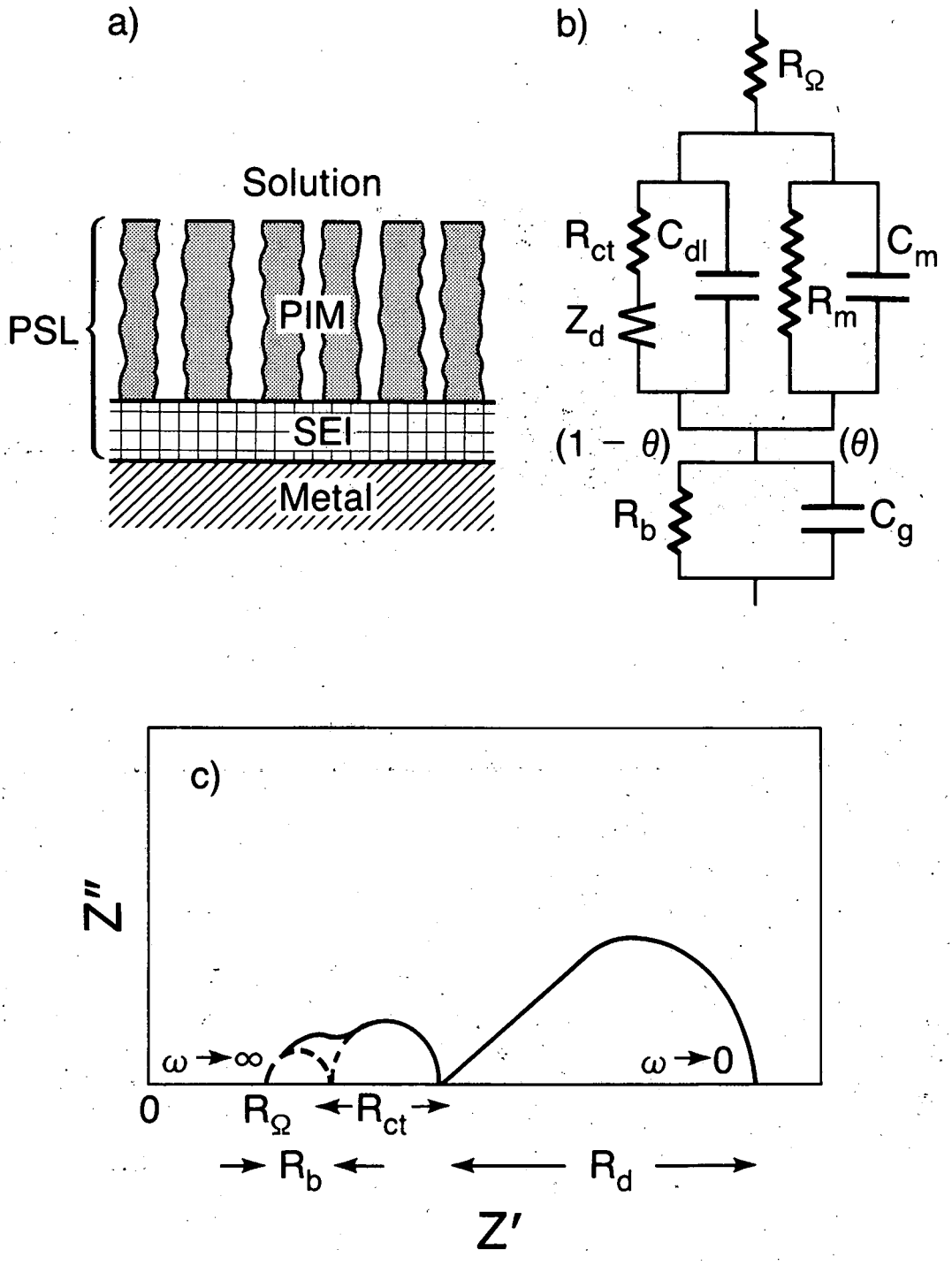

XBL 861-344

Fig. 3-8

4. EXPERIMENTAL

4.1 Organic Electrolyte

The electrolyte studied was the molar solution of lithium perchlorate in propylene carbonate with a residual water content of a few ppm. Propylene carbonate (Burdick and Jackson Lab) was dehydrated on molecular sieves of 3-A mesh for about two weeks. Lithium perchlorate (Smith Chem. Co.) was dessicated at 240^{o}C for one day under a vacuum created by a rotary pump.

Three different solutions were used. Solution A was prepared directly with the dehydrated solvent and the dessicated solute. Solution B was Solution A submitted to a preliminary polarization between two lithium electrodes (charge density of 50 C/cm^2 at a current density of 1 mA/cm^2 for 50 cm^3 of the molar solution). Solution C was Solution A with lithium amalgam immersed for 7 hours (50 cm^3 of solution for 1 cm^3 of lithium amalgam). The gray Li(Hg) powder was formed with 1.5 wt% or more of lithium immersed in mercury.

4.2 Electrolytic Cell

The electrolytic cell, made of polypropylene, had two opposing holes for the electrode holders and a compartment for extruding the lithium reference electrode, as shown in Fig. 4-1. The counterelectrode was a lithium disc 2 cm in diameter by 0.1 cm thick, which was inserted into a polypropylene holder. The working electrode was the cross section of a lithium cylinder 0.2 cm in diameter inserted into a polypropylene holder. The reference electrode was the cross section of a lithium cylinder

extruded close to the side of the working electrode. The reference and working lithium electrodes were cut with a blade just before immersion into the electrolyte. The reference electrode was cut frequently during the experiment to avoid any artefacts due to its impedence.

4.3 Electrode Impedance Measurements

The electrode impedance was determined using the lock-in amplifier technique in the high-frequency range ($5x10^4$ to 5 Hz) and the Lissajous-figure technique in the low-frequency range (5 to $5x10^{-3}$ Hz). The system was used in the galvanostatic mode near the open-circuit potential of the lithium electrode. The alternating-current density was about 0.05 mA/cm^2, which provided a linear response, as required for valid electrode-impedance measurements. As shown in Fig. 4-2, the equipment included an oscillator (Hewlett Packard Model 3310A), which drove a potentiostat-galvanostat (Princeton Applied Research Model 173). The oscillating current and voltage were measured by a differential preamplifier (Princeton Applied Research Model 113). The in-phase and out-of-phase components of the current and voltage were determined with two lock-in amplifiers (Princeton Applied Research Model 5101). Current versus voltage was displayed on a storage oscilloscope (Tektronix Model 5111).

4.3.1 Lock-in Amplifier Technique

Any ac-current vector can be defined as the sum of its real and imaginary components and can be expressed as $I(wt) = I' + jI''$; similarly, any ac-voltage vector can be expressed as $E(wt) = E' + jE''$,

as shown in Fig. 4-3a. The real component is in phase with the reference waveform, and the imaginary component is exactly 90^{o} out of phase. The reference waveform allows expression of the current and voltage waveforms as vectors with respect to the same coordinate axes. When the perturbated current (voltage) and the reference signal are applied to a lock-in amplifier, the real and imaginary components of the current (voltage) are determined independently. Specifically, this allows us to calculate the impedance vector as the quotient of the voltage and current vectors:

$$Z' + jZ'' = \frac{E' + jE''}{I' + jI''}$$

Consequently, the real and imaginary components of the electrode impedance are easily calculated by the following equations:

$$Z' = \frac{E'I' + E''I''}{(I')^2 + (I'')^2} \qquad Z = \frac{E''I' - E'I''}{(I')^2 + (I'')^2}$$

4.3.2 Lissajous-Figure Technique

When the ac current ($R^{*}\Delta I$) and potential (ΔE) are connected to the horizontal and vertical plates of an oscilloscope by differential amplifiers with a dc offset capability, an ellipse is observed on the display. The geometric parameters of the ellipse are related by simple equations to the complex impedance. The following

characteristic quantities can then be determined, as shown in Fig. 4-3b; knowing that

$$E(\omega t) = E_o + \Delta E \sin(\omega t)$$

$$I(\omega t) = I_o + \Delta I \sin(\omega t + \varphi)$$

where E_o and I_o are the dc voltage and current applied to the cell, respectively.

$$OA = E(\omega t) - E_o = \Delta E \qquad \text{when } (\omega t) = \pi/2;$$

$$OB = R^* I(\omega t) - R^* I_o = R^* \Delta I \qquad \text{when } (\omega t + \varphi) = \pi/2;$$

$$OC = E(\omega t) - E_o = E \sin(\varphi) \qquad \text{when } (\omega t) = \varphi.$$

Hence, the modulus /Z/ and the phase (φ) of the impedance $Z = \Delta E/\Delta I$ can be calculated:

$$/Z/ = R^*.OA/OB$$

$$\sin \varphi = OC/OA,$$

and the real (Z') and imaginary (Z") components are determined by the following equation:

$$Z' = R^* \, OA/OB \, \sqrt{1-(OC/OA)^2},$$

$$Z'' = R^* \, OC/OB.$$

FIGURE CAPTIONS

Fig. 4-1. Cross-section of the electrochemical cell.

Fig. 4-2. Experimental set-up for electrode impedance spectroscopy.

Fig. 4-3. (a) Vector analysis by means of lock-in amplifiers.
(b) Analysis of the Lissajous figure on a storage oscilloscope.

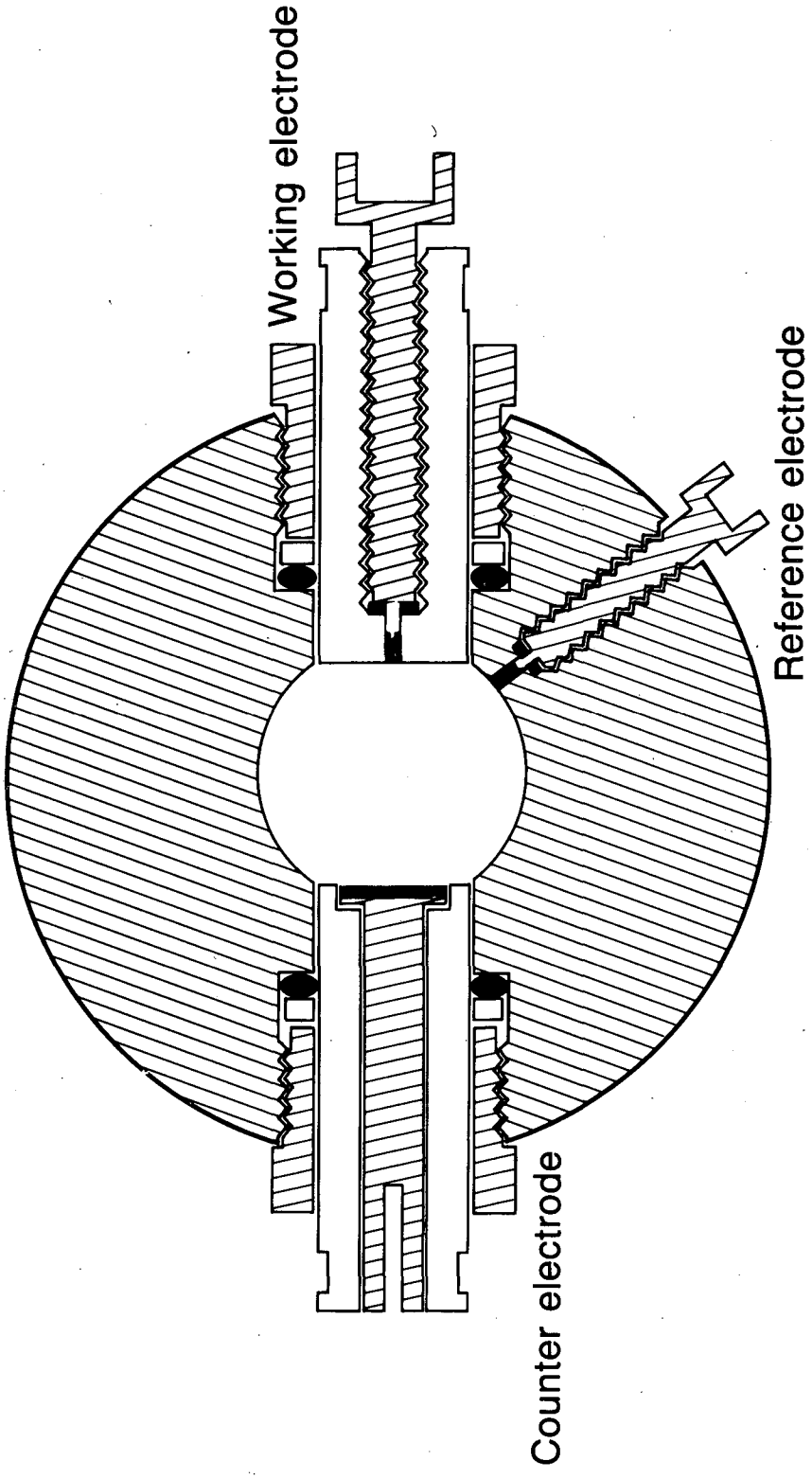

XBL 861-6033

Fig. 4-1

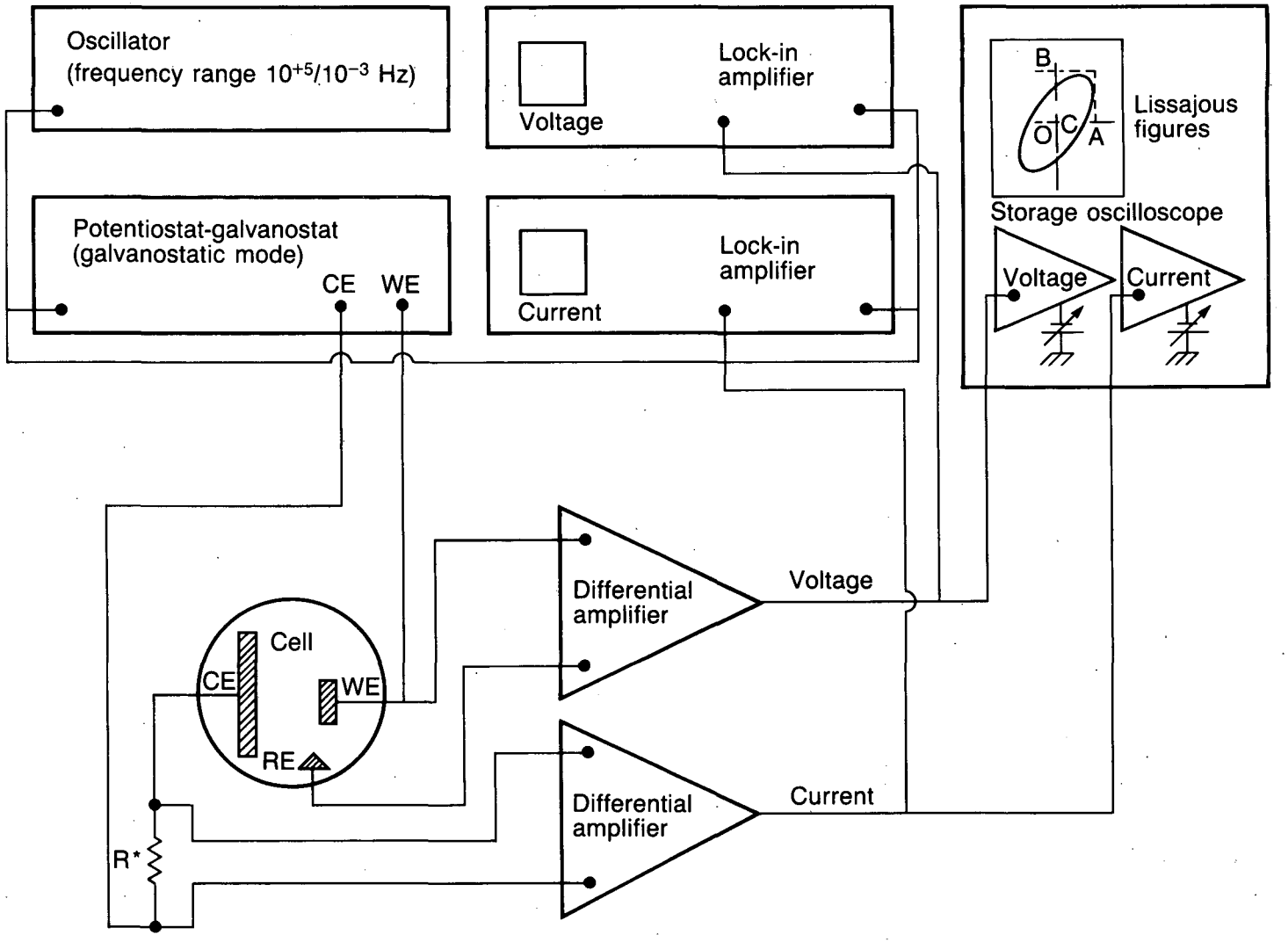

XBL 861-343

Fig. 4-2

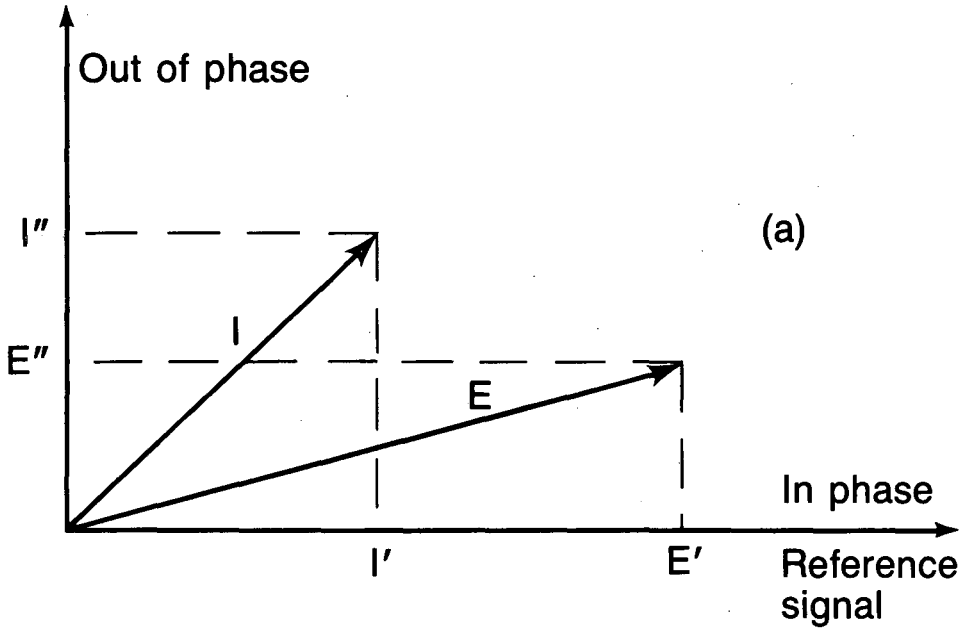

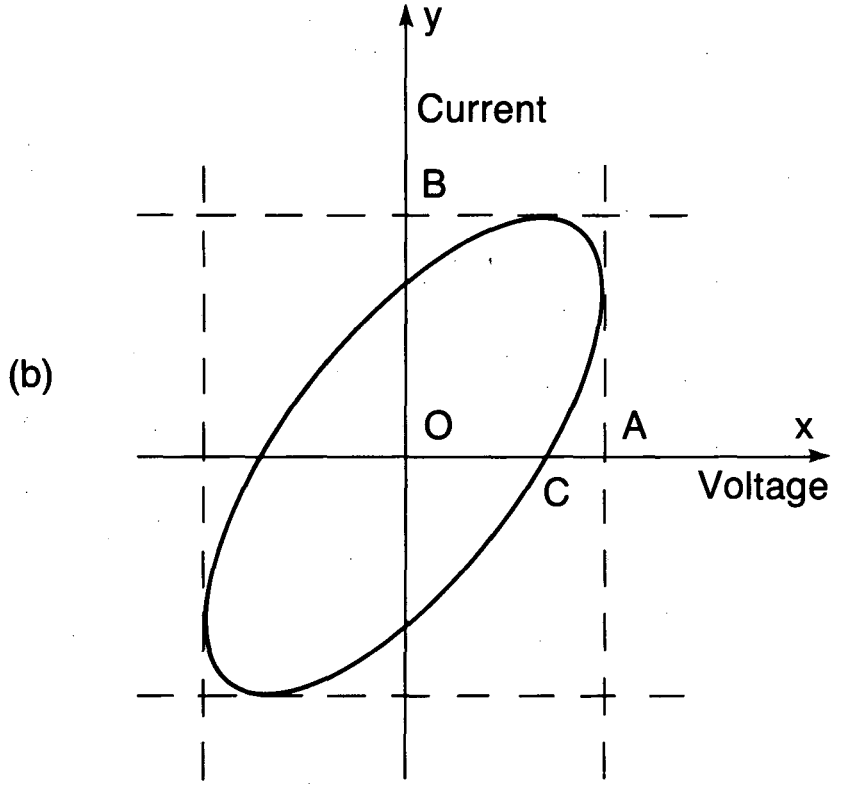

XBL 861-6037

Fig. 4-3

5. RESULTS AND DISCUSSION

5.1 Preliminary Study:

5.1.1 Reactivity of the Lithium Amalgam

In order to eliminate the impurities of the solution and reduce the value of its residual water content, a molar solution of $LiClO_4$ in propylene carbonate was brought in contact with lithium amalgam. In fact, this experiment has provided a study of the possible methods of complete decomposition of the PC/$LiClO_4$ solution in the presence of the lithium amalgam.

After a few minutes of immersion of 1 cm^3 of lithium amalgam in 50 cm^3 of electrolyte, many gas bubbles were produced. After one hour the electrolyte gradually became cloudy, and a white precipitate formed. After several hours there was a considerable decrease in the volume of clear liquid electrolyte available. This effect seemed to indicate that the amalgam reacted with the whole electrolyte and did not permit a selective reaction with the residual water content of the electrolyte. After one day of immersion of the lithium amalgam, the electrolyte had decomposed completely to form propylene gas, (lost in the glove box), and a gray-white powder, made of a combination of lithium carbonate and lithium perchlorate.

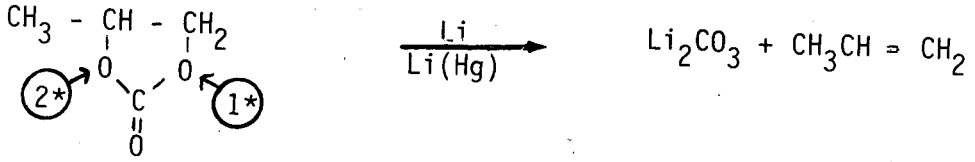

The above chemical reaction, which is in agreement with the reaction described by Dousek, Jansta, and Riha,[18] corresponds to the double opening of the characteristic ring of propylene carbonate (positions 1* and 2*).

The immersion of a smaller volume of lithium amalgam, for example, 0.1 cm^3 in 50 cm^3 of the molar solution, leads during the first hours to the same decomposition process. But after a few hours, the formation of a colorless polymer that contains gas bubbles appears. The polymerization of propylene carbonate can be initiated as follows:

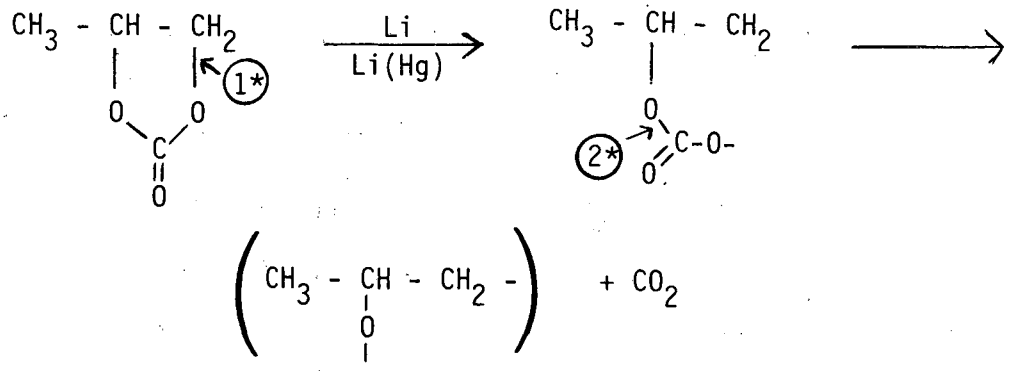

An initial opening (position 1^*) of the characteristic ring of propylene carbonate is probably followed by another opening (position 2^*), to form carbon dioxide and the repeat unit of polypropylene oxide. This reaction, which explains the presence of carbon dioxide in the gaseous phase, seems too simple because propylene carbonate can be polymerized by many causes. For example, by impurities of the solvent and salt and/or certain specific radicals that are due to reactions of these impurities with lithium. Traces of water, propylene glycol, and any acid are not taken into account, while their presence can be the cause of the decomposition of the solvent. (See Appendices XI and XII).

5.1.2 Reactivity of Lithium Metal

To attempt to assess every possible reaction between lithium and propylene carbonate-based electrolytes due to the thermodynamic instability of this system would be a futile exercise. (See Appendix XI) The most likely reactions expected to occur are as follows:

(1) $2\ Li + H_2O \rightarrow Li_2O + H_2$

(2) $Li + R\text{-}OH \rightarrow LiO\text{-}R + 1/2\ H_2$

(3) $2\ Li + PC \rightarrow Li_2CO_3 + CH_3 - CH = CH_2$

(4) $Li + PC \rightarrow CO_2 + (CH_3 - \underset{\underset{O}{|}}{CH} - CH_2\text{-})$

Since the major reactive impurities in propylene carbonate are water and propylene glycol, reactions (1) and (2) are expected. Even if the impurities are kept at the ppm level, these reactions cannot be avoided, and they influence the electrochemical behavior of lithium. (See Appendix XII) The formation of Li_2O is much more probable than the formation of LiOH, according to the values of their respective energies of formation.[62] But Li_2O is expected to be on the lithium surface, while LiOH is assumed to be between the oxide and the wet solution.[29]

Reaction (3), which can be a chemical or electrochemical reduction of propylene carbonate in the presence of the lithium electrode, corresponds to the classic formation of lithium carbonate and propylene. Reaction (4), which can intervene at the same time with the preceeding reaction, corresponds to the polymerization of propylene carbonate to form polypropylene oxide and derivatives. With regard to the lithium

perchlorate/propylene carbonate electrolyte, it is also necessary to remember the formation of LiCl due to an unknown decomposition mechanism of $LiClO_4$ in the presence of lithium. This reaction, involving the transient formation of HCl, may be the cause of other decomposition products. For example, different chlorinated molecules and polymers can be obtained by selected reactions in which H_2O and HCl may be involved. (See Appendix XII)

This survey of the most likely decomposition products of the lithium perchlorate/propylene carbonate electrolytes shows that the surface layer formed on the lithium electrode has a complex composition, including different organic and inorganic compounds.

5.2 General Study: Interphase Model of the Surface Layer

The evolution of the electrochemical properties of surface layers was studied for two weeks at the open-circuit potential in Solution C, which is the molar solution of lithium perchlorate in propylene carbonate treated with lithium amalgam. A preliminary comparative study of the impedance obtained with surface layers of the same age in the three solutions (A, B, and C) showed that the electrode impedance was always lower in Solution C than in Solutions A and B. Thus, Solution C is assumed to be the best electrolyte, with the minimum of impurities and water.

The evolution of impedance behavior of the lithium electrode covered by a surface layer is detailed in Figs. 5-1 through 5-4, all showing Cole-Cole plots as a function of the storage time.

During the first day of formation of the surface layer, as shown in

Figs. 5-1 and 5-2a, each impedance diagram in the complex plane exhibits two features: (1) a semicircle in the high-frequency range, which can be related to a charge transfer process, and (2) a straight line in the low-frequency range which is characteristic of a diffusion process. The increase of the semicircle with the decrease of the straight line as a function of the storage time indicates a fast change of the processes involved in the surface layer which is related to its composition and structure. During the next days, as shown in Figs. 5-2 through 5-4, the impedance diagrams exhibit only one depressed loop over the whole frequency range. This loop can be defined by apparent resistance R_a and capacitance C_a. Because the product R_aC_a has an increasing value as a function of the storage time, it seems too simple to attribute the single loop to a conduction process in a solid electrolyte according to the Solid-Electrolyte Interphase (SEI) model. Nevertheless, it is interesting to use this model for a rough estimation of the thickness of the surface layer. By taking into account the apparent capacitance C_a, as shown in Fig. 5-6, the thickness Y of the surface-layer increases as an exponential function of the storage time from 15 (30) to 25 (50) Å for a relative permittivity ε_r equal to 5 (10), by assuming that the solid electrolyte is similar to Li_2CO_3 (Li_2O). As shown in Fig. 5-7, by taking into account the apparent resistance R_a, the layer thickness increases as another exponential function of the storage time from 5 (10) to 100 (200) Å for a conductivity σ equal to 1 (2)x10^{-9} $\Omega^{-1}cm^{-1}$ during two weeks of storage. These values determined by impedance measurements according to the SEI model are much lower than the values (up to 1500 Å) determined by ellipsometric measurements performed by Schwager, Geronov and Muller,[8]

using similar experimental conditions. According to these authors, the discrepancy between the optical and electrochemical thicknesses can be attributed to the sensitivity of the respective methods in detecting different parts of the surface layer.

The surface layer can also be considered to be made of two sublayers with different permittivities and conductivities according to the Compact-Stratified Layer (CSL) model. The use of this model, as shown in Figs. 5-6 and 5-7, leads to an estimation of the thicknesses of sublayers. (See Appendix VI) For a ratio $\varepsilon_2/\varepsilon_1$ equal to 10 ($\varepsilon_{r1} = 5$), the total thickness L ranges from 75 to 125 Å, while for a ratio σ_1/σ_2 equal to 50 ($\sigma_1 = 1\text{x}10^{-9}\Omega^{-1}\text{cm}^{-1}$), the thickness ranges from 100 to 1500 Å during two weeks of storage. For this condition, the thickness d of the first sublayer ranges from 10 to 100 Å, and the thickness (L-d) of the second sublayer ranges from 90 to 1400 Å, during two weeks of storage. These last values of the thickness of the surface layer deduced from the CSL model appear in better agreement with those determined by optical measurements.[8]

Another possible assumption is to consider that the surface layer is essentially made of a polymer electrolyte with insertion of different solid electrolytes. The depressed loop in the complex plane is not due to a simple conduction process, but is caused by three elementary processes (conduction, charge transfer, diffusion) the time constants of which are not well separated according to the Solid-Polymer Interphase (SPI) model (See also Appendix V for the general study of a Polymer-Electrolyte Interphase (PEI) model). The analysis of the Figs. 5-2 through 5-4 demonstrates that the impedance diagrams can show the

occurrence of more than one time constant for the case of thick surface layers. Considering successive resistance/capacitance circuits with a depression parameter, an approximate geometrical fitting between the experimental and theoretical Cole-Cole and Bode plots can be obtained, for one time constant in Fig. 5-8, two time constants in Fig. 5-9, and three time constants in Fig. 5-10. The study of the apparent resistance R_a (capacitance C_a) in order to define the different components R_1, R_2 and R_3 (C_1, C_2 and C_3) deduced from the Figs. 5-3 and 5-4, is shown in Fig. 5-11 between the 7th and 15th day of storage. Assuming that the first loop in the high-frequency range (coupling R_1/C_1) is related to the conduction process in the surface layer, the layer thickness can be determined for a given permittivity or conductivity. As shown in Fig. 5-12, by assuming that the surface layer is a polymer electrolyte such as $P(PO)_n$ $LiClO_4$, (See Appendix XIII), the thickness X increases exponentially from 500 to 1000 $\mathring{A}$ for a relative permittivity equal to 50, and from 175 to 1125 $\mathring{A}$ for a conductivity equal to 50×10^{-9} Ω^{-1} cm^{-1}. These values of the thickness of the surface layer also appear in agreement with those deduced from ellipsometric measurements.[8]

FIGURE CAPTIONS

Fig. 5-1. Impedance diagram in the complex plane obtained with a lithium electrode immersed in the molar solution of lithium perchlorate in propylene carbonate. a) after 30 min., b) after 2 hours, c) after 6 hours.

Fig. 5-2. Impedance diagram in the complex plane obtained with a lithium electrode immersed in the molar solution of lithium perchlorate in propylene carbonate. a) after 1 day, b) after 3 days, c) after 4 days.

Fig. 5-3. Impedance diagram in the complex plane obtained with a lithium electrode immersed in the molar solution of lithium perchlorate in propylene carbonate. a) after 7 days, b) after 8 days, c) after 10 days.

Fig. 5-4. Impedance diagram in the complex plane obtained with a lithium electrode immersed in the molar solution of lithium perchlorate in propylene carbonate. a) after 11 days, b) after 14 days, c) after 15 days.

Fig. 5-5. a) Study of the apparent resistance R_a [o] and apparent capacitance C_a [Δ] as a function of the storage time. b) Study of the product R_aC_a as a function of the storage time.

Fig. 5-6. Study of the layer thickness as a function of the storage time according to the apparent capacitance C_a for the Solid-Electrolyte Interphase (SEI) and the Compact-Stratified Layer (CSL) models. [o] Y, SEI model (ε_r =5). [●] Y, SEI model (ε_r=10). [Δ] L, CSL model ($\varepsilon_2/\varepsilon_1$ =10, ε_{r1}=5). [□] d, CSL model ($\varepsilon_2/\varepsilon_1$=10, ε_{r1}=5).

Fig. 5-7. Study of the layer thickness as a function of the storage time

according to the apparent resistance R_a for the Solid-Electrolyte Interphase (SEI) and the Compact-Stratified Layer (CSL) models. [o] Y, SEI model ($\sigma = 10^{-9}\Omega^{-1}cm^{-1}$). [•] Y, SEI model ($\sigma = 2\times10^{-9}\Omega^{-1}cm^{-1}$). [Δ] L, CSL model ($\sigma_1/\sigma_2 = 50$, $\sigma = 10^{-9}\Omega^{-1}cm^{-1}$). [□] d, CSL model ($\sigma_1/\sigma_2 = 50$, $\sigma = 10^{-9}\Omega^{-1}cm^{-1}$).

Fig. 5-8. Analysis of the impedance data by the Cole-Cole and Bode plots for the case of a surface layer formed after 3 days of storage. The experimental diagrams [Δ] are compared to the theoretical ones [o] according to the Solid-Polymer Electrolyte (SPI) model. Case of one time constant. $\alpha = 0.2$, $R_0 = 15\Omega cm^2$, $R_1 = 85\Omega cm^2$, $C_1 = 2.6\mu F/cm^2$, $f_1 = 750$ Hz.

Fig. 5-9. Analysis of the impedance data by the Cole-Cole and Bode plots for the case of the surface layer formed after 7 days of storage. The experimental diagrams [Δ] are compared to the theoretical ones [o] according to the Solid-Polymer Electrolyte (SPI) model. Case of two time constants. $\alpha = 0.1$, $R_0 = 15\Omega cm^2$ $R_1 = 35\Omega cm^2$, $C_1 = 0.9\ \mu F/cm^2$, $f_1 = 5000$Hz, $R_2 = 180\Omega cm^2$, $C_2 = 3.5\ \mu F/cm^2$, $f_2 = 250$ Hz.

Fig. 5-10. Analysis of the impedance data by the Cole-Cole and Bode plots for the case of the surface layer formed after 11 days of storage. The experimental diagrams [Δ] are compared to the theoretical ones [o] according to the Solid-Polymer Electrolyte (SPI) model. Case of three time constants. $\alpha = 0.15$, $R_0 = 15\Omega cm^2$, $R_1 = 120\Omega cm^2$, $C_1 = 0.5\ \mu F/cm^2$, $f_1 = 2250$ Hz, $R_2 = 320\Omega cm^2$, $C_2 = 4.1\ \mu F/cm^2$, $f_2 = 125$ Hz, $R_3 = 60\Omega cm^2$, $C_3 = 530\ \mu F/cm^2$, $f_3 = 5$Hz.

Fig. 5-11. Study of the resistances R_1 and capacitances C_1 as functions of the storage time according to the Solid-Polymer Electrolyte (SPI) model. R_1, C_1 for the conduction process; R_2, C_2 for the charge transfer

process; R_3,C_3 for the diffusion process.

Fig. 5-12. Study of the layer thickness as a function of the storage time according to the Solid-Polymer Interface (SPI) model. [o] for $\sigma = 5 \times 10^{-9}\ \Omega^{-1}cm^{-1}$. [•] for $\varepsilon_r = 50$.

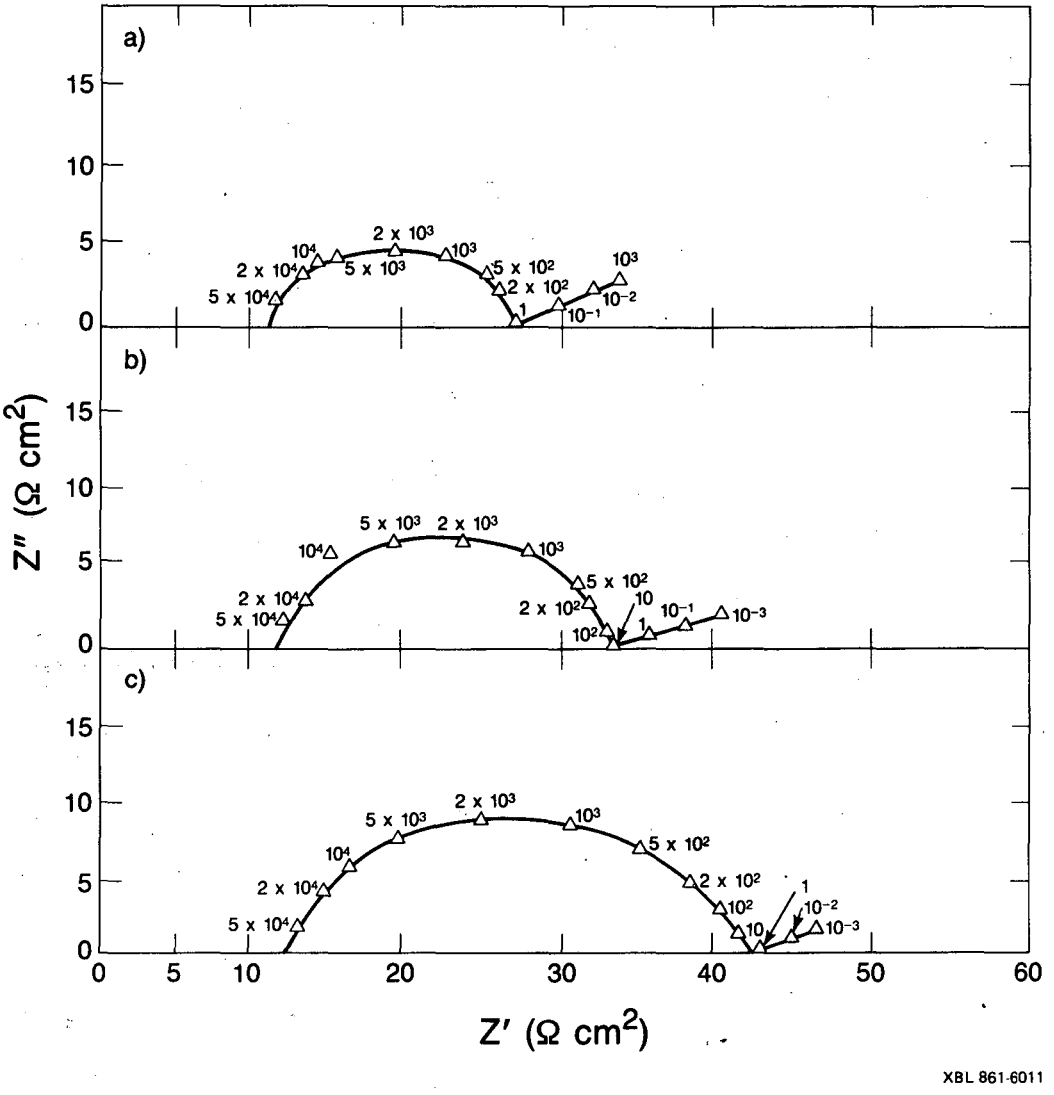
a)
b)
c)
Z'' (Ω cm²)
Z' (Ω cm²)
0
5
10
15
20
30
40
50
60
5 x 10⁴
2 x 10⁴
10⁴
5 x 10³
2 x 10³
10³
5 x 10²
2 x 10²
10²
10
1
10⁻¹
10⁻²
10⁻³
XBL 861-6011

Fig. 5-1

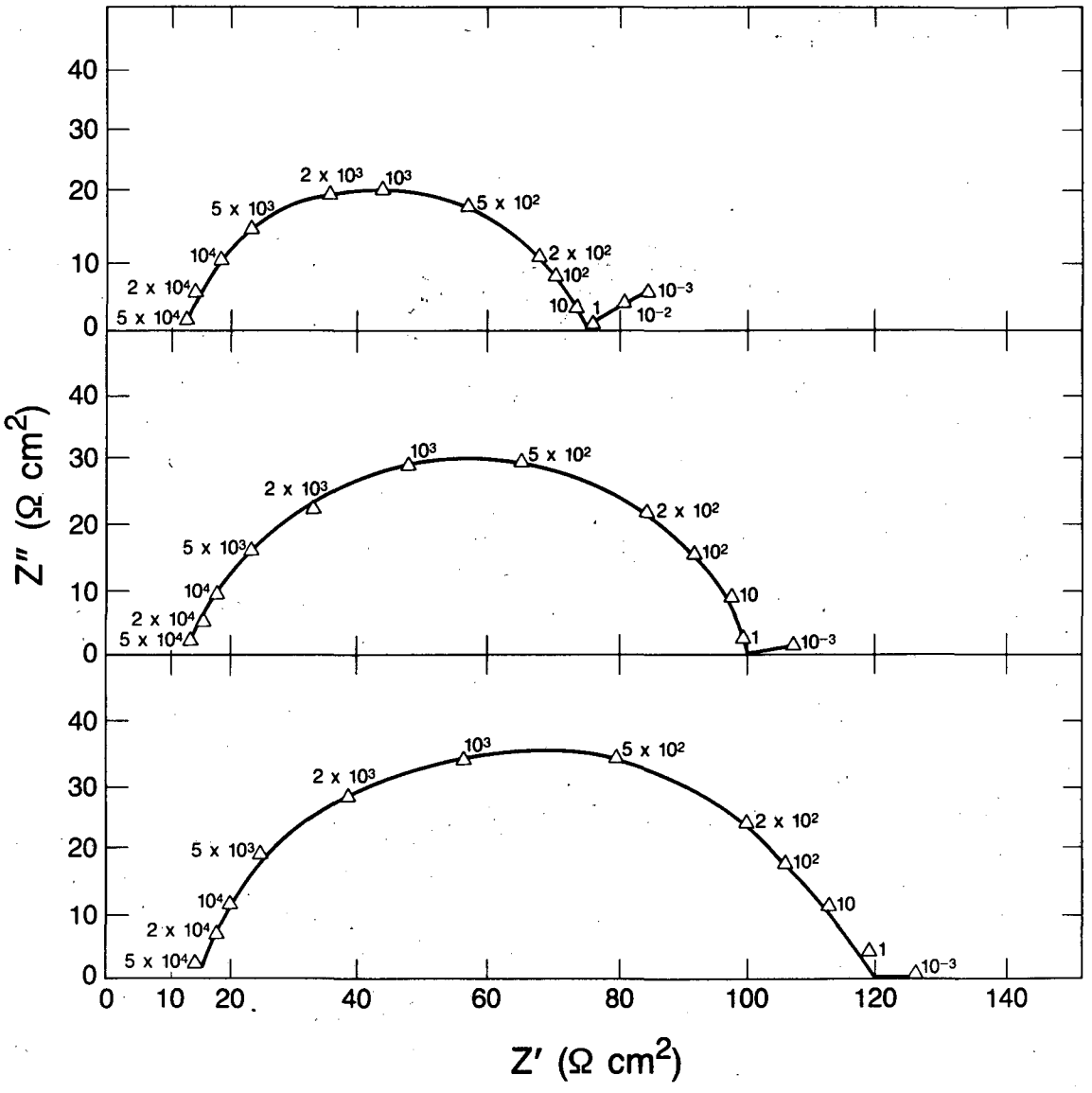
Z'' (Ω cm²)
Z' (Ω cm²)
0
10
20
30
40
0
10
20
40
60
80
100
120
140
2 x 10³
10³
5 x 10³
5 x 10²
10⁴
2 x 10²
2 x 10⁴
10²
5 x 10⁴
10
10⁻³
1
10⁻²
XBL 861-6009

Fig. 5-2

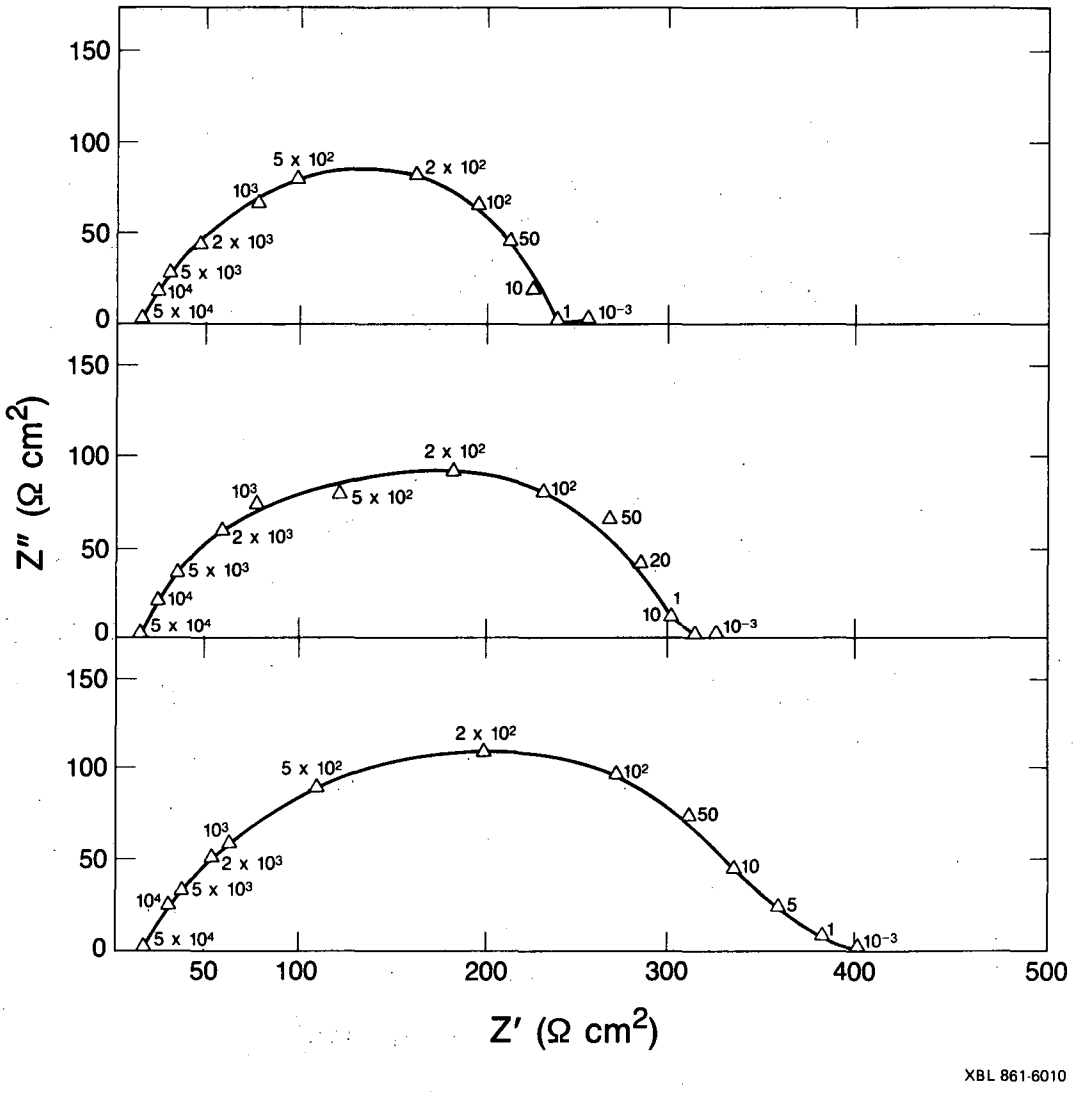

XBL 861-6010

Fig. 5-3

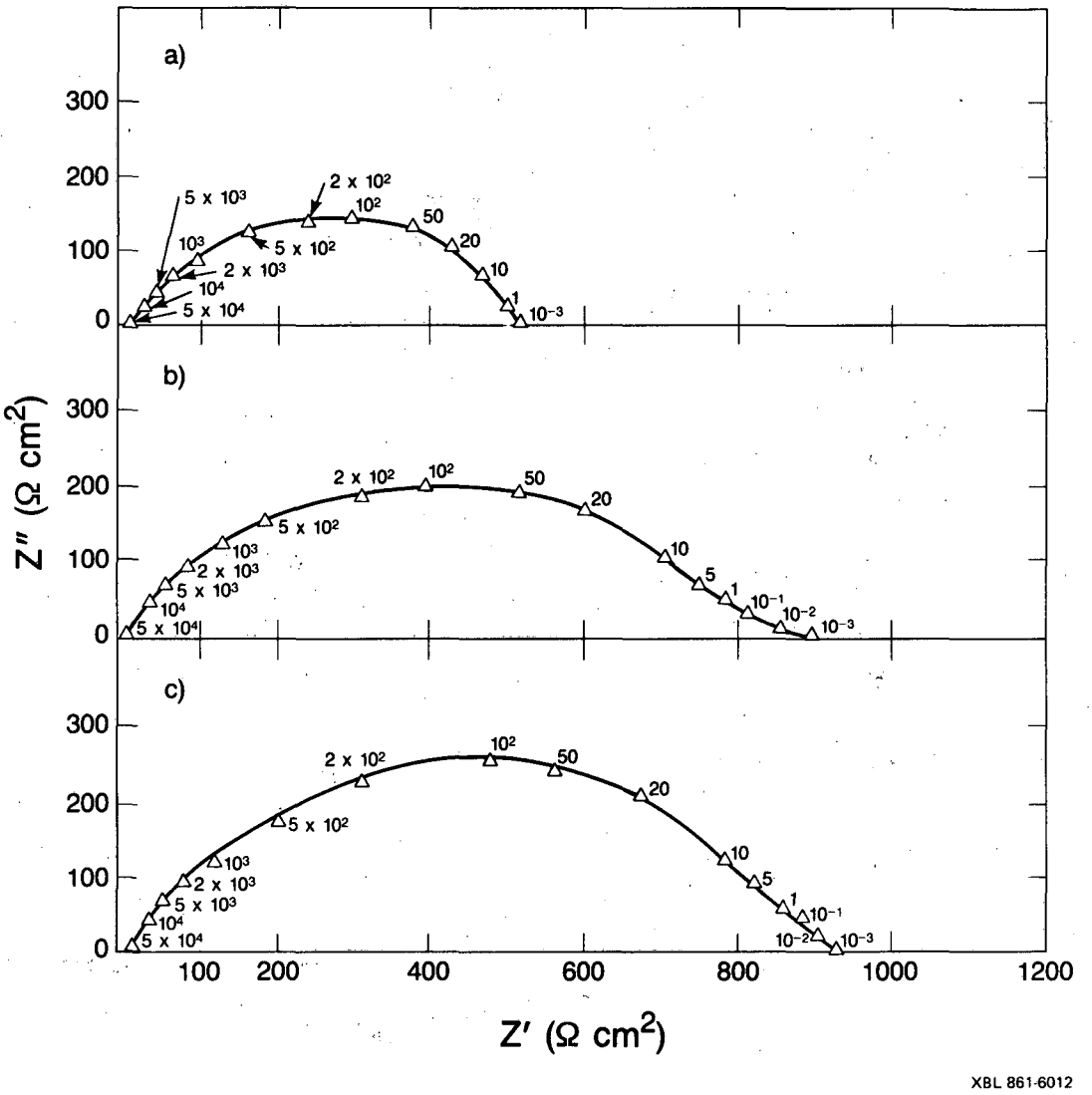
a)
b)
c)
300
200
100
0
5 x 10³
2 x 10²
10²
50
20
10
1
10⁻³
10³
5 x 10²
2 x 10³
10⁴
5 x 10⁴
5
10⁻¹
10⁻²
100
200
400
600
800
1000
1200
Z″ (Ω cm²)
Z′ (Ω cm²)
XBL 861-6012

Fig. 5-4

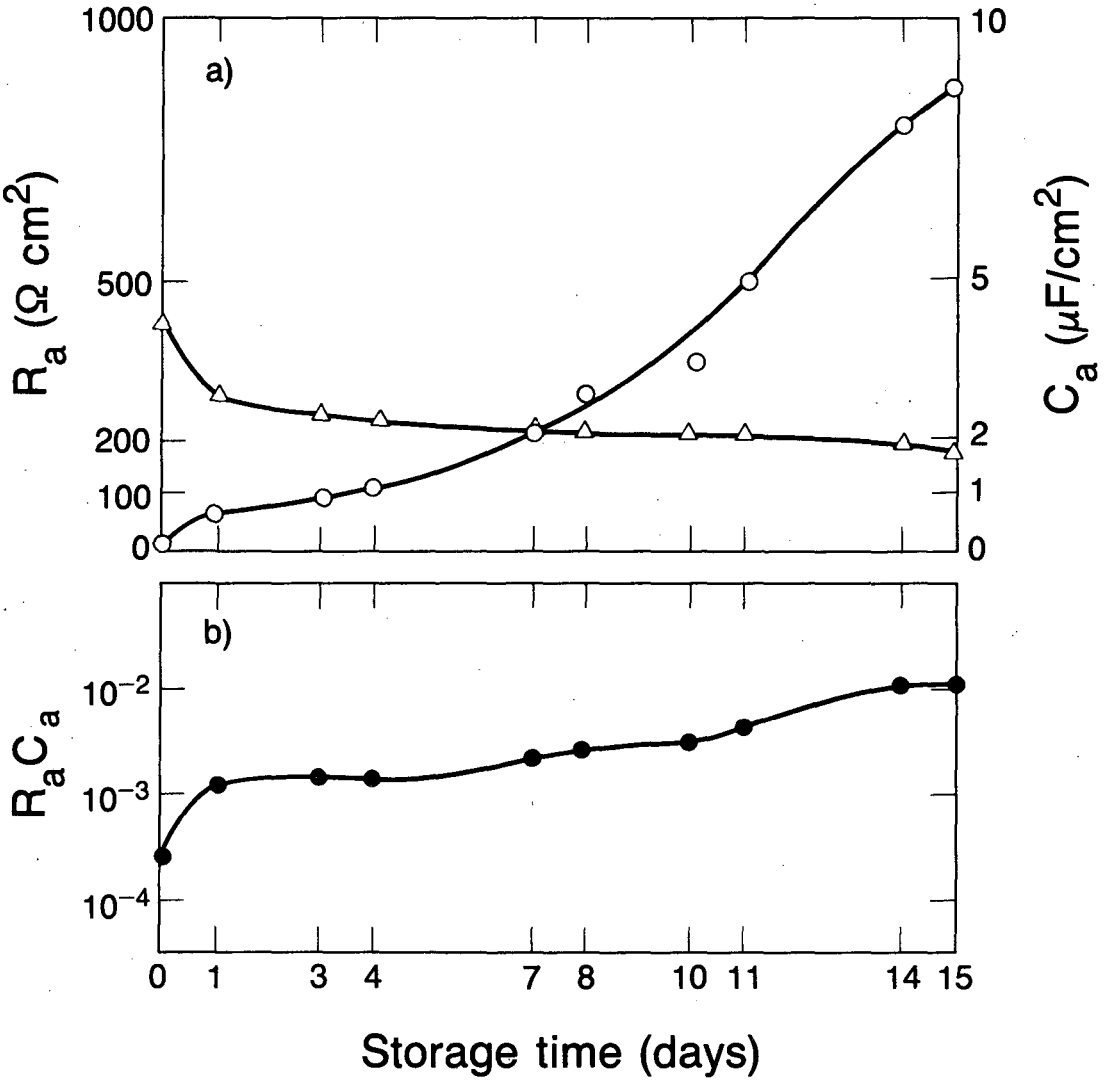

XBL 861-6004

Fig. 5-5

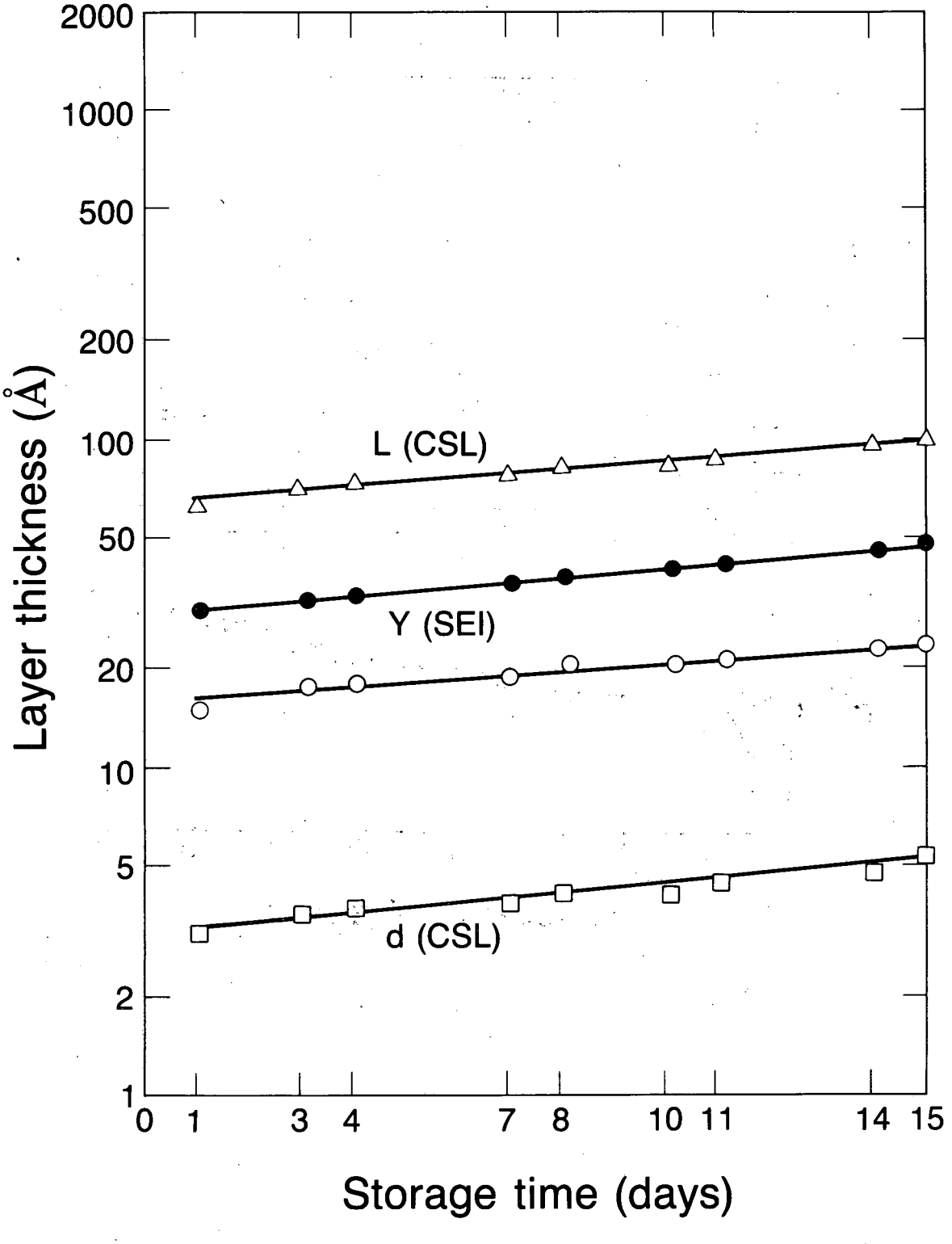
2000
1000
500
200
100
50
20
10
5
2
1
Layer thickness (Å)
L (CSL)
Y (SEI)
d (CSL)
0
1
3
4
7
8
10
11
14
15
Storage time (days)
XBL 861-6002

Fig. 5-6

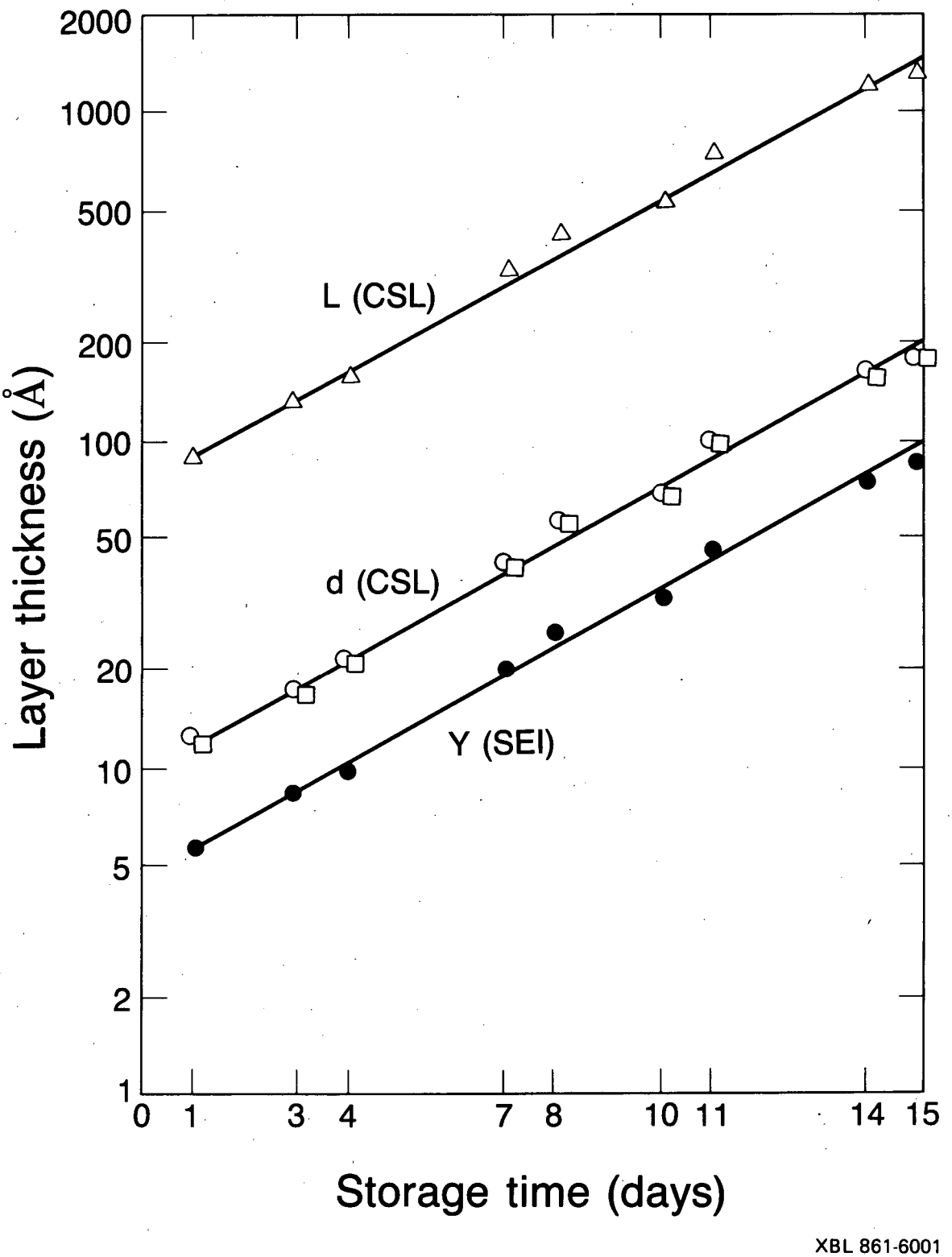
2000
1000
500
200
100
50
20
10
5
2
1
Layer thickness (Å)
L (CSL)
d (CSL)
Y (SEI)
0 1 3 4 7 8 10 11 14 15
Storage time (days)
XBL 861-6001

Fig. 5-7

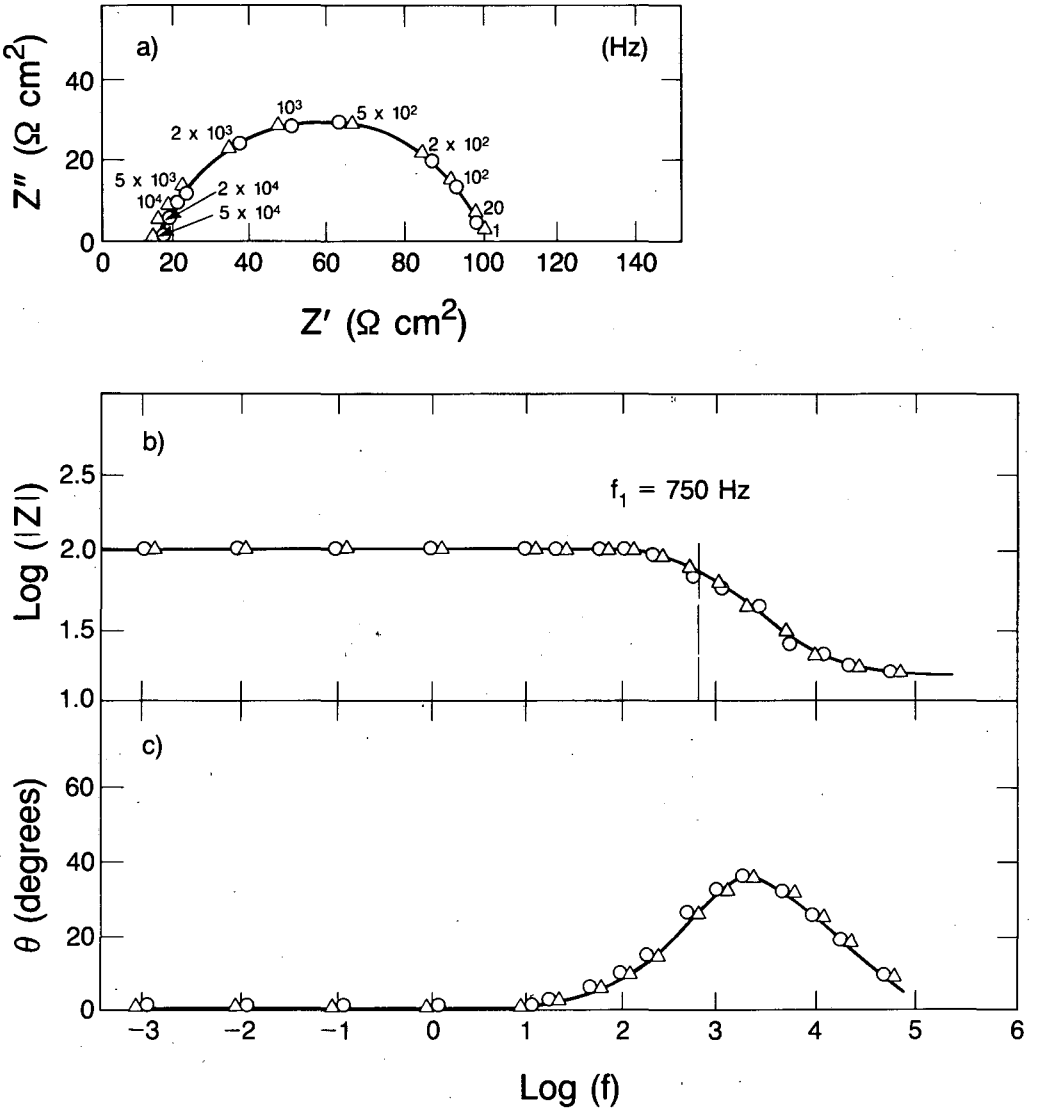
a)
(Hz)
Z″ (Ω cm²)
Z′ (Ω cm²)
10³
5 x 10²
2 x 10³
2 x 10²
5 x 10³
10²
2 x 10⁴
10⁴
20
5 x 10⁴
1
b)
f₁ = 750 Hz
Log (|Z|)
c)
θ (degrees)
Log (f)
XBL 861-6013

Fig. 5-8

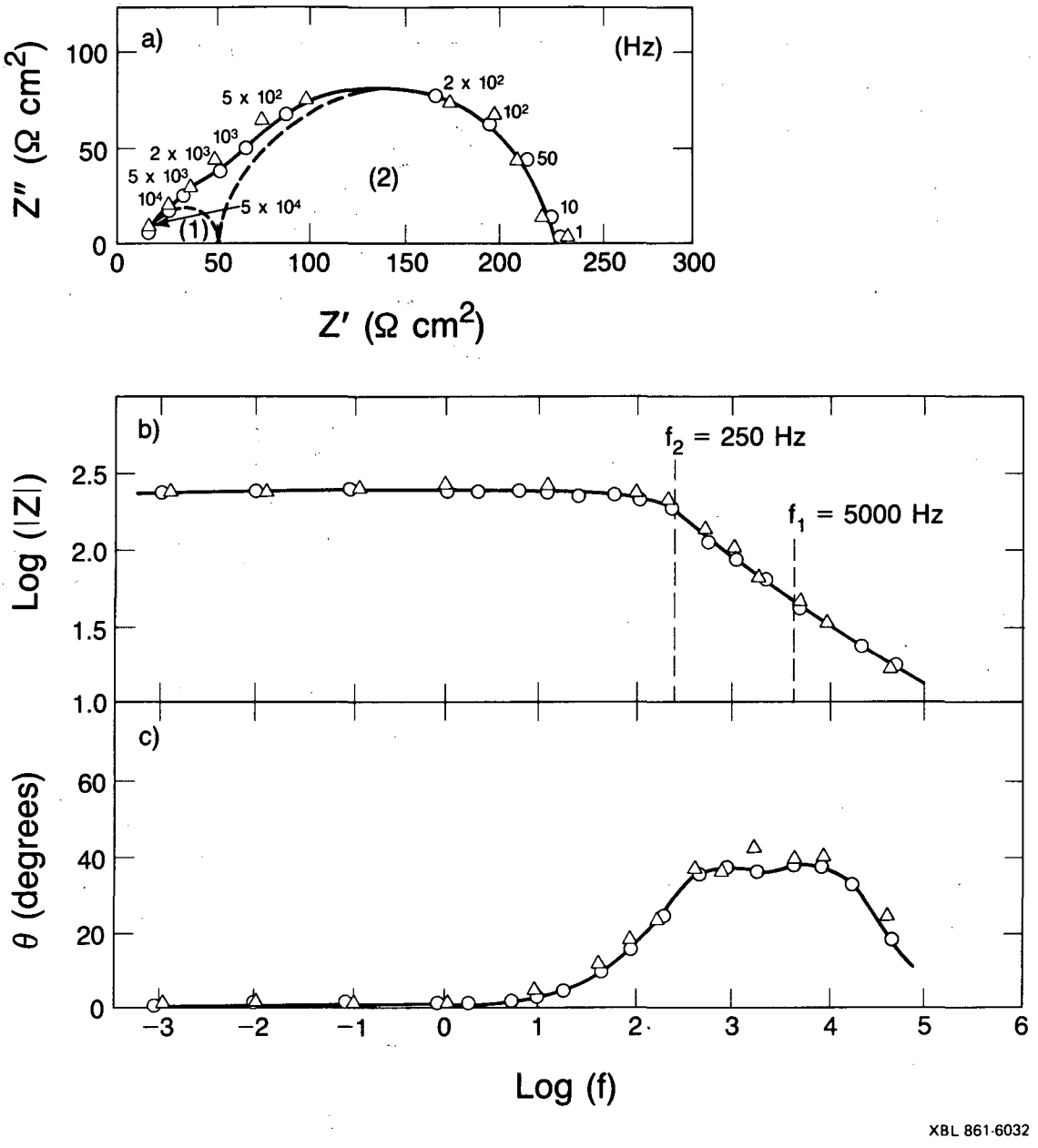
a)
(Hz)
Z'' (Ω cm²)
Z' (Ω cm²)
5 x 10²
2 x 10²
10²
10³
2 x 10³
5 x 10³
10⁴
5 x 10⁴
50
10
1
(1)
(2)
b)
Log (|Z|)
f₂ = 250 Hz
f₁ = 5000 Hz
c)
θ (degrees)
Log (f)
XBL 861-6032

Fig. 5-9

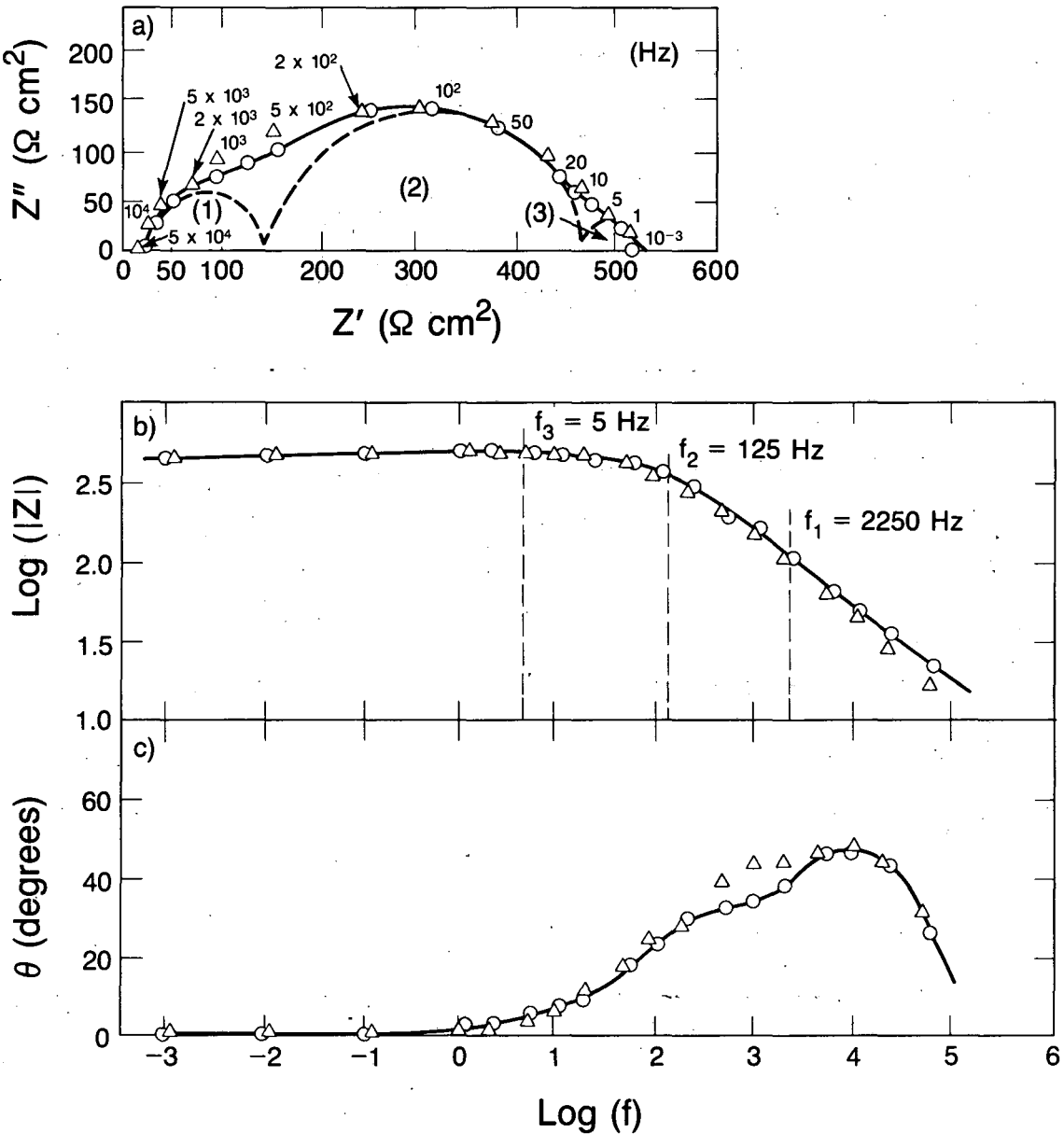
a)
(Hz)
2 x 10²
5 x 10³
2 x 10³
5 x 10²
10³
10²
50
20
10
5
1
10⁻³
10⁴
5 x 10⁴
(1)
(2)
(3)
Z″ (Ω cm²)
Z′ (Ω cm²)
b)
f₃ = 5 Hz
f₂ = 125 Hz
f₁ = 2250 Hz
Log (|Z|)
c)
θ (degrees)
Log (f)
XBL 861-6025

Fig. 5-10

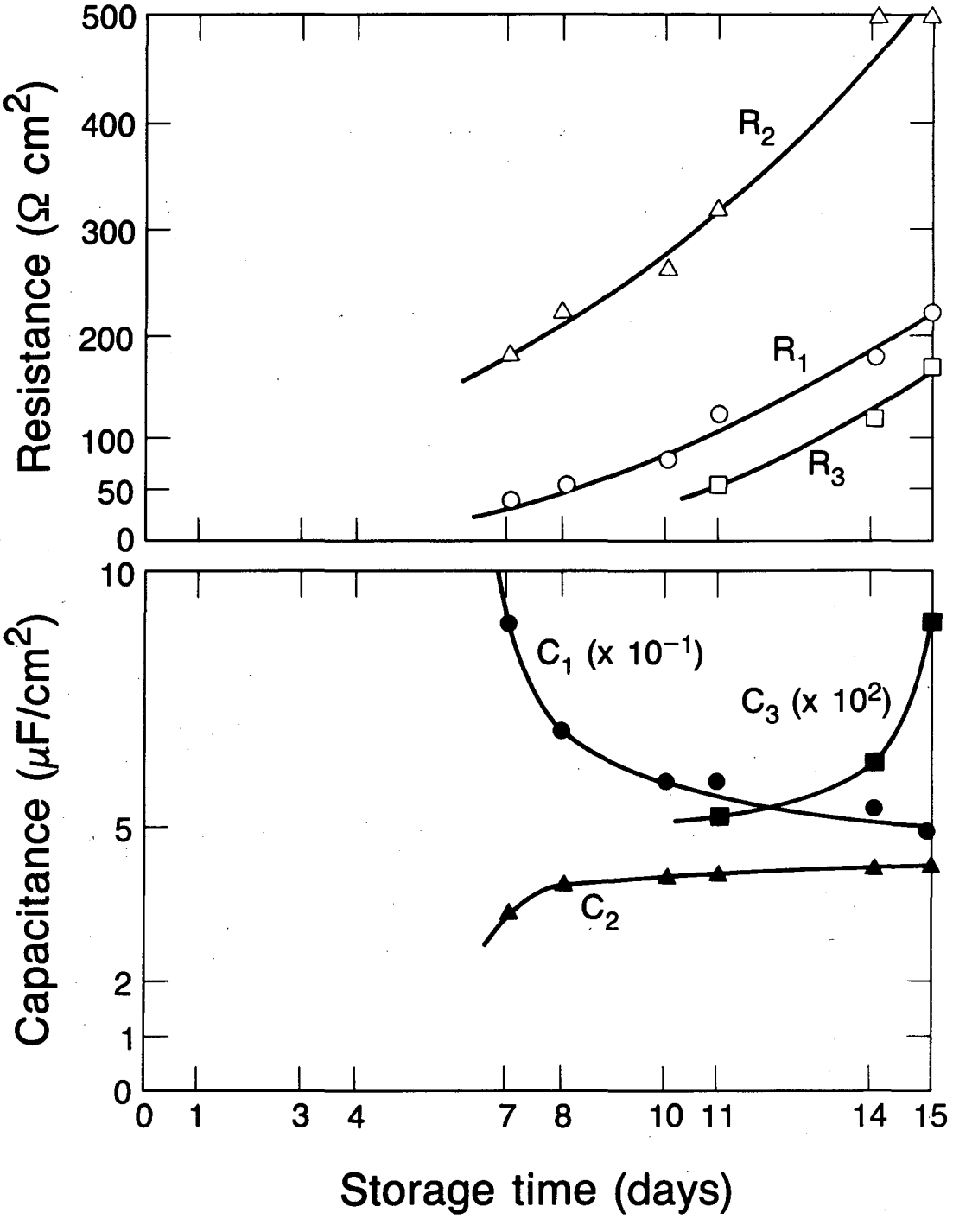
Resistance (Ω cm²)
500
400
300
200
100
50
0
R₂
R₁
R₃
Capacitance (μF/cm²)
10
5
2
1
0
C₁ (x 10⁻¹)
C₃ (x 10²)
C₂
0 1 3 4 7 8 10 11 14 15
Storage time (days)
XBL 861-6003

Fig. 5-11

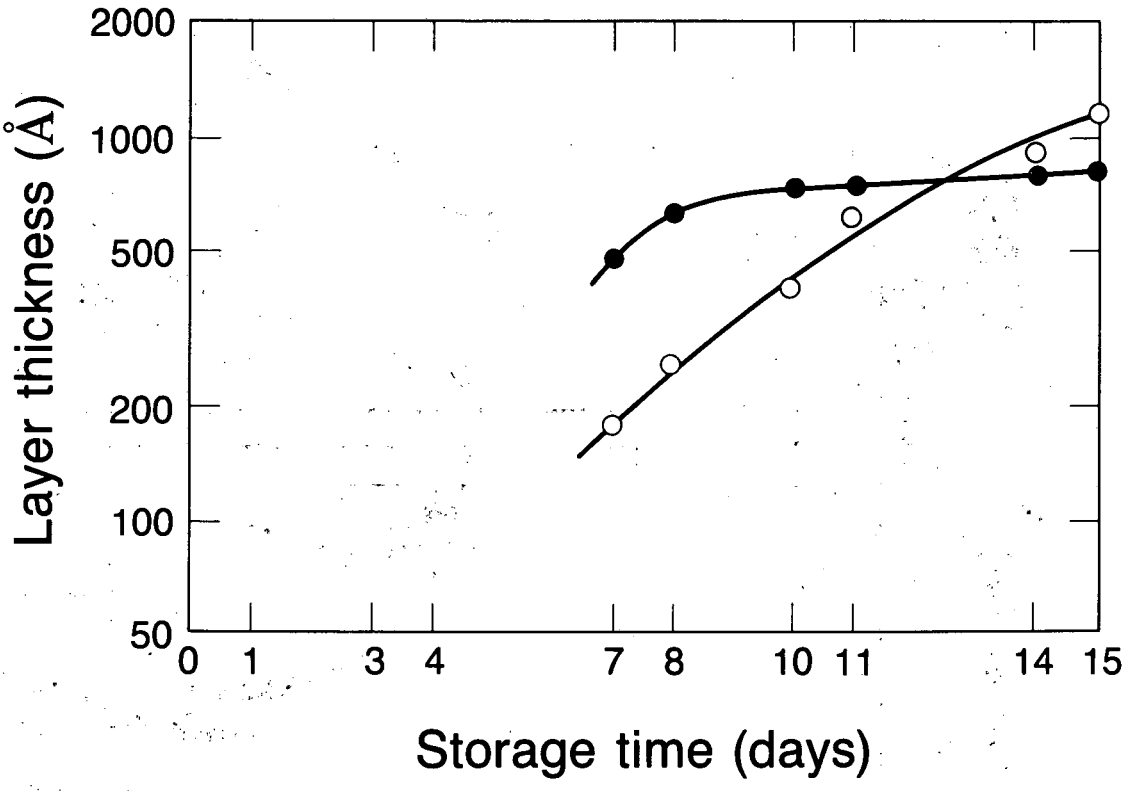
2000
1000
500
200
100
50
Layer thickness (Å)
0
1
3
4
7
8
10
11
14
15
Storage time (days)
XBL 861-6005

Fig. 5-12

6. CONCLUSION

The study of the impedance behavior of the metal/surface-layer/solution system has shown that the interphase models can be defined for simple compositions and structures of the surface layer. Besides, the determination of the thickness of the surface layer is only possible when the permittivity or the conductivity of the surface layer is known by another method. For the case of good ionic conductors, different interphase models have been discussed for surface layers having the general properties of a solid or a polymer electrolyte. The equivalent circuit and the corresponding impedance diagram has been presented for compact, porous and multilayer systems. For the case of ionic and electronic conductors, it has been shown that the impedance behavior of the layer cannot be useful for the determination of its thickness, especially when the time constants of the processes at the interface surface-layer/solution are not well separated from those involved in the surface layer.

The study of the impedance behavior of the lithium electrode in a lithium perchlorate/propylene carbonate solution has shown that the surface layer can be considered as either a solid electrolyte with two sublayers or as a solid-polymer electrolyte. If the electrode impedance is considered to be due to a conduction process in a stratified-layer interphase, the Compact-Stratified Layer (CSL) Model allows one to determine the respective thicknesses of two sublayers made of different solid electrolytes. If the electrode impedance is considered to be due to the occurrence of conduction, charge-transfer, and diffusion processes with

overlapping time constants, the Solid-Polymer Interphase (SPI) Model leads to the determination of the thickness of a surface layer made essentially of a polymer electrolyte. The fact that the layer thicknesses deduced from the impedance measurements are in good agreement with those deduced from ellipsometric measurements suggests that the CSL and SPI Models may be of value in understanding the main properties of the surface layers formed on the lithium electrode in propylene carbonate-based electrolytes.

ACKNOWLEDGMENTS

This work was supported by the Assistant Secretary for Conservation and Renewable Energy, Office of Advanced Conservation Technologies, Electrochemical Research Division of the U.S. Department of Energy under Contract No. DE-AC03-76SF00098.

The authors wish to thank Mr. Joseph Katz for his help and suggestions for the use of differential and lock-in amplifiers needed for the electrode-impedance spectroscopy.

REFERENCES

1. A.N. Dey, Thin Solid Films 43 (1977), 131.

2. J.O. Besenhard and G. Eichinger, J. Electroanal. Chem. 68 (1976), 1.

3. T. Broadhead and F.A. Trumbore, in 10th International Power Sources Symposium, Brighton, England, 1976.

4. M. Garreau and J. Thevenin, J. Microscopie et Spectr. Electron. 3 (1978), 27.

5. M. Froment, M. Garreau, J. Thevenin, and D. Warin, J. Microscopie et Spectr. Electron. 4 (1979), 111.

6. Y. Geronov, F. Schwager, and R.H. Muller, Electrochemical Society Meeting, Hollywood, FL, 80-2, (1980), p. 102.

7. J.P. Contour, A. Salesse, M. Froment, M. Garreau, J. Thevenin, and D. Warin, J. Microscopie Spectr. Electron. 4 (1979), 483.

8. F. Schwager, Y. Geronov, and R.H. Muller, J. Electrochem. Soc. 132 (1985), 285.

9. G. Nazri and R.H. Muller, J. Electrochem. Soc. 132 (1985), 2050.

10. S.G. Meibuhr, J. Electrochem. Soc. 117 (1970), 56.

11. R.F. Scarr, J. Electrochem. Soc. 117 (1970),

295.

12. B. Burrows and S. Kirkland, J. Electrochem. Soc. 115 (1958), 1164.

13. Y. Geronov, F. Schwager, and R.H. Muller, J. Electrochem. Soc. 129 (1982), 1422.

14. M. Garreau and J. Thevenin, Electrochemical Society Meeting, Washington, DC, 83-2, (1983).

15. R. Jasinski, in Advances in Electrochemistry and Electrochemical Engineering, edited by P. Delahay and C.W. Tobias, Interscience Publishers, Vol. 8 (1971), p. 253.

16. K.M. Abraham and S.B. Brummer, in Ambient Temperature Lithium Batteries, edited by J.P. Gabano, Academic Press, 1983, p. 371.

17. A.N. Dey and B.P. Sullivan, J. Electrochem. Soc. 117 (1970), 222.

18. F.P. Dousek, J. Jansta, and L. Riha, J. Electroanal. Chem. 46 (1973), 281.

19. G.L. Holleck, K.M. Abraham, and S.B. Brummer, in Power Sources for Biomedical Implantable Applications and Ambient Temperature Batteries, edited by B.B. Owens and N. Margalit, The Electrochemical Soc., Inc., 80-4 (1980), p. 384.

20. E. Peled, in Ambient Temperature Lithium Batteries, edited by J.P. Gabano, Academic Press, London, 1983, p. 43.

21. M. Garreau, J. Thevenin, and D. Warin, in Progress in Batteries and Solar Cells, edited by A. Kozawa et al., JEC Press, Inc., Vol. 2, 1979, p. 54.

22. M. Garreau, J. Thevenin, D. Warin, and P. Campion, in Lithium Nonaqueous Battery Electrochemistry, edited by E.B. Yeager, et al., The Electrochemical Society, Inc., 80-7 (1980), p. 158.

23. G. Nazri and R.H. Muller, International Society of Electrochemistry, 35th Meeting, Berkeley, CA, 1984, n^{o} A4-16.

24. G. Nazri and R.H. Muller, J. Electrochem. Soc., 132 (1985), 2054.

25. E. Peled, J. Electrochem. Soc. 126 (1979), 2047.

26. E. Peled, J. Electrochem. Soc. 128 (1981), 825.

27. R.D. Armstrong, M.F. Bell, and A.A. Metcalfe, in Electrochemistry, Specialist Periodical Reports, edited by H.R. Thirsk, The Chemical Society, Burlington House, London, Vol. 6, 1978, p. 98.

28. W.I. Archer and R.D. Armstrong, in Electrochemistry Specialist Periodical Reports, edited by H.R. Thirsk, The Chemical Society, Burlington House, London, Vol. 6, 1980, p. 157.

29. D.M. Radman, Electrochemical Society Meeting, New Orleans, LA, 84-2 (1984), p. 188.

30. L. Young, Anodic Oxide Films, Academic Press, New

York, 1961.

31. J. Thevenin, C.R. Acad. Sci. Paris, France 294 (1982), 697.

32. J. Thevenin, J. Power Sources 14 (1985), 45.

33. M. Garreau and J. Thevenin, submitted to J. Electrochem. Soc. (1986).

34. I. Epelboin, M. Froment, M. Garreau, J. Thevenin, and D. Warin, J. Electrochem. Soc. 127 (1980), 2100.

35. M. Garreau, B. Milandou, and J. Thevenin, submitted to J. Electrochem. Soc. (1986).

36. M. Armand, in Workshop on Lithium Nonaqueous Electrochemistry, The Electrochemical Society, Inc., 80-7 (1980), p. 261.

37. M. Armand, Solid State Ionics 9/10 (1983), 745.

38. P.R. Sorensen and T. Jacobsen, Electrochimica Acta 27 (1982), 1671.

39. J.E. Weston and B.C.H. Steele, Solid State Ionics 7 (1982), 75; Solid State Ionics 7 (1982), 81.

40. J.R. MacDonald, J. Chem. Phys. 61 (1974), 3977.

41. J.R. MacDonald, J. Chem. Phys., 58 (1973), 4982.

42. Handbook of Chemistry and Physics, edited by CRC Press, 64th edition (1984).

43. D.D. MacDonald, Transients Techniques in Electrochemistry, Plenum Press (1977).

44. H.A. Laitenen and J.E.B. Randles, Trans. Faraday Soc. 51 (1955), 54.

45. R. Parsons, in Advances in Electrochemistry and Electrochemical Engineering, edited by P. Delahay and C.W. Tobias, Interscience Publishers, Vol. 7, 1970, p. 177.

46. G.C. Barker, Pure Applied Chem. 15 (1967), 239.

47. J.L. Dawson and D.G. John, J. Electroanal. Chem. 110 (1980) 37.

48. E. Warburg, Wied. Ann. 67 (1899), 493; Drud. Ann. 6 (1901), 125.

49. P. Drossbach and J. Schultz, Electrochimica Acta 9 (1964), 1391.

50. K.S. Cole and R.H. Cole, J. Chem. Phys. 9 (1941), 341.

51. H.W. Bode, Network Analysis and Feedback Amplifier Design, D. Van Nostrand Co., New York, 1945.

52. B.D. Cahan and C.T. Chen, J. Electrochem. Soc. 129 (1982), 474; J. Electrochem. Soc. 129 (1982),700.

53. M. Kleitz and J.H. Kennedy, in Fast Ion Transport in Solids, edited by P. Vashishta, J.N. Mundy and G.K. Shenoy, North-Holland, Amsterdam, 1979.

54. J.R. McDonald in Electrode Processes in Solid State Ionics, edited by M. Kleitz and J. Dupuy, Reidel Publishing Co., Dordrecht, Holland, 1976.

55. J.R. MacDonald and J.A. Garber, J. Electrochem. Soc.

124 (1977), 1022.

56. J.R. MacDonald, J. Shoonman, and A.P. Lehnen, J. Electroanal. Chem. 67 (1982), 77.

57. Y.T. Tsai and D.H. Whitmore, Solid State Ionics 7 (1982), 129.

58. W.S. Harris, UCRL-8381, (1958).

59. J. Jorne, LBL-1111, (1972).

60. H.H. Law, LBL-9207, (1979).

61. D.W. Van Krevelen and H.A.G. Chermin, Chem. Eng. Sci. 1 (1951), 66; Chem. Eng. Sci. (1952), 236.

62. Lange's Handbook of Chemistry, Edited by J.A. Dean, McGraw-Hill Book Co., Twelfth edition, 1979 .

63. B. Gosse and A. Denat, J. Electroanal. Chem. 56 (1974), 129.

64. L.F. Silvester and C.W. Tobias, LBL-2528, (1973).

65. R.D. Armstrong and K. Edmondson, Electrochimica Acta 18 (1973) 937.

66. R.D. Armstrong and M. Henderson, J. Electroanal. Chem. 39 (1972) 81.

APPENDIX I: Randles Interface Model

The equivalent circuit and corresponding impedance diagram in the complex plane for an electrode free of any passivating layer and placed in a liquid electrolyte have been given by the Randles Interface Model,[44,45] As shown in Fig. A1-1, the electrode kinetics is governed by the charge-transfer process that is partially controlled by a diffusion process.

The components of the electrode impedance can be described as follows:

- R_{Ω}, the electrolyte resistance, contributes to the real component of the impedance in the very high-frequency range.

- R_{ct}, the charge-transfer resistance, is placed in parallel with C_{dl}, the double-layer capacitance. The charge-transfer resistance is determined by the Butler-Volmer equation and is related to the polarization conditions. C_{dl}, the double-layer capacitance, is a characteristic of the organic electrolyte. The corresponding impedance diagram is a semicircle observed in the high-frequency range.

- Z_{w}, the Warburg impedance, is generally placed in series with the charge-transfer impedance and in parallel with the double-layer capacitance. The corresponding impedance diagram in the low-frequency range, which is caused by the diffusion of the ions in a concentration gradient near the electrode, is responsible for a Warburg straight line for an infinite diffusion thickness, according to the equation

$$Z_w = K\omega^{-1/2}(i-j) \tag{A1.1}$$

where K is the Warburg constant.

The measured total impedance[43] is expressed as $Z = Z' - jZ''$

$$Z' = R_\Omega + \frac{R_{ct} + K\omega^{-1/2}}{(C_{dl}\, K\, \omega^{-1/2}+1)^3 + \omega^2 C_{dl}{}^2 (R_{ct} + K\omega^{-1/2})^2} \tag{A1.2a}$$

$$Z'' = \frac{\omega C_{dl}(R_{ct} + K\omega^{-1/2})^2 + K\omega^{-1/2}(\omega^{1/2} C_{dl}\, K+1)}{(C_{dl}\, K\, \omega^{-1/2}+1)^2 + \omega^2 C_{dl}{}^2 (R_{ct} + K\omega^{-1/2})^2} \tag{A1.2b}$$

At the low-frequency limit ($\omega \to 0$), the real and imaginary components approach the limiting forms:

$$Z' = R_\Omega + R_{ct} + K\omega^{-1/2}, \tag{A1.3a}$$

$$Z'' = K\omega^{-1/2} + 2\, K^2 C_{dl} \tag{A1.3b}$$

Elimination of ω between these two equations gives:

$$Z'' = Z' - R_\Omega - R_{ct} + 2\, K^2\, C_{dl}. \tag{A1.3c}$$

Thus, the plot of Z" versus Z' should be linear and have a unit slope. The extrapolated line intersects the real axis at

$$(R_\Omega + R_{ct} - 2\, K^2 C_{dl}) \tag{A1.3d}$$

At the high-frequency limit ($\omega \to \infty$), the Warburg impedance becomes insignificant in relation to R_{ct}, and the real and imaginary components of the impedance are given by:

$$Z' = R_{\Omega} + \frac{R_{ct}}{1 + \omega^2 C_{dl}^2 R_{ct}^2} \tag{A1.4a}$$

$$Z'' = \frac{\omega C_{dl} R_{ct}^2}{1 + \omega^2 C_{dl}^2 R_{ct}^2} \tag{A1.4b}$$

Elimination of ω from these equations yields:

$$(Z' - R_{\Omega} - \frac{R_{ct}}{2})^2 + Z''^2 = (\frac{R_{ct}}{2})^2. \tag{A1.4c}$$

Hence, Z" versus Z' should give a circular plot centered at

$$Z' = R_{\Omega} + R_{ct}/2 \tag{A1.5}$$

and Z" = 0 and having a radius $R_{ct}/2$. The radial frequency ω^0 at the maximum of the imaginary component $Z'' = R_{ct}/2$ is defined by the equation $R_{ct} C_{dl} \cdot \omega^0 = 1$.

APPENDIX II: Analysis of Diffusion Impedance

Even with the possibilities realized by the circuit networks utilizing a variety of series and parallel combinations of the resistances and capacitances, many electrochemical interfaces can not be modeled adequately without an additional circuit component known as the Warburg impedance, Z_w, which is associated with the mass transport of electrolyte species to (or from) the interface before (or after) the charge transfer. A more detailed study shows that the Warburg impedance can be represented by an infinite RC transmission line:[46] one of the conductors has a uniform resistance R_{tl} per unit length, and the other has a zero resistance. Between the two conductors, there is a uniform capacitance C_{tl} per unit length.

The classical study of diffusion impedance[47] as a function of thickness of the diffusion layer shows that the Warburg impedance is a limiting case corresponding to an infinite thickness,[48] while the Drossbach-Schultz impedance corresponds to a finite thickness of the diffusion layer:[49]

Warburg impedance:

$$Z_w = K\,\omega^{-1/2}(i-j). \qquad \text{(A2.1)}$$

Drossbach-Schultz impedance:

$$Z_d = K\,\omega^{-1/2}(i-j)\,\tanh\sqrt{j\omega d^2/D}, \qquad \text{(A2.2)}$$

where K is the Warburg constant, d is the thickness of the diffusion layer, and D is the diffusion coefficient of the species.
(It is easy to verify that $Z_d \rightarrow Z_w$ when $d \rightarrow \infty$ for which $\tanh\sqrt{j\omega d^2/D} \rightarrow 1$.)

The Drossbach-Schultz impedance Z_d can be written in another useful form: [49]

$$Z_d = \frac{R_d \tanh\sqrt{j\omega d^2/D}}{\sqrt{j\omega d^2/D}} \qquad \text{(A2.3)}$$

where R_d, the diffusion resistance, is the limiting value of the real component of the impedance knowing that at the zero frequency limit,

$$\frac{\tanh\sqrt{j\omega d^2/D}}{\sqrt{j\omega d^2/D}} \longrightarrow 1$$

Such a diffusion resistance is defined as a function of the parameters of the diffusion process:

$$R_d = \frac{RTd}{\sqrt{2}\, AF^2 C_o D}, \qquad \text{(A2.4)}$$

knowing that the Warburg constant K is given by:

$$K = \frac{RT}{\sqrt{2}\, AF^2 C_o D^{1/2}} \qquad \text{(A2.5)}$$

The analysis of the ratio $\dfrac{\tanh\sqrt{j\omega d^2/D}}{\sqrt{j\omega d^2/D}}$

as a function of the radial frequency shows that this ratio becomes a maximum for $\omega^* \approx 2.5\ D/d^2$. The corresponding frequency

$$f^* \approx 0.4\ D/d^2 \tag{A2.6}$$

can be called the Drossbach-Schultz frequency.

From a more general point of view, the diffusion impedance[47] can be developed in order to define the real and imaginary components:

$$Z_d = Z_d' - jZ_d''.$$

With $\Delta = d(2/D)^{1/2}$,

$$Z_d' = K\,\omega^{-1/2}\left\{\frac{\sinh(\Delta\omega^{1/2}) + \sin(\Delta\omega^{1/2})}{\cosh(\Delta\omega^{1/2}) + \cos(\Delta\omega^{1/2})}\right\} \tag{A2.7a}$$

$$Z_d'' = K\,\omega^{-1/2}\left\{\frac{\sinh(\Delta\omega^{1/2}) - \sin(\Delta\omega^{1/2})}{\cosh(\Delta\omega^{1/2}) + \cos(\Delta\omega^{1/2})}\right\} \tag{A2.7b}$$

The characteristic shape of the diffusion impedance is shown in Fig. A2-1. Two main frequency domains can be distinguished: (1) For relatively high frequencies, the impedance diagram is a straight line with a 45^o slope versus the real and imaginary axes. This part of the

impedance diagram corresponds to the Warburg impedance. The Warburg constant K can be determined from the slope of the Randles plot, which is given by the modulus of the impedance as a function of the inverse of the square root of the radial frequency. (2) For relatively low frequencies, the impedance diagram shows a characteristic loop. The maximum value of the real component of the impedance is equal to R_d, and the maximum value of the imaginary component is obtained for the Drossbach-Schultz frequency f^*.

APPENDIX III: Analysis of the SEI Model.

The basic equation of the classical theory of ionic conduction in solids[30] allows one to determine the electrode kinetics of solid electrolytes:

$$i = 4q\nu_+ Fan \exp(-W/RT) \sinh(aqFE/RT), \qquad (A3.1)$$

where R, T, and F have their classical meanings in electrochemistry, i is the current density, q is the charge of the mobile ion, ν_+ is the vibration frequency, W is the barrier energy, a is the half-jump distance, and E is the electric-field strength. At high electric fields, the equation can be simplified to a Tafel-like equation:

$$i + i_o \exp(BE) = i_o \exp(B\eta/Y), \qquad (A3.2)$$

where i_o is the zero-field ionic current density, B is the field coefficient, η is the potential difference across the solid, and Y is the thickness. Thus, the bulk resistance R_b of the solid electrolyte is expressed as:

$$1/R_b = (di/d\eta) = [i_o B/Y] \exp(B\eta/Y). \qquad (A3.3)$$

When the potential difference approaches zero, Ohm's law applies, and the bulk resistance per unit surface area is:

$$R_b = (1/i_o\ B)Y = (1/\sigma)Y,$$

where σ is the specific conductivity.

A solid electrolyte is usually represented by a simple equivalent circuit.[27,28] As shown in Fig. A3-1, the bulk resistance R_b, which represents the conductive properties of the solid electrolyte, is placed in parallel with the geometric capacitance C_g, which represents its dielectric properties. The corresponding impedance plot, which is caused by the coupling of the geometric capacitance and bulk resistance, is represented by a semicircle in the complex plane over the whole frequency range. The radial frequency ω^* at the maximum of the imaginary component of the bulk impedance is given by:

$$R_b C_g \omega^* = 1 \qquad (A3.5)$$

and permits the determination of the value of the geometric capacitance for any value of the bulk resistance.

The equivalent electrical circuit of the passivated lithium electrode for the SEI Model is shown in Fig. A3-2b. The impedance of the solid electrolyte is placed in series with the solution resistance R_Ω. The impedance diagram related to the SEI electrode is represented as shown in Fig. A3-2c. Under these conditions, the experimental diagram can be analyzed easily by considering a planar system for which C_g and R_b are given by the equations of the parallel-plate capacitor and

cylindrical resistor per unit surface area:

$$C_g = \varepsilon_r \varepsilon_o / Y \qquad \text{(A3.6a)}$$

$$R_b = Y/\sigma \qquad \text{(A3.6b)}$$

where ε_r is the dielectric constant and σ is the conductivity of the solid electrolyte. Consequently, the measurement of C_g and R_b leads to the evaluation of the layer thickness Y for a known relative permittivity ε_r or conductivity σ of the solid electrolyte.

APPENDIX IV; ANALYSIS OF THE PIM MODEL.

The equivalent circuit and corresponding impedance diagram of an electrode free of any passivating layer in the presence of a liquid electrolyte are given by the Randles Interface Model, as shown in Fig. A4.1. (See appendices I and II) For an electrode covered by a porous insulating material, the equivalent circuit and impedance diagram remain the same, but with a reduced active area of the electrode surface. This simple behavior is taken into account in the study of the electrode kinetics occurring on a lithium electrode covered by a porous polymeric membrane.

As shown in Fig. A4.2, the electrode surface in contact with the insulating membrane defines a passive area Θ. Its properties can be represented by a simple equivalent circuit (R_m and C_m). The pores of the polymeric membrane define an active area $(1-\Theta)$ on which the electrochemical processes can be represented by the Randles circuit (R_{ct} C_{dl},Z_d). Thus, when the impedance of the layer/solution interface can be assumed to be negligible, the equivalent circuit and corresponding impedance diagram related to the PIM layer are shown in Fig. A4-2. The semicircle in the high- and intermediate-frequency range is related to the charge-transfer process on the base of the pores, while the characteristic loop in the low-frequency range is determined by the diffusion process through the pores of the surface layer.

The classical study of the electrode kinetics gives the basic equation:

$$i = i_o \left\{ \frac{c}{C_o} \exp\left[\frac{\alpha F\eta}{RT}\right] - \exp\left[\frac{-(1-\alpha)}{RT} F\eta\right] \right\} \qquad (A4.1)$$

where i and i_o are the current and exchange current densities, respectively, η is the overpotential, and α is the charge-transfer coefficient. The concentrations c and c_o are the concentrations at the electrode/layer and layer/electrolyte interfaces, respectively. The symbols R, T, and F have their usual electrochemical meanings.

For a highly concentrated electrolyte of anions and cations of the same charge (unity), the effects of the migration and diffusion processes are equal. Thus, the current density can be defined by the Nernst hypothesis of a linear concentration gradient:

$$i = 2D\ F\ (c - c_o)/d. \qquad \text{(A4.2)}$$

The charge-transfer resistance R_{ct} is given by the derivative of the overpotential versus the current for a concentration c considered as a constant, while the polarization resistance R_p is given by the same derivative when the concentration is considered as a function of the overpotential.

$$R_{ct} = \left(\frac{\partial i}{\partial \eta}\right)^{-1}_{c=ct} \qquad \text{(A4.3)}$$

$$R_p = \left(\frac{\partial i}{\partial \eta}\right)^{-1}_{c=f(\eta)} \qquad \text{(4.4)}$$

The diffusion resistance Rd defined by

$$R_d = R_p - R_{ct} \qquad \text{(A4.5)}$$

is expressed at the open-circuit potential as follows:

$$R_d = \frac{RT_d}{2F^2 C_o D} \qquad (A4.6)$$

With these equations in mind, the analysis of the impedance data gives the necessary and sufficient equations to determine the main parameters of the surface layer: the ratio $(1-\Theta)$, its thickness d, and the ionic-diffusion coefficient D.

The ratio $(1-\Theta)$ can be evaluated by considering the value of the interfacial capacitance C_i, which is determined from the study of the charge-transfer semicircle. Assuming that the resistance R_m is much greater than the charge-transfer resistance R_{ct}, the effect of R_m must be negligible in the intermediate-frequency range. Thus, the charge-transfer semicircle is characterized by the radial frequency ω_o:

$$R_{tg} \; C_i \; \omega^o = 1 \qquad (A4.7)$$

where R_{tg} is the charge-transfer resistance related to the geometric area of the electrode surface. The interfacial capacitance C_i is defined by the parallel coupling of the capacitance C_m on the passivated area and the double-layer capacitance C_{dl} on the active area:

$$C_i = C_{dl} \; (1-\Theta) + C_m \Theta \qquad (A4.8)$$

Because the capacitance of a polymeric membrane is very low, the

relative value of $C_m \Theta$ can be considered as negligible compared to the relative value of C_{dl} $(1-\Theta)$, the measurement of C_i leads to an evaluation of the ratio $(1-\Theta)$ according to:

$$(1-\Theta) \approx C_i/C_{dl}, \tag{A4.9}$$

when a standard value of the double-layer capacitance C_{dl} is known for the electrolyte being studied.

The thickness and diffusion-coefficient results can be obtained by considering the parameters of the diffusion impedance. (See Appendix II). The diffusion process is characterized by the Warburg constant K or the Drossbach-Schultz frequency f^*, which are given by:

$$K = \frac{RT}{2\sqrt{2}\, F^2 C_o \sqrt{D}} \tag{A4.10}$$

$$f^* \approx 0.4\, D/d^2, \tag{A4.11}$$

and by the diffusion resistance related to the active area:

$$R_d = R_{dg}(1-\Theta) \tag{A4.12}$$

where R_{dg} is the diffusion resistance defined by the geometric area of the electrode.

Combining equations (A4.10) and (A4.12), the parameters d and D can be calculated:

$$d = \frac{RT}{C_o F^2} \frac{R_{dg}}{4K_g^2(1-\Theta)}, \tag{A4.13}$$

$$D = \frac{R^2T^2}{C_o^2F^2\ 8\ K_g^2(1-\Theta)^2}, \tag{A4.14}$$

where K_g is the Warburg constant defined by the geometric area of the electrode.

Combining equations (A4.11) and (A4.12), the parameters d and D are calculated as follows:

$$d \approx 0.2\ \frac{RT}{C_o F^2 f^*\ R_{dg}(1-\Theta)}, \tag{A4.15}$$

$$D \approx 0.1\ \frac{R^2T^2}{C_o^2F^4f^*\ R_{dg}^2(1-\Theta)^2}. \tag{A4.16}$$

APPENDIX V: Analysis of the PEI Model

Polymers containing heteroatoms can form conductive complexes with low-lattice-energy alkali salts.[36] These new materials have been recently called polymer electrolytes.[37-39] The equivalent circuit and corresponding impedance diagram for a polymer electrolyte are shown in Fig. A5-1. The bulk resistance R_b and the geometric capacitance C_g are related to the conduction process. The charge-transfer resistance R_{ct} and the double-layer capacitance C_{dl} are coupled for the charge-transfer process, and the Warburg impedance Z_w (or diffusion impedance Z_d) is characteristic of the diffusion process. The corresponding impedance diagram shows two semicircles and a straight line (or a characteristic loop) in the complex plane. The R_b/C_g coupling is responsible for the semicircle in the high-frequency range, and the R_{ct}/C_{dl} coupling is responsible for the semicircle in the intermediate-frequency range, while Z_w is responsible for the straight line (or Z_d for the characteristic loop) in the low-frequency range.

In a polymer electrolyte as well as in other electrolytes, the diffusion resistance R_d is related to the conduction resistance R_b, as demonstrated by MacDonald,[40] according to the following equation:

$$R_d = R_b\ (\mu^-/\mu^+), \qquad \text{(A5.1)}$$

where μ^+ is the mobility of the cation and μ^- is the mobility of the anion, respectively.

For a mono-monovalent electrolyte, the transference number of the cation t^+ is given by:

$$t^+ = \frac{\mu^+}{\mu^+ + \mu^-}, \qquad \text{(A5.2)}$$

and the diffusion resistance can be given as a function of the transference number of the cation:

$$R_d = R_b \frac{(1-t^+)}{t^+}. \qquad \text{(A5.3)}$$

The equivalent circuit for the PEI model is shown in Fig. A5-2. The impedance of the polymer electrolyte is placed in series with the solution resistance. Under these conditions, the experimental diagram can be analyzed by considering a planar system. The analysis of the conduction semicircle in the high-frequency range leads to the determination of the layer thickness X for a known permittivity or conductivity by using the equations of the resistance and capacitance per unit area:

$$C_g = \varepsilon_r \varepsilon_0 / X \quad \text{and} \quad R_b = X/\sigma. \qquad \text{(A5.4)}$$

The analysis of the diffusion loop in the low-frequency range leads to the determination of the diffusion coefficient of the lithium ion according to the value of the Warburg constant K or the Drossbach-Schultz

frequency f^*,

$$K = \frac{RT}{\sqrt{2}\, f^2 C_o D^{1/2}} \text{ and } f^* \approx 0.4\ D/X^2 \qquad \text{(A5.5)}$$

The conductivity deduced from the diffusion coefficient by the Nernst-Einstein equation must be of the same order as the conductivity deduced from the conduction resistance.

APPENDIX VI: Analysis of the CSL Model

The equivalent circuit of a lithium electrode covered by two sublayers having the properties of different electrolytes is given in Fig. A6-1a. The two circuits R_1C_1 and R_2C_2 can be identified when the dielectric and resistive properties of these sublayers are considered separately (Fig. A6-1b). When these sublayers cannot be simply separated, the equivalent circuit can be considered as a single R_1C_1 circuit taking into account the integral values of the bulk resistance and geometric capacitance of the surface layer (Fig. A-6-1b'). Under these conditions, the resistive and dielectric properties of the surface layer are considered as functions of the distance x from its top to its bottom, as shown in Fig. A6-2a. Two main regions can be defined along L, which is the total thickness of the surface layer: d is the minimum thickness of the first sublayer, and $(L-d)$ is the maximum thickness of the second sublayer. In an attempt to understand the properties of the surface layer, an inverse function of second order f(x) has been considered for $\rho(x)$, the resistivity, and $1/\varepsilon(x)$, the inverse of the permittivity. (See Footnote 1):

$$f(x) = \frac{f_2}{1-(x/L)^2}\,, \qquad 0 \leqslant x \leqslant L-d \tag{A6-1}$$

and with

$$L/2d = f_1/f_2\,,$$

Footnote 1

$$f(o) = f_2; \qquad f(L-d) = f_1 = \frac{f_2}{1-(\frac{L-d}{L})^2} \approx \frac{f_2 L^2}{2Ld-d^2}$$

$$\text{if } d \ll L \quad \text{then} \quad f_1 \approx \frac{f_2 L}{2d}$$

where f_2 and f_1 are the limiting values of each parameter for the solid electrolytes, respectively.

Thus, the equations of the integral value of the resistance R and the inverse of the capacitance 1/C per unit surface area can be calculated. (See Footnote 2)

$$R = \int_0^{L-d} \frac{\rho_2}{1 - (x/L)^2}\, dx + \int_{L-d}^{L} \rho_1\, dx \qquad \text{(A6-2a)}$$

with $L/2d = \rho 1/\rho_2$;

$$R = (\rho_2\, L/2)\, \log(2L/d) + \rho_1\, d = \rho_2\, L/2[1 + \log(4\rho_1/\rho_2)]; \qquad \text{(A6.2b)}$$

and

$$1/C = \int_0^{L-d} \frac{(1/\varepsilon_2)}{1 - (x/L)^2}\, dx + \int_{L-d}^{L} (1/\varepsilon_1).dx \qquad \text{(A6.3a)}$$

with $L/2d = \varepsilon_2/\varepsilon_1$

$$1/C = (L/2\varepsilon_2)\, \log(2L/d) + d/\varepsilon_1 = (L/2\varepsilon_2)\, [1 + \log(4\varepsilon_2/\varepsilon_1)] \qquad \text{(A6.3b)}$$

Footnote 2

$$\int \frac{dx}{a^2 - b^2x^2} = \frac{1}{2ab} \log \frac{a+bx}{a-bx}$$

with a=1 , b=1/L.

These equations deduced from the CSL model can be easily compared to those obtained from the SEI model:

$$R = \rho_1 \, Y, \tag{A6.4a}$$

$$1/C = Y/\varepsilon_1 \tag{A6.4b}$$

where Y is the apparent thickness of the surface layer considered as a simple solid electrolyte. It is possible to evaluate the ratio Y/L as a function of the ratio f_2/f_1 for the same measured capacitance and resistance:

$$Y/L = (\varepsilon_1/2\varepsilon_2) \, [1 + \log(4\varepsilon_2/\varepsilon_1)] \tag{A6.5a}$$

or

$$Y/L = (\rho_2/2\rho_1) \, [1 + \log(4\rho_1/\rho_2)]. \tag{A6.5b}$$

Under these assumptions, Fig. A6-2b shows the evolution of L/Y as a function of the ratio f_2/f_1. For example, the total thickness L is nearly 4.25 times larger than the apparent thickness Y for the case of a given ratio f_2/f_1 equal to 10. Besides, the thickness d of the first sublayer is nearly 0.05 times lower than the total thickness.

APPENDIX VII: Cole-Cole and Bode Plots

It is common practice in the electrochemical literature to use the Cole-Cole plot[50] (often called the Nyquist plot). In this plot, the impedance is presented in the complex plane, the imaginary component (Z") plotted versus the real component (Z') with the sinusoidal frequency as a parameter. The Bode plot is a useful alternative for the presentation of the impedance data.[51] But in this case, two curves are required that are not completely independent: log(/Z/) versus log(f), and Θ versus log(f), where /Z/ is the modulus of the impedance, Θ is the phase angle of the impedance, and f is the excitation frequency.

The following section discusses the respective advantages and disadvantages of the Cole-Cole and Bode plots for better understanding the impedance data obtained when studying RC equivalent circuits. An illustration of the principles involved has been given recently by Cahan and Chen.[52]

An electrochemical system can be represented by the simple equivalent circuit, as shown in Fig. A7-1a. A Cole-Cole plot gives a semicircle over the whole frequency range, as shown in Fig. A7-1b. The presence of R_o contributes to the real portion of the impedance at very high frequencies. The frequency of the top of the semicircle corresponds to the R_1/C_1 time constant. This Cole-Cole plot has the advantage of giving an immediate and simple shape to the electrode impedance diagrams. A change of R_1 leads to another semicircle for the same C_1. With the same R_1, the frequency points move around the arc for a change of C_1.

One of the disadvantages of the Cole-Cole plot is that the spacing of frequencies along the whole curve is highly nonlinear.

For the same circuit, as shown in Figs. A7-1c/d, the Bode plot consists of different lines of characteristic slopes for different ranges of log(f). At very high frequencies, $\log(/Z/)$ is a line of slope zero and corresponds to R_Ω, the electrolyte resistance. At high frequencies, $\log(/Z/)$ is a straight line with a slope zero which corresponds to the resistance R_0. At intermediate frequencies, the straight line has a slope of (-1), which corresponds to the impedance of C_1. At low frequencies, the line with slope zero corresponds to (R_0+R_1). The study of the phase angle (Θ) versus log(f) shows a maximum related to the coupling R_1/C_1. The Bode plot is a useful alternative to the Cole-Cole plot for avoiding the longer measurement times associated with the low-frequency resistance determination, because the $\log(/Z/)$ versus log(f) plot sometimes allows a more effective extrapolation of data from higher frequencies. In general, the Bode plot provides a clearer description of the frequency-dependent behavior of the electrochemical system than does the Cole-Cole plot, where the frequency values are implicit. The Bode format also has the advantage of giving an immediate view of the evolution of the individual components of the equivalent circuit. For example, a change of R_0 or R_1 causes a shift of the lines of slope zero, while a change of C_1 causes a shift of the line of slope (-1).

In some electrochemical systems, there is more than one rate-determining step and consequently more than one time constant. The ac-impedance experiment can often distinguish among these steps and

provide information about their respective relaxation times. An illustration of the principles involved can be obtained by considering the electrochemical equivalent circuit in Fig. A7.2a. While it is true that more than one equivalent circuit can represent a given set of measureable impedance-frequency relations, it is possible to uniquely identify all of the circuit components when the time constants are very different. For the Cole-Cole plot, two semicircles can be observed for the simple determinations of the respective couplings R_1/C_1 and R_2/C_2, as shown in Fig. A7.2b. In the case of the Bode plot, as shown in Figs. A7-2c/d, the lines of slope zero correspond to the resistances R_o, $(R_o + R_1)$, and $(R_o + R_1 + R_2)$, while the lines of slope (-1) correspond to the impedance of C_1 and C_2.

APPENDIX VIII: Case of Depressed Semicircles

The observed complex impedance spectra for an electrochemical system often show semicircular arcs whose centers lie below the real axis. This effect can be attributed to the fact that the equivalent circuit cannot be reduced to a simple resistance/capacitance network. In fact, the equivalent circuit must be modeled as a series of numerous RC circuits with different time constants (each R and C are considered to be frequency independent parameters).

A depressed semicircle in the complex plane can be described adequately by the Cole-Cole formula for an RC equivalent circuit.[50,57] The classic equation of the impedance:

$$\frac{1}{Z(\omega)} = \frac{1}{R} + jC\omega, \qquad \text{(A8.1)}$$

is reduced to the following equation:

$$Z(\omega) = \frac{R}{1 + (jRC\omega)^{(1-\alpha)}} \qquad \text{(A8.2)}$$

in which α is the depression parameter whose value is between 0 and 1/2. (The value 0 corresponds to a semicircle with its center on the real axis.)

For a multistep electrochemical system, the total impedance, which corresponds to an equivalent circuit consisting of several RC circuits in series with the solution resistance, For example, a two-step system can be defined by the following equation:

$$Z(\omega) = R_o + \frac{R_1}{1 + (j\frac{\omega}{\omega_1})^{(1-\alpha_1)}} + \frac{R_2}{1 + (j\frac{\omega}{\omega_2})^{(1-\alpha_2)}} \qquad (A8.3)$$

where α_1 and α_2 are the depression parameters of the different semicircles, and ω_1 and ω_2 are the time constants of the R_1C_1 and R_2C_2 circuits ($R_1C_1\omega_1 = 1$ and $R_2C_2\omega_2 = 1$).

Figure A8.1 gives an example of the influence of the depression parameter α on the Cole-Cole and Bode plots corresponding to an equivalent circuit made of two RC circuits placed in series with a resistance. The example is given for the same depression paramater (α = 0.2) on both plots in order to show in the Cole-Cole plot that the center of each semicircle lies below the real axis with an angle equal to $\alpha\pi/2$. Besides, the Bode plot of the same equivalent circuit easily shows that the interpretation of the impedance data can be difficult for large depression parameters.

APPENDIX IX: Case of Overlapping Time Constants

Significant distortions in the shape of the impedance spectrum occur when the time constants differ by less than a factor of 100, as demonstrated by Kleitz and Kennedy.[53] An illustration of the distortion of the Cole-Cole and Bode plots is given in Fig. A9-1 for an equivalent circuit made of two RC networks placed in series. When the time constants are extremely different (ω_1/ω_2 = 333), the Cole-Cole plot shows two semicircles, while the Bode plot shows two straight lines of slope (-1). When the time constants are of the same order (ω_1/ω_2 = 10), the Cole-Cole plot is a depressed semicircle (See Appendix V), but the Bode plot continues to demonstrate the existence of two time constants.

In such cases, it has proved to be very difficult to obtain accurate circuit parameters using customary graphical methods. Sophisticated methods are necessary to extract meaningful results from the impedance data. The Kleitz-Kennedy procedure is a geometrical curve-fitting ofthe impedance spectrum to a Cole-Cole-type function and/or a Warburg-type impedance. Based on an analytical model, MacDonald, et al.[54] have developed a nonlinear least-squares fitting technique that is able to simultaneously fit the real and imaginary parts of impedance data. MacDonald, et al.[55,56] have also discussed up-to-date versions of their nonlinear complex least-squares fitting routine, based in part on the Marquardt algorithm. More recently Tsai and Whithmore[57] have described a procedure that combines the Kleitz-Kennedy method with the nonlinear least-squares fitting technique of Marquardt to accurately evaluate the circuit parameters.

APPENDIX X: Physical properties of propylene carbonate and of the molar solution of lithium perchlorate in propylene carbonate.[15]

Structure

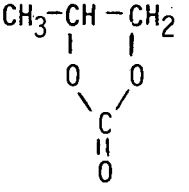

Molecular Weight	102.09
Melting Point, ^{o}C	-49.2
Boiling Point at 760 mm Hg, ^{o}C	241.7
Vapor Pressure at $25^{o}C$, mm Hg	0.069
Density at $25^{o}C$, gm/cm^3	1.203
Viscosity at $25^{o}C$, millipoise	24.8
Dielectric Constant at $25^{o}C$	65.1
Specific Conductivity at $25^{o}C$, $\Omega^{-1}cm^{-1}$	1.2 to 8.6×10^{-7}
Conductivity of the molar solution of $LiClO_4$, at $25^{o}C$, $\Omega^{-1}\,cm^{-1}$	
1N	5.6×10^{-3}
1.1N	4.97×10^{-3}
0.9N	5.2×10^{-3}
Transference number of the Li^+ ion	0.4
Diffusion coefficient of the Li^+ ion, $cm^2\,sec^{-1}$	3.5×10^{-6}

APPENDIX XI: Thermodynamic Instability of Propylene Carbonate with Lithium

The thermodynamic instability of this system can be evaluated by means of the free energy of the reaction corresponding to the most likely decomposition reactions of propylene carbonate (PC) and lithium. As previously shown by H.H. Law,[60] the Gibbs free energy of formation of propylene carbonate can be estimated by using the method of van Krevelen and Chermin.[61] (See Table and Note below.) This energy was estimated to be -59 kcal/mole at 300°K.

The classical reaction involving Li and PC is the following:

$$2\ Li + PC \rightarrow Li_2CO_3 + C_3H_6. \qquad (a)$$

Since the free energies of formation of Li_2CO_3 and C_3H_6 are -270.6 and 15 kcal/mole, respectively,[62] the change in the free energy of the reaction is -196.6 kcal/mole.

Another decomposition reaction of PC in presence of Li is the following:

$$Li + PC \rightarrow CO_2 + (C_3H_6O). \qquad (b)$$

According to the method of van Krevelan and Chermin,[61] the free energy of formation of the repeat unit of polypropylene oxide can be estimated to be -12.5 kcal/mole. Since the free energy of formation of CO_2 is -94.3 kcal/mole,[62] the change in the free energy of the last reaction is -47.8 kcal/mole.

Therefore, one can expect that propylene carbonate is more likely decomposed according to the reaction (a) than to the reaction (b). The reaction (b) must be catalyzed to be comparable to the reaction (a). In any case, it appears evident that PC is thermodynamically unstable in presence of Li even if the method of estimating the free energy of propylene carbonate and polypropylene oxide is not very accurate.

Table 1. Estimation of Gibbs Free Energy of Formation of Different Compound Groups.[62]

Compound Group	A	B x 10^2
H_3C-	-10.943	2.215
$>CH_2$	- 5.193	2.43
$-CH<$	- 0.705	2.910
$>C=O$	-28.08	0.91
-O-	-15.79	-0.85
correction for the symmetry 5-membered ring	4.275	-2.35

Note:[62]

The Gibbs free energy of a compound can be estimated by the summation of the contributions ΣC of the compound groups:

$$\Delta G = \Sigma C + \emptyset$$

in which ∅ represents the correction for the symmetry of the compound. The group contributions are represented as a linear function of the temperature:

$$C = A + B.T$$

In comparison to the expression $\Delta G = \Delta H - T.\Delta S$, it follows that the term A has the dimension of enthalpy of formation and the term B has the dimension of an entropy of formation.

APPENDIX XII: Influence of Impurities on the Decomposition of Propylene Carbonate

The presence of impurities adds another dimension to the stability problem of propylene carbonate-based electrolytes. The role of water and propylene glycol in propylene carbonate electrochemistry is not well understood.[58-60] Alkali metals such as lithium are known to react spontaneously with water and propylene glycol:

$$Li + H_2O \rightarrow LiOH + 1/2\ H_2$$

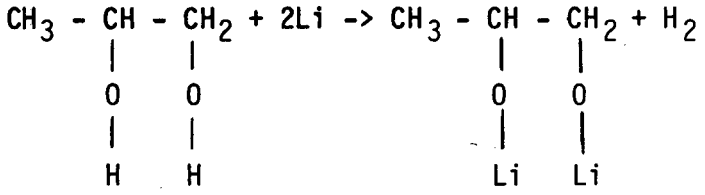

The electrochemical behavior of lithium should be affected by the presence of these compounds. Furthermore, the decomposition of PC may possibly be catalyzed by these impurities.

Gosse and Denate[63] found that hydroxide ions resulting from water reduction reacted with PC to form bicarbonate ions and propylene glycol:

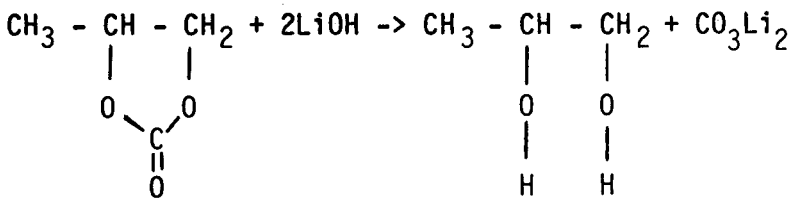

On the other hand, the presence of an acid medium, for example HCl, due to the hydrolysis or decomposition of the solute, can also catalyze another decomposition reaction of PC, as shown by Silvester and Tobias[64] for PC/LiAlCl electrolytes:

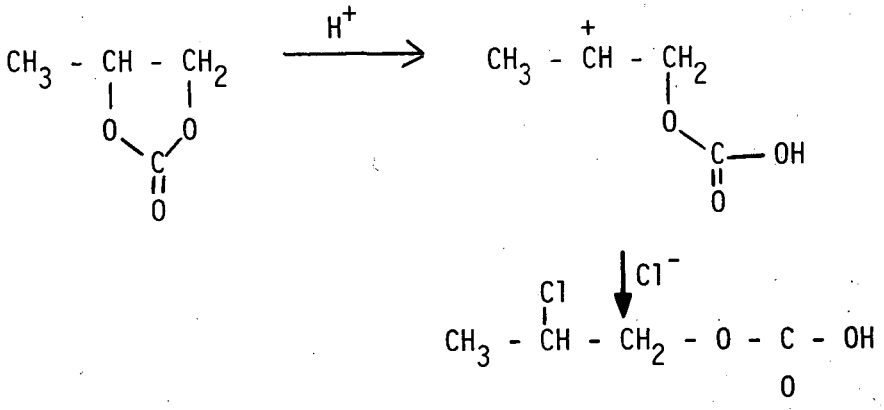

This last compound can be transformed into other compounds such as:

(1)

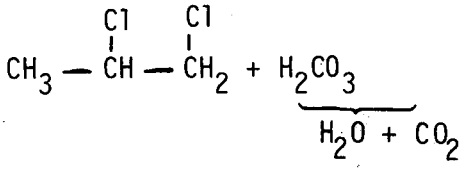

(2)

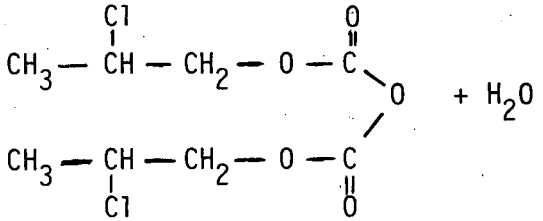

(3)

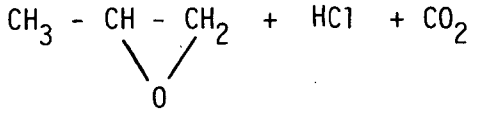

APPENDIX XIII: Properties of Selected Solid and Polymer Electrolytes.

Solid electrolytes.

	Li_2O	Li_2CO_3
relative permittivity	8.9	4.9
conductivity, $\Omega^{-1}cm^{-1}$		10^{-9}

Polymer electrolytes.[36,37]

P(PO) = polypropylene oxide. P(PE) = polyethylene oxide.
The subscript between polymer and salt is the oxygen/lithium ratio.

	$P(PO)_8$ $LiClO_4$	$P(PE)_8$ $LiClO_4$
relative permittivity	50	50
conductivity, $\Omega^{-1}cm^{-1}$	9×10^{-6}	3×10^{-4}
transference number of the Li^+ ion	0.5	0.5
diffusion coefficient of the Li^+ ion cm^2/sec	10^{-9}	10^{-9}

(For the analysis of the impedance data, the electrode surface area is 2 cm^2, and the thickness of the polymer electrolyte is 10^{-2}cm.)

APPENDIX XIV: Analysis of the Impedance of the Metal/ Solution Interface

The aim of this analysis is to identify the different terms of the impedance of the metal/surface-layer interface by assuming that the Faradaic current I_F and the charging current of the double-layer capacitance C_{dl} are separated. Hence, in this model, it is assumed that the interface can be represented for small perturbations by a Faradaic impedance Z_F placed in series with the double-layer capacitance.

In the simplest case of the dissolution and deposition of a metal:

$$M^+ + e^- \leftrightharpoons M$$

it is generally assumed that the charge-transfer reaction is quasi-reversible and controlled by mass transport.

The Faradaic current I_F is expressed by the Butler-Volmer equation, which is a function of the electrode potential E and the concentration c of the metal cations. The rate of transfer ν, is related to the Faradaic current I_F as follows:

$$\nu = I_F/F, \qquad [1]$$

where F is the Faraday constant. The concentration c of the metal cations, which diffuse linearly in the direction z toward and from the solution bulk, is ruled by the following equation (known as the second Fick's law):

$$\frac{\partial c}{\partial t} = D \frac{\partial^2 c}{\partial z^2} , \qquad [2]$$

where D is the diffusion coefficient of the metal ions. The rate of transfer ν on the electrode surface is determined by the mass and charge balance (known as the first Fick' law):

$$D \frac{\partial c}{\partial z} = \nu \qquad [3]$$

Using a Taylor-series expansion for a perturbation in the potential ΔE, the perturbation of the rate of transfer is given by:

$$\Delta\nu = \left(\frac{\partial \nu}{\partial E}\right)_c \Delta E + \left(\frac{\partial \nu}{\partial c}\right)_E \Delta c. \qquad [4]$$

The resulting perturbation of concentration Δc as a function of $\Delta\nu$ can be deduced from Eqs. 2 and 3 for the cases of infinite thickness (Eq. 5a) and finite thickness d (Eq. 5b) of the diffusion layer (see Footnote):

$$\Delta c = \left(-1/\sqrt{j\omega D}\right)\Delta\nu = -\lambda_w \Delta\nu, \qquad [5a]$$

$$\Delta c = \left(-\tanh d\sqrt{j\omega/D} \,/\, \sqrt{j\omega D}\right)\Delta\nu = -\lambda_d \Delta\nu, \qquad [5b]$$

where ω is the radial frequency of the sinusoidal perturbation. Thus Eq. 5 can be rewritten as:

$$\Delta\nu = \left(\frac{\partial \nu}{\partial E}\right)_c \Delta E - \left(\frac{\partial \nu}{\partial c}\right)_E \lambda \Delta\nu \qquad [6]$$

where $\lambda=\lambda_w$ or $\lambda=\lambda_d$, according to the thickness of the diffusion layer.

The Faradaic admittance Y_F of the reaction is defined by

$$Y_F = \frac{\Delta I_F}{\Delta E} = F \frac{\Delta \nu}{\Delta E} . \qquad [7]$$

According to Eq. 7, one obtains

$$Y_F = F \left(\frac{\partial \nu}{\partial E}\right)_c - \lambda \mu Y_F, \qquad [8]$$

where

$$\left(\frac{\partial \nu}{\partial c}\right)_E = \mu; \qquad [9]$$

and a more simple equation can be developed:

$$Y_F = \left(\frac{1}{1+\lambda\mu}\right) F \left(\frac{\partial \nu}{\partial E}\right)_c . \qquad [10]$$

The Faradaic impedance $Z_F = 1/Y_F$ is given by

$$Z_F = R_{ct} (1+\lambda\mu), \qquad [11]$$

where $R_{ct} = [F \left(\frac{\partial \nu}{\partial E}\right)_c]^{-1}$ [11a]

which is called the charge-transfer resistance.

The last term of the Faradaic impedance can be defined as a function of the thickness of the diffusion layer, according to Eqs. 5a and 5b. For an infinite thickness,

$$Z_F = R_{ct} + Z_W, \qquad [12]$$

where Z_W is the Warburg impedance ($\lambda = \lambda_W$):

$$Z_W = R_{ct}\left[\frac{\mu}{\sqrt{j\omega D}}\right] \qquad [12a]$$

For a finite thickness d,

$$Z_F = R_{ct} + Z_d, \qquad [13]$$

where Z_d is the Drossbach-Schultz impedance ($\lambda = \lambda_d$):

$$Z_d = R_{ct}\,\mu\,\frac{\tanh\, d\sqrt{j\omega/D}}{\sqrt{j\omega\, D}} \qquad [13a]$$

The total impedance Y of the metal/surface-layer interface determined by considering the double-layer capacitance C_{dl} is given by:

$$Y = Y + j\,\omega\, C_{dl}. \qquad [14]$$

The general shape of the impedance plot in the complex plane consists of

a circle related to the charge-transfer process (R_{ct}/C_{dl} coupling) in the high-frequency range, and a straight line (Z_w) or a characteristic loop (Z_d) related to the diffusion process in the low-frequency range. (See Appendices I and II)

Footnote: Analysis of the diffusion impedance.

The resulting concentration perturbation:

$$\Delta c(z,t) = \Delta c(z) \exp(j\omega t)$$

written as the product of functions of time and distance, can be obtained from the general solution of Eq. 2 where

$$\Delta c(z) = M \exp(+z\sqrt{j\omega/D}) + N \exp(-z\sqrt{j\omega/D}) .$$

The integration constants M and N can be calculated from the boundary conditions, using the following two hypotheses about the thickness of the diffusion layer:

i) Diffusion layer of infinite thickness (Warburg impedance).

In this case M = 0 and hence:

$$\Delta c(z) = N \exp(-z\sqrt{j\omega/D})$$

by Eq. 3

$$\Delta v = [-D\sqrt{j\omega/D}\,]\, N \exp(-z\sqrt{j\omega/D})$$

the equation becomes:

$$\Delta c = \left(-1/\sqrt{j\omega D}\right)\Delta v = \lambda_w \Delta v.$$

ii) Diffusion layer of finite thickness (Drossbach-Schultz impedance).

By considering a thickness d for the diffusion layer, the boundary condition at z=d implies that the resulting concentration perturbation $\Delta c(d) = 0$. It becomes:

$$M = -N \exp(-2d\sqrt{j\omega/D}).$$

The following equation of $\Delta c(z)$ can be obtained:

$$\begin{aligned}\Delta c &= -N \exp(-2d\sqrt{j\omega/D}\,)\exp(z\sqrt{j\omega/D}) + N\exp(-z\sqrt{j\omega/D}) \\ &= -2\,N\exp(-d\sqrt{j\omega/D})\sinh[(z-d)\sqrt{j\omega/D}].\end{aligned}$$

Thus, by Eq. 3,

$$\Delta\nu = +2N\ D\sqrt{j\omega/D}\ \exp(-d\sqrt{j\omega/D})\ \cosh[(z-d)\ \sqrt{j\omega/D}].$$

and hence on the electrode surface (z = 0), the equation becomes:

$$\Delta c = -(1/\sqrt{j\omega D})\ \tanh[d\sqrt{j\omega/D}]\ \Delta\nu = \lambda_d \Delta\nu$$

APPENDIX XV: Analysis of the Impedance of the Surface-Layer/Solution Interface.

In this study we assume that the surface layer (at least the sublayer facing the solution) is an ionic and electronic conductor. Nonstoichiometric compounds formed by the reaction of lithium with water in the organic electrolyte (based on Li_2O and/or LiOH) can be considered in this study.

According to Armstrong and Edmondson,[65] in order to deduce the impedance of the surface-layer/ solution interface, we shall consider the model shown in Fig. A15.-1, where we separate the monolayer facing the solution from the rest of the system.

Let ν_1 and ν_2 be the transfer rates of metal cations (Li^+) into the monolayer from the bulk of the surface layer and the bulk of the solution, respectively. Let ν_3 and ν_4 be the transfer rates of anions (e.g. OH^-) into the monolayer from the bulk of the surface layer and from the bulk of the solution, respectively. In the following discussion ν^+ and ν^- are the sums $(\nu_1+\nu_2)$ and $(\nu_3+\nu_4)$, respectively.

If Γ is the excess concentration of cations over anions in the monolayer, then we can write the derivative with time of the concentration perturbation $\Delta\Gamma$ as follows:

$$\frac{\partial\Delta\Gamma}{\partial t} = \Delta\nu^+ - \Delta\nu^- \qquad [14]$$

a) Case of no diffusion of metal cations.

Using a Taylor-series expansion for a potential perturbation ΔE across the layer/solution interface, the transfer-rate perturbation is given by:

$$\Delta\nu_i = \left(\frac{\partial\nu_i}{\partial E}\right)_\Gamma \Delta E + \left(\frac{\partial\nu_i}{\partial\Gamma}\right)_E \Delta\Gamma, \qquad [15]$$

with i = 1, 2, 3 or 4, leading to the determination of $\Delta\nu^+$ amd $\Delta\nu^-$:

$$\Delta\nu^+ = \left(\frac{\partial\nu^+}{\partial E}\right)_\Gamma \Delta E + \left(\frac{\partial\nu^+}{\partial\Gamma}\right)_E \Delta\Gamma, \qquad [16a]$$

$$\Delta\nu^- = \left(\frac{\partial\nu^-}{\partial E}\right)_\Gamma \Delta E + \left(\frac{\partial\nu^-}{\partial\Gamma}\right)_E \Delta\Gamma. \qquad [16b]$$

According to Eqs. 14 and 15, $\Delta\Gamma$ can be defined as a function of ΔE:

$$\Delta\Gamma = \frac{\left\{\left(\frac{\partial\nu^+}{\partial E}\right)_\Gamma - \left(\frac{\partial\nu^-}{\partial E}\right)_\Gamma\right\}\Delta E}{\left[j\omega - \left(\frac{\partial\nu^+}{\partial\Gamma}\right)_E + \left(\frac{\partial\nu^-}{\partial E}\right)_E\right]}. \qquad [17]$$

The Faradaic admittance Y_F is defined by

$$Y_F = F\,(\Delta\nu^+ + \Delta\nu^-)/\Delta E, \qquad [18]$$

$$Y_F = \frac{1}{R_\infty^+} + \frac{1}{R_\infty^-} + \frac{k}{(j\omega+k)}\left(\frac{1}{R_o^+} + \frac{1}{R_o^-}\right) \qquad [19]$$

where

$$k = \left(\frac{\partial \nu^-}{\partial \Gamma}\right)_E - \left(\frac{\partial \nu^+}{\partial \Gamma}\right)_E , \qquad [20]$$

and the resistances are

$$\frac{1}{R_\infty^+} = F\left(\frac{\partial \nu^+}{\partial E}\right)_\Gamma , \qquad [21a]$$

$$\frac{1}{R_\infty^-} = F\left(\frac{\partial \nu^-}{\partial E}\right)_\Gamma , \qquad [22b]$$

$$\frac{1}{R_o^+} = \frac{F}{k}\left[\left(\frac{\partial \nu^-}{\partial E}\right)_\Gamma - \left(\frac{\partial \nu^+}{\partial E}\right)_\Gamma\right]\left(\frac{\partial \nu^+}{\partial \Gamma}\right)_E , \qquad [23a]$$

$$\frac{1}{R_o^-} = \frac{F}{k}\left[\left(\frac{\partial \nu^+}{\partial E}\right)_\Gamma - \left(\frac{\partial \nu^-}{\partial E}\right)_\Gamma\right]\left(\frac{\partial \nu^-}{\partial \Gamma}\right)_E . \qquad [23b]$$

Each resistance R_∞ is a charge-transfer resistance, and each resistance R_o can be called an additional charge-transfer resistance.

According to Armstrong and Henderson,[66] in the general case, the equivalent circuit for Y_F is shown in Fig. A15-2a, where R_∞, R_o, R_p, and C_p are all frequency-independent elements and where

$$\frac{1}{R_\infty} = \frac{1}{R_\infty^+} + \frac{1}{R_\infty^-} , \qquad [24a]$$

$$\frac{1}{R_o} = \frac{1}{R_o^+} + \frac{1}{R_o^-} , \qquad [24b]$$

$$R_p = -R_\infty^2/(R_o+R_\infty), \qquad [25]$$

$$C_p = -R_o\tau/R_\infty^2, \qquad [26]$$

with

$$\tau = 1/k, \qquad [27]$$

which is the relaxation time.

The general shapes that can be generated in the complex plane by $(Y_F + j\omega C_{dl})$ are quite complicated and are considered below.

(i) $R_o >> R_\infty$. Here the circuit reduces to R_∞ in parallel with C_{dl}, which generates a semicircle in the complex plane.

(ii) $R_o << R_\infty$. The resistance is approximately R_o, and two semicircles in the complex plane are of approximately the same diameter.

(iii) R_o comparable to R_∞. Two semicircles are generated in the complex plane, one at high frequencies from R_∞ in parallel with C_{dl} with a radial frequency ω_∞ at the maximum of the semicircle, and the other at low frequencies with a center at $Z' = (R_r/2 + R_\infty)$, $Z'' = 0$, and a radius $R_r/2$ where

$$R_r = \frac{R_o R_\infty}{R_o+R} - R_\infty. \qquad [28]$$

The value of τ can be estimated from the frequency ω_o at the maximum of the low-frequency semicircle, since

$$\omega_o R_p C_p = 1 = \omega_o\left(\frac{R_o}{R_o+R_\infty}\right) \tau, \qquad [29a]$$

$$\text{i.e. } \tau = \frac{1}{\omega_o} \frac{R_o+R_\infty}{R_o}. \qquad [29b]$$

This behavior, when R_o and R_∞ are of the same order for cases when R_o is negative and R_∞ is positive, is shown in Fig. A15-2, where the deviations from two separate semicircles as τ becomes comparable to ω_o are also shown.

As demonstrated in Appendices VIII and IX, serious distortions from the case where the time constants were well separated can occur. Finally, when $\tau \lesssim \omega_\infty$, it becomes impossible to distinguish two semicircles in the complex plane, so that the relaxation is not experimentally observable.

When the anions, for example OH^-, are in equilibrium in the steady state between the solution and the hydroxide, the requirement

$$R_\infty^- = -R_0^- \qquad [30]$$

leads to the following equation of the Faradaic admittance:

$$Y_F = \frac{1}{R_\infty^+} + \left(\frac{k}{j\omega+k}\right) \frac{1}{R_0^+} + \left(\frac{j\omega}{j\omega+k}\right) \frac{1}{R_\infty^-} . \qquad [31]$$

When the surface monolayer has a composition that does not vary with the potential, $\Delta\Gamma/\Delta E$ must tend to zero. This will normally be achieved by a very large value of the parameter k given by Eq. 20. For large k (i.e., $k \gg \omega$) then $k/(j\omega+k) \to 1$, and $j\omega/(j\omega+k) \to j\omega/k$, and Y_F becomes:

$$Y_F = \frac{1}{R_\infty^+} + \frac{1}{R_0^+} + \frac{j\omega}{kR_\infty^-} . \qquad [32]$$

Under these conditions, as shown in Fig. A15-3, the shape of the impedance diagram generated by $\left(Y_F + j\,\omega\,C_{dl}\right)$ is a semicircle resulting from a resistance R_X:

$$R_X = \left[\frac{1}{R_\infty^+} + \frac{1}{R_0^+}\right]^{-1}, \qquad [33]$$

in parallel with a capacitance C_x associated with the double-layer capacitance C_{dl}:

$$C_x = 1/kR_\infty^- . \qquad [34]$$

b) Case of diffusion of metal cations.

When diffusion is important, Eq. 15 must be replaced by:

$$\Delta\nu_i = \left(\frac{\partial\nu_i}{\partial E}\right)_{\Gamma,c_i^+} \Delta E + \left(\frac{\partial\nu_i}{\partial\Gamma}\right)_{E,c_i^+} \Delta\Gamma + \left(\frac{\partial\nu_i}{\partial c_i^+}\right)_{E,\Gamma} \Delta c_i^+ . \qquad [35]$$

For example, this equation applies for the diffusion of a concentration c_i^+ of the metal cations on side i (i = 1, surface-layer side) (i = 2, solution side) of the surface-layer/solution interface. When the diffusion process can be defined by Fick's laws, Eqs. 5a or 5b are sufficient to determine the concentration perturbation Δc_i^+ as a function of the transfer-rate perturbation $\Delta\nu_i$. Thus, Eq. 15 is modified as follows:

$$\Delta\nu_i = \frac{1}{\alpha_i}\left\{\left(\frac{\partial\nu_i}{\partial E}\right)_{\Gamma_i c_i^+} \Delta E + \left(\frac{\partial\nu_i}{\partial\Gamma}\right)_{E_i c_i^+} \Delta\Gamma\right\}, \qquad [36]$$

where $\alpha_i = \left[1 + \lambda_i^+ \ \mu_i^+\right]$, [37]

and $$\mu_i^+ = \left(\frac{\partial\nu_i}{\partial c_i^+}\right)_{E,\Gamma}, \qquad [38]$$

with

$$\lambda_i^+ = \begin{cases} \lambda_{iw}^+ = 1/\sqrt{j\omega D_i} & [39a] \\ \lambda_{id}^+ = \dfrac{\tanh d_i \sqrt{j\omega/D_i}}{\sqrt{j\omega D_i}}, & [39b] \end{cases}$$

When the metal cations diffuse on the surface-layer and solution sides of the surface-layer/solution interface, the Faradaic admittance given by Eq. 32 is modified as follows:

$$Y_F' = \frac{1}{R_\infty^+} + \frac{1}{R_o^+} + \frac{j\omega}{k R_\infty^-}, \qquad [40]$$

where

$$\frac{1}{R_\infty^+} = F\left\{\frac{1}{\alpha_1}\left(\frac{\partial \nu_1}{\partial E}\right)_{\Gamma_1 c_1^+} + \frac{1}{\alpha_2}\left(\frac{\partial \nu_2}{\partial E}\right)_{\Gamma_1 c_2^+}\right\}, \qquad [41a]$$

$$\frac{1}{R_\infty^-} = F\left(\frac{\partial \nu^-}{\partial E}\right)_\Gamma, \qquad [41b]$$

and

$$\frac{1}{R_o^+} = \frac{F}{k}\left\{\left(\frac{\partial \nu^-}{\partial E}\right)_\Gamma - \left[\frac{1}{\alpha_1}\left(\frac{\partial \nu_i}{\partial E}\right)_{\Gamma_1 c_1^+} + \frac{1}{\alpha_2}\left(\frac{\partial \nu_2}{\partial E}\right)_{\Gamma_1 c_2^+}\right]\right\} \times \left[\frac{1}{\alpha_1}\left(\frac{\partial \nu_1}{\partial \Gamma}\right)_{E_1 c_1^+} + \frac{1}{\alpha_2}\left(\frac{\partial \nu_2}{\partial \Gamma}\right)_{E_1 c_2^+}\right], \qquad [42a]$$

$$\frac{1}{R_o^-} = \frac{F}{k}\left\{\left[\frac{1}{\alpha_1}\left(\frac{\partial \nu_1}{\partial E}\right)_{\Gamma_1 c_1^+} + \frac{1}{\alpha_2}\left(\frac{\partial \nu_2}{\partial E}\right)_{\Gamma_1 c_2^+}\right] - \left(\frac{\partial \nu^-}{\partial E}\right)_\Gamma\right\}\left(\frac{\partial \nu^-}{\partial \Gamma}\right)_E, \qquad [42b]$$

$$k = \left(\frac{\partial \nu^-}{\partial \Gamma}\right)_E - \left\{\frac{1}{\alpha_1}\left(\frac{\partial \nu_1}{\partial \Gamma}\right)_{E_1 c_1^+} + \frac{1}{\alpha_2}\left(\frac{\partial \nu_2}{\partial \Gamma}\right)_{E_1 c_2^+}\right\}. \qquad [43]$$

It is immediately apparent that Y_F' cannot be written as a simple function of Y_F by adding Warburg or Drossbach-Schultz impedances. In general, the complicated equation of the Faradaic admittance does not allow one to determine a simple equation of the Faradaic impedance. Thus the shape of the impedance plot in the complex plane, which depends on the specific values of a large number of parameters, cannot be simply defined.

FIGURE CAPTIONS (APPENDICES)

Fig. A1-1. Randles Interface Model. (a) equivalent circuit, (b) impedance diagram (Warburg impedance).

Fig. A2-1. Drossbach-Schultz and Warburg impedances. (a) Cole-Cole plot, (b) Randles plot.

Fig. A3-1. Kinetic properties of a solid electrolyte. (a) equivalent circuit, (b) impedance diagram.

Fig. A3-2. The Solid-Electrolyte Interphase (SEI) model. (a) schematic view of the surface layer, (b) equivalent circuit, and (c) corresponding impedance diagram for an electrode covered by a solid electrolyte. [The increase of the semi-circle diameter is related to the increase of the thickness of the solid electrolyte interphase.]

Fig. A4-1. Randles Interface Model. (a) equivalent circuit, (b) impedance diagram (Drossbach-Schultz impedance).

Fig. A4-2. The Porous-Insulating Membrane (PIM) model. (a) schematic view of the surface layer, (b) equivalent circuit, and (c) corresponding impedance diagram for an electrode covered by a porous insulating membrane. [The increase of the semi-circle and loop sizes is related to the increase of the thickness of the porous polymeric membrane.]

Fig. A5-1. Kinetic properties of a polymer electrolyte. (a) equivalent circuit, (b) impedance diagram.

Fig. A5-2. The Polymer-Electrolyte Interphase (PEI) model. (a) schematic view of the surface layer, (b) equivalent circuit, and (c) corresponding impedance diagram for an electrode covered by a polymer electrolyte.

Fig. A6-1. The Compact-Stratified Layer (CSL) Model. (a) schematic view of the surface layer, (b) equivalent circuit, and (c) corresponding impedance diagram for an electrode covered by two sublayers.

Fig. A6-2. (a) Study of the parameter f as a function of distance x from the solution to the electrode, (b) study of the ratio L/Y as a function of the ratio f_2/f_1.

Fig. A7-1. Analysis of the impedance data. Equivalent circuit (a) and corresponding impedance diagrams: (b) Cole-Cole plot, (c) and (d) Bode plot.

Fig. A7-2. Analysis of the impedance data. Equivalent circuit (a) and corresponding impedance diagrams: (b) Cole-Cole plot, (c) and (d) Bode plot.

Fig. A8-1. Influence of the depression parameter ($\alpha=\alpha_1=\alpha_2$), α=o [Δ], α=0.2 [o]. Equivalent circuit (a) and corresponding impedance diagrams: (b) Cole-Cole plot, (c) and (d) Bode plot. Circuit parameters: R_o=15 Ωcm^2, R_1=100 Ωcm^2, C_1=0.3 $\mu F/cm^2$, R_2=100 Ωcm^2, C_2=100 $\mu F/cm^2$.

Fig. A9-1. Influence of the frequency ratio, ω_1/ω_2=333 [Δ], ω_1/ω_2 =10 [o]. Equivalent circuit (a) and corresponding impedance diagrams: (b) Cole-Cole plot, (c) and (d) Bode plot. Circuit parameters: R_o=15 Ωcm^2, R_1=100 Ωcm^2, R_2=100 Ωcm^2, C'_1=0.3 $\mu F/cm^2$, C'_2 =100 $\mu F/cm^2$, ω_1/ω_2=333. C''_1=0.3 $\mu F/cm^2$, C''_2=100 $\mu F/cm^2$, ω_1/ω_2=10.

Fig. A15-1. Schematic view of the surface-layer/solution interface showing the movement of species from the solution and from the surface layer.

Fig. A15-2. Study of the surface-layer/solution interface. General case without diffusion of the species. (a) equivalent circuit, (b) corresponding impedance diagram.

Fig. A15-3. Study of the surface-layer/solution interface. Case of a stable composition of the surface layer with the potential (a) equivalent circuit, (b) corresponding impedance diagram.

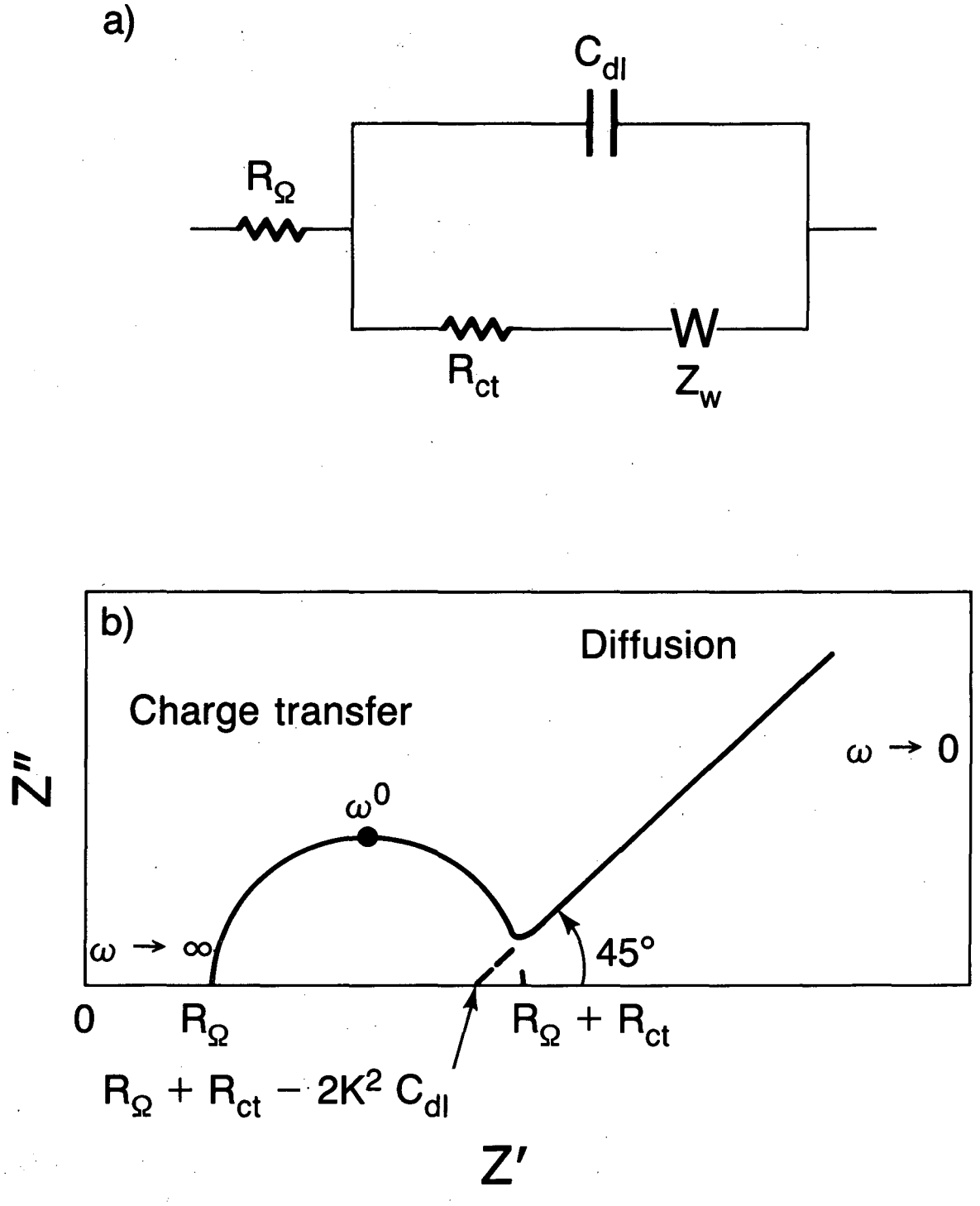

XBL 861-6018

Fig. A1-1

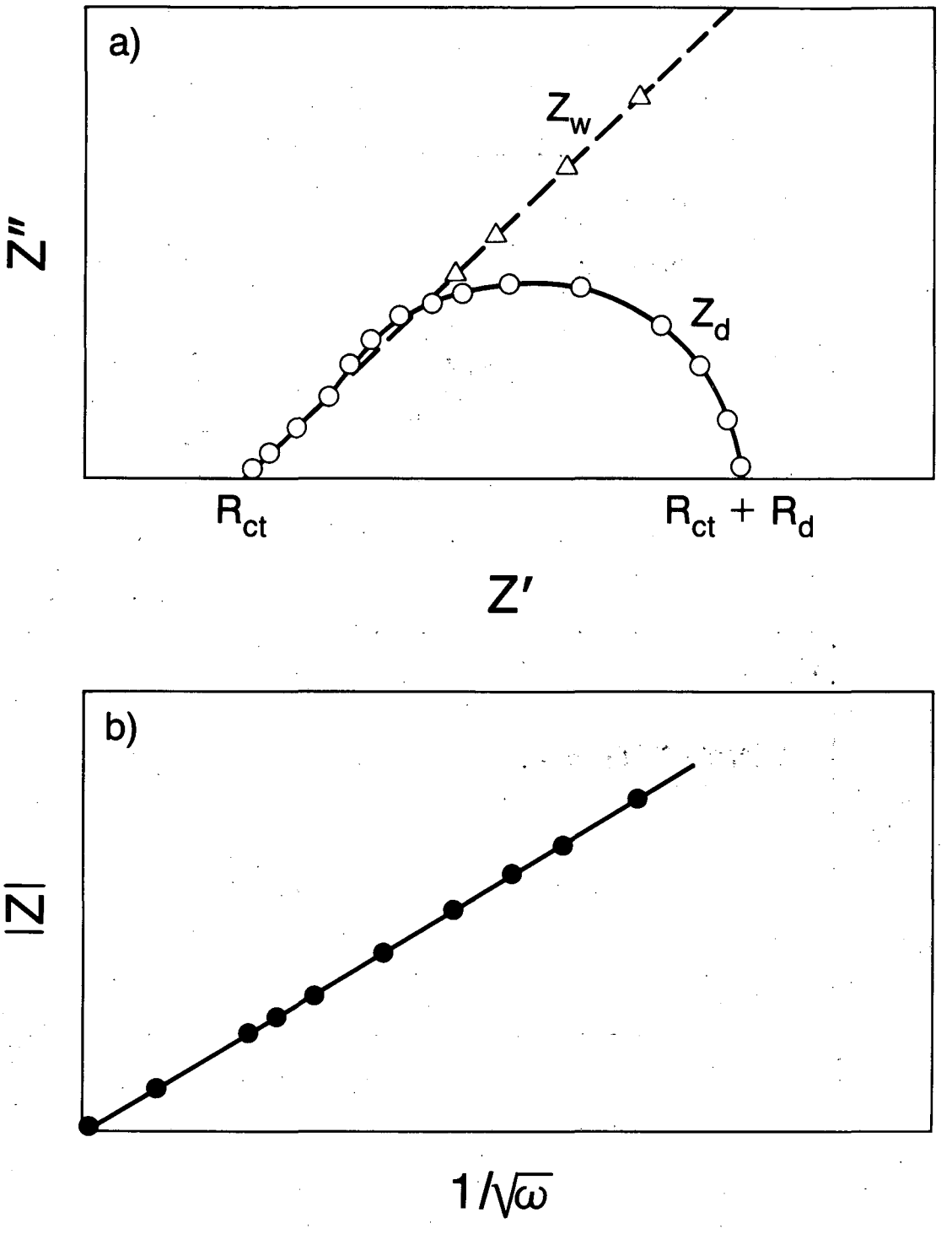

XBL 861-6007

Fig. A2-1

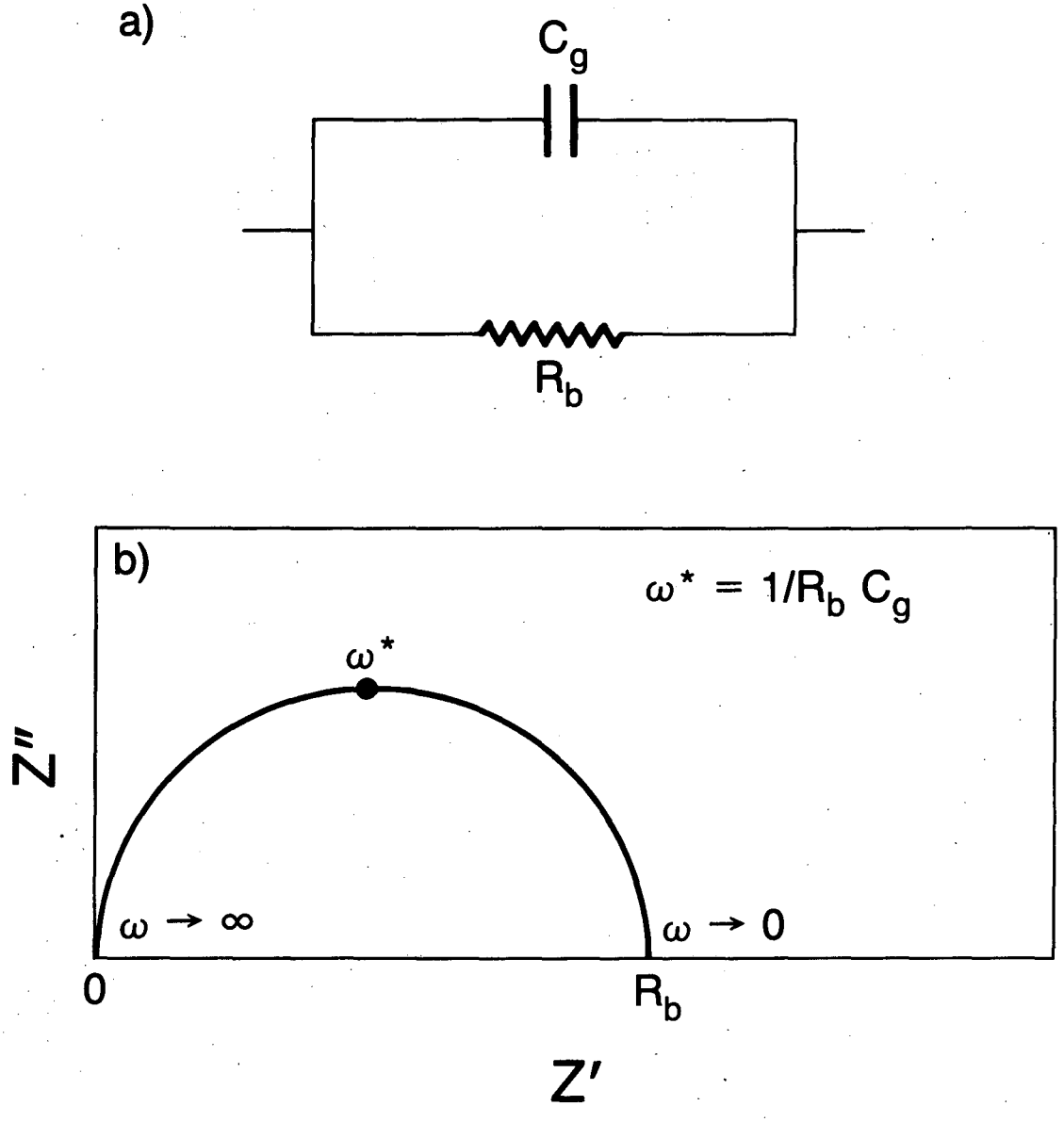

XBL 861-6016

Fig. A3-1

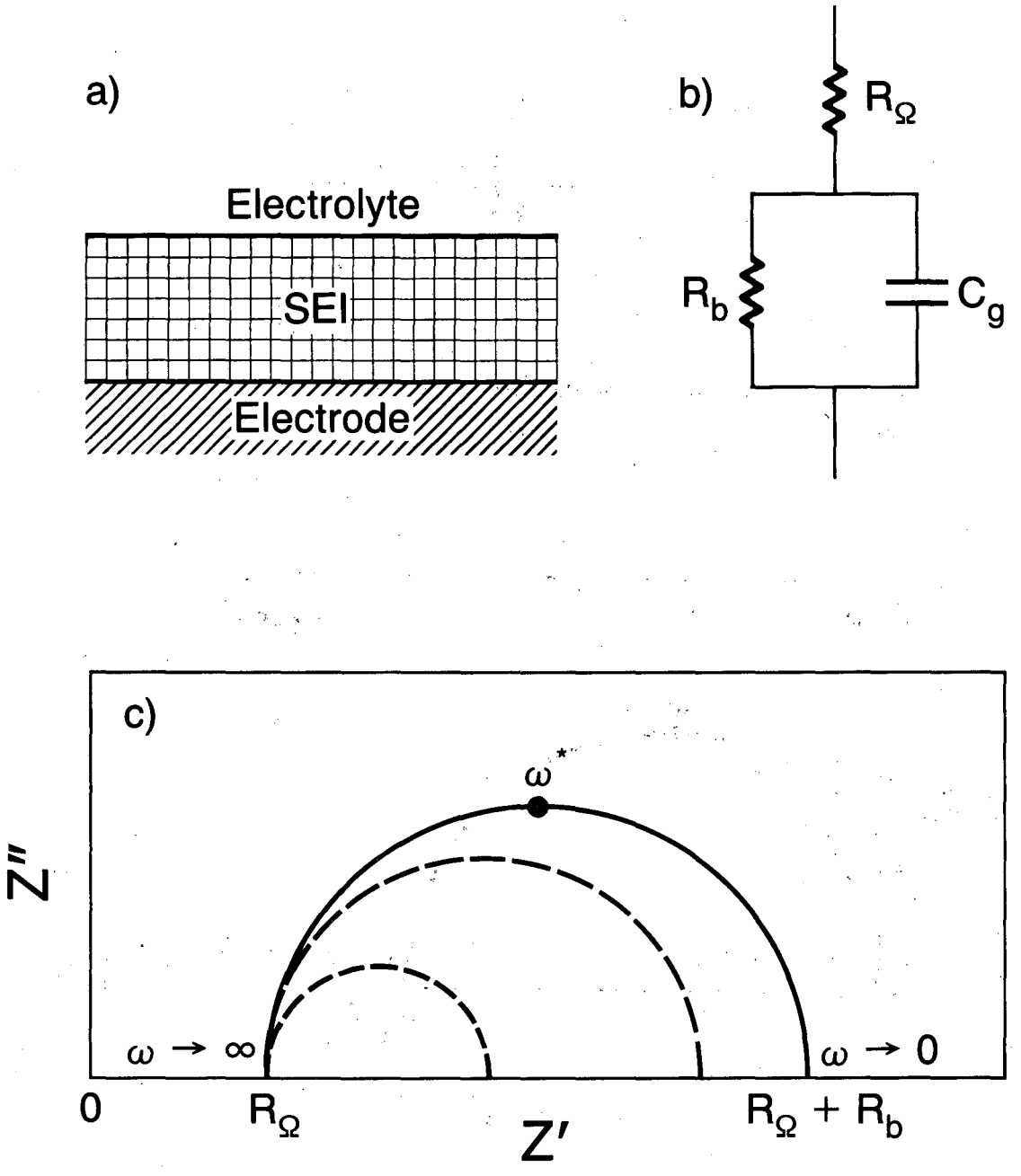
a)
Electrolyte
SEI
Electrode
b)
R_Ω
R_b
C_g
c)
ω^*
Z″
$\omega \to \infty$
$\omega \to 0$
0
R_Ω
$R_\Omega + R_b$
Z′
XBL 861-6021

Fig. A3-2

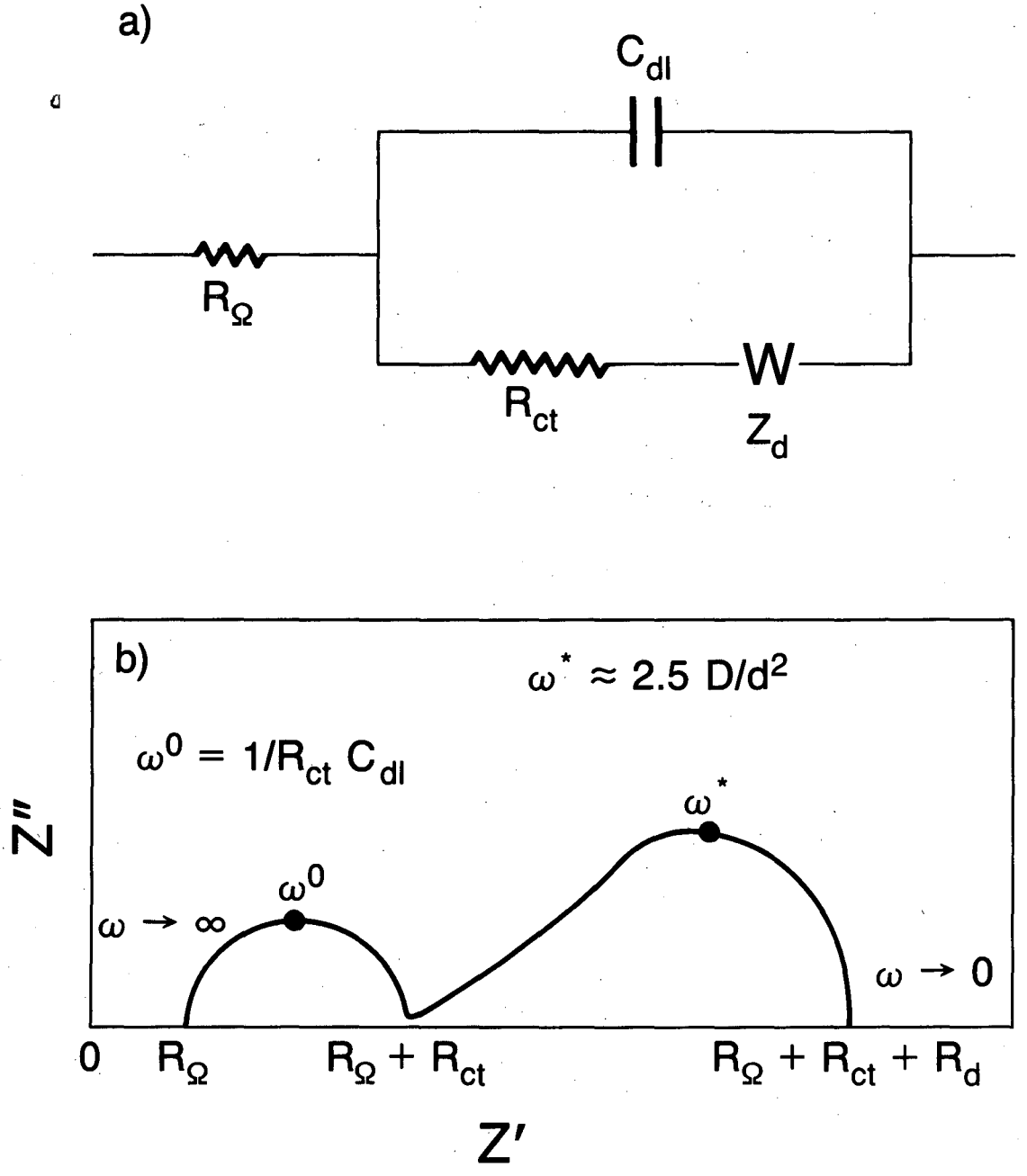

XBL 861-6019

Fig. A4-1

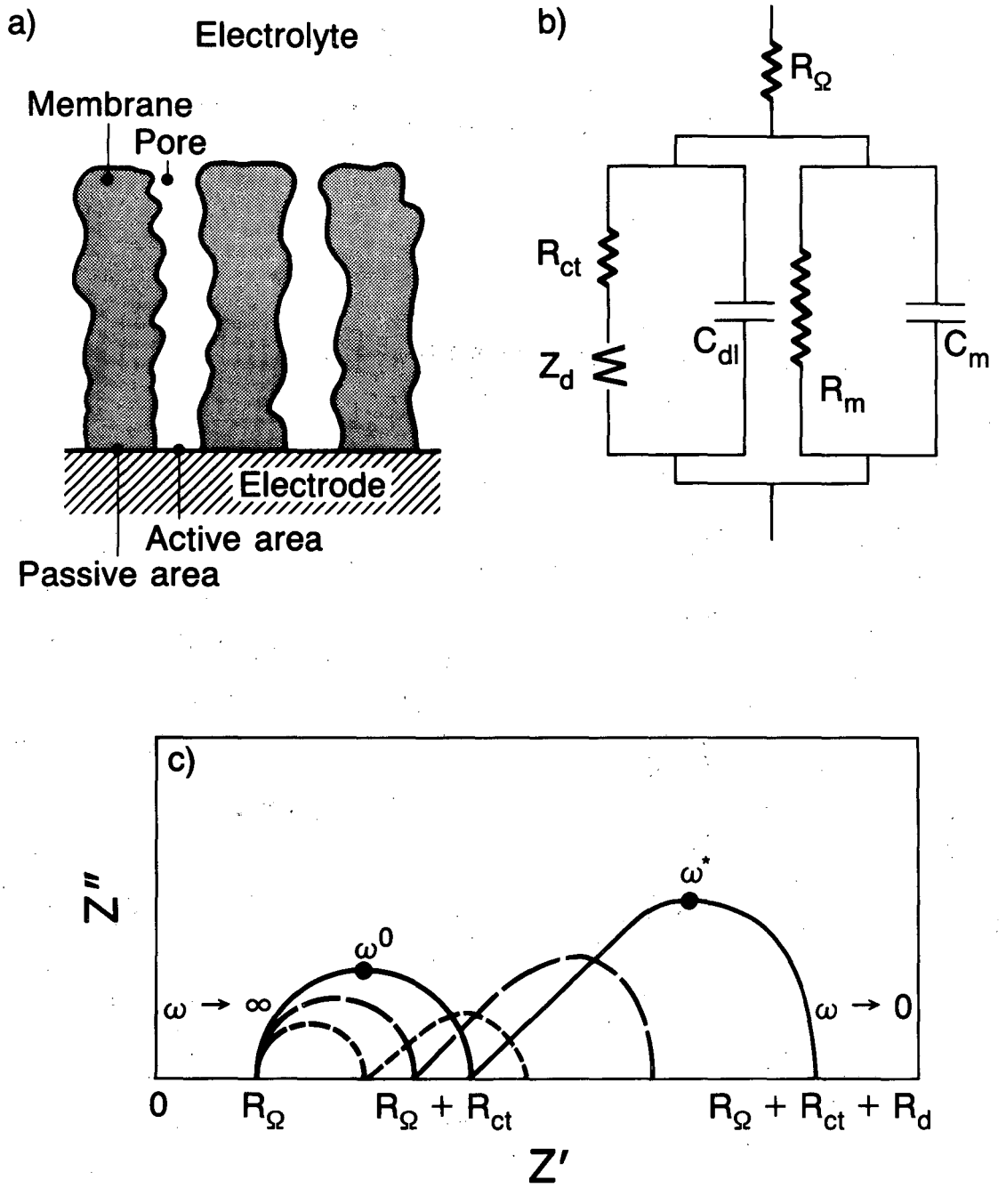

XBL 861-6034

Fig. A4-2

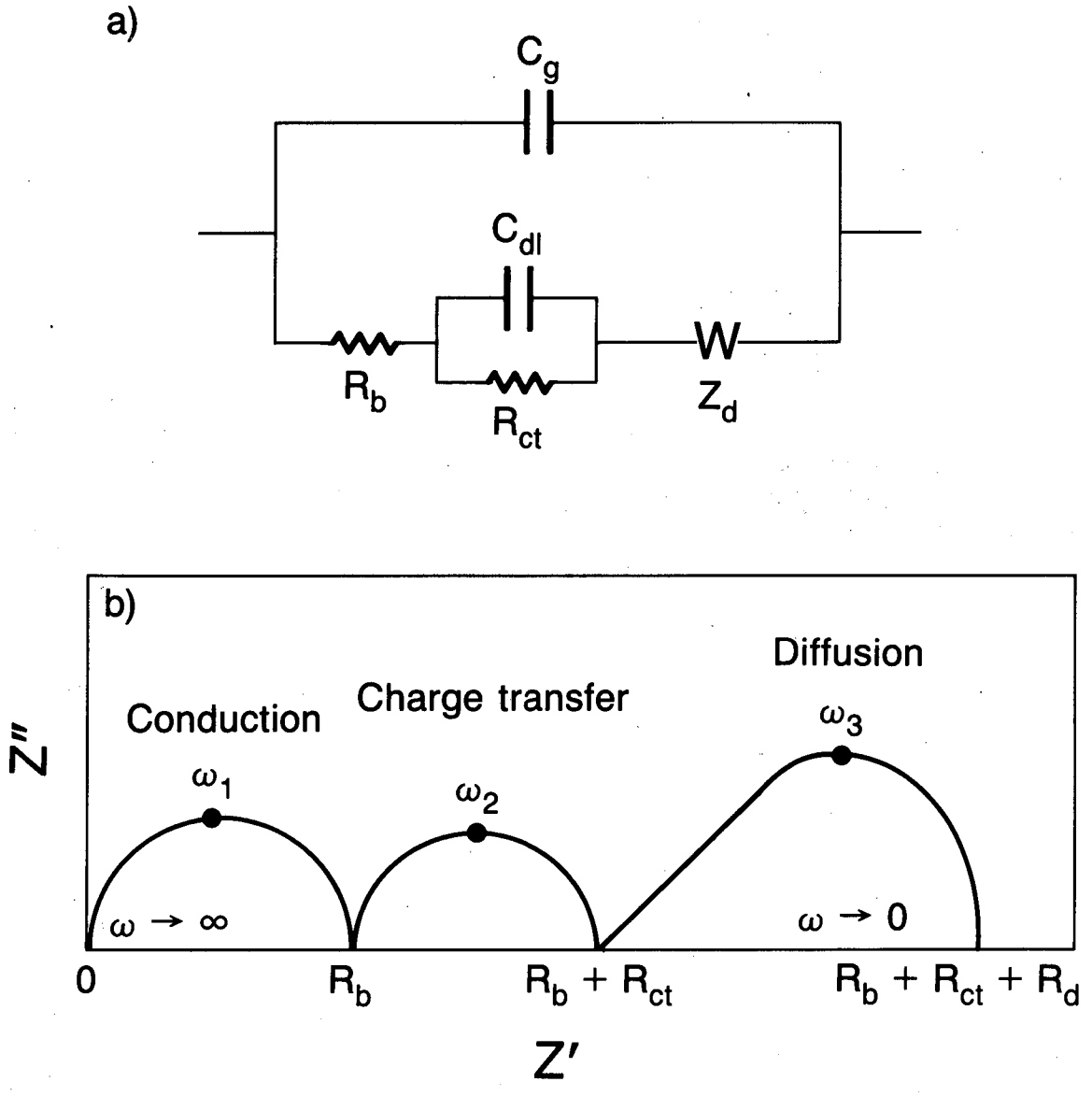

XBL 861-6020

Fig. A5-1

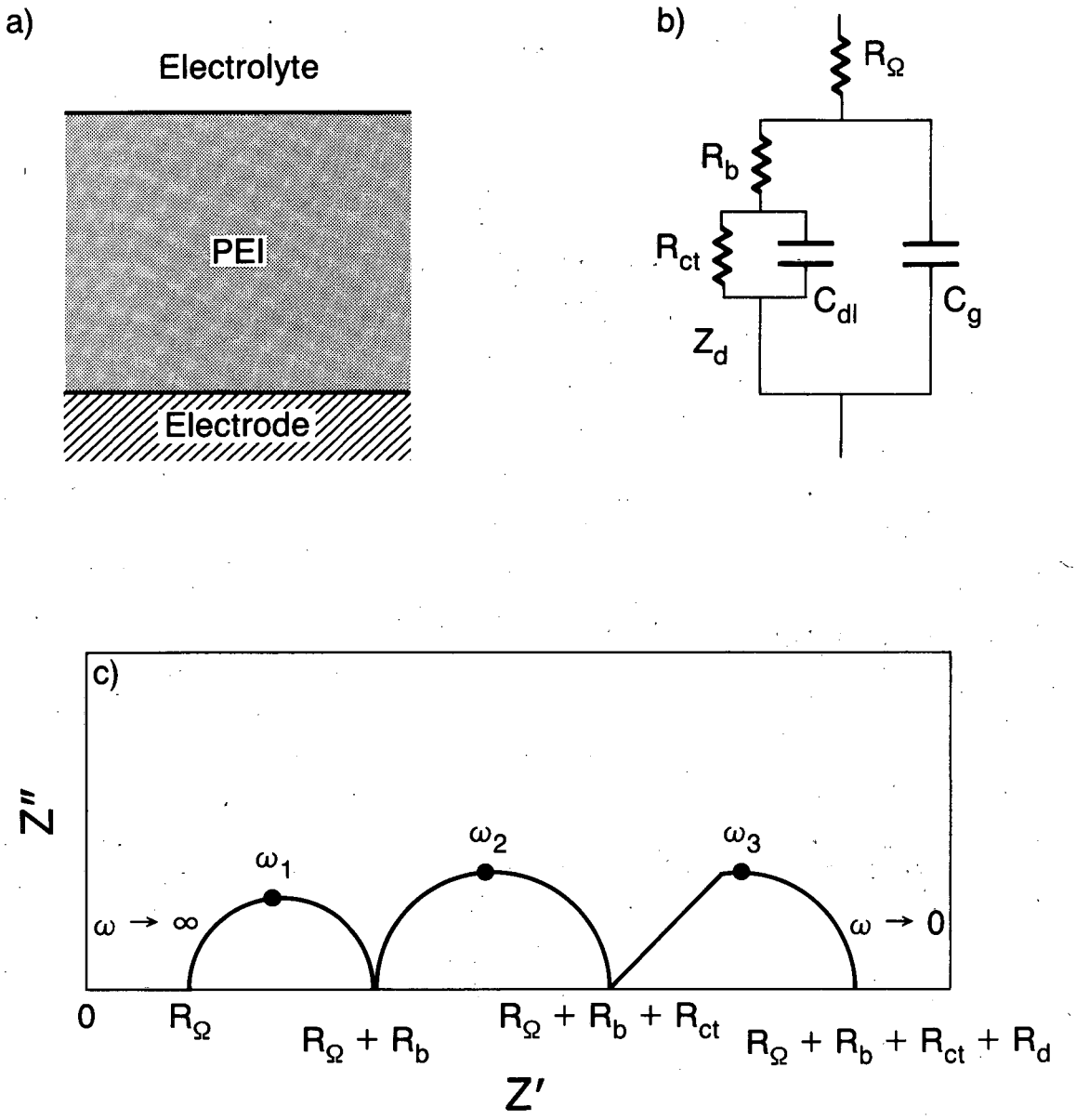
a)
Electrolyte
PEI
Electrode
b)
R_Ω
R_b
R_{ct}
C_{dl}
C_g
Z_d
c)
Z″
ω_1
ω_2
ω_3
$\omega \to \infty$
$\omega \to 0$
0
R_Ω
$R_\Omega + R_b$
$R_\Omega + R_b + R_{ct}$
$R_\Omega + R_b + R_{ct} + R_d$
Z′
XBL 861-6028

Fig. A5-2

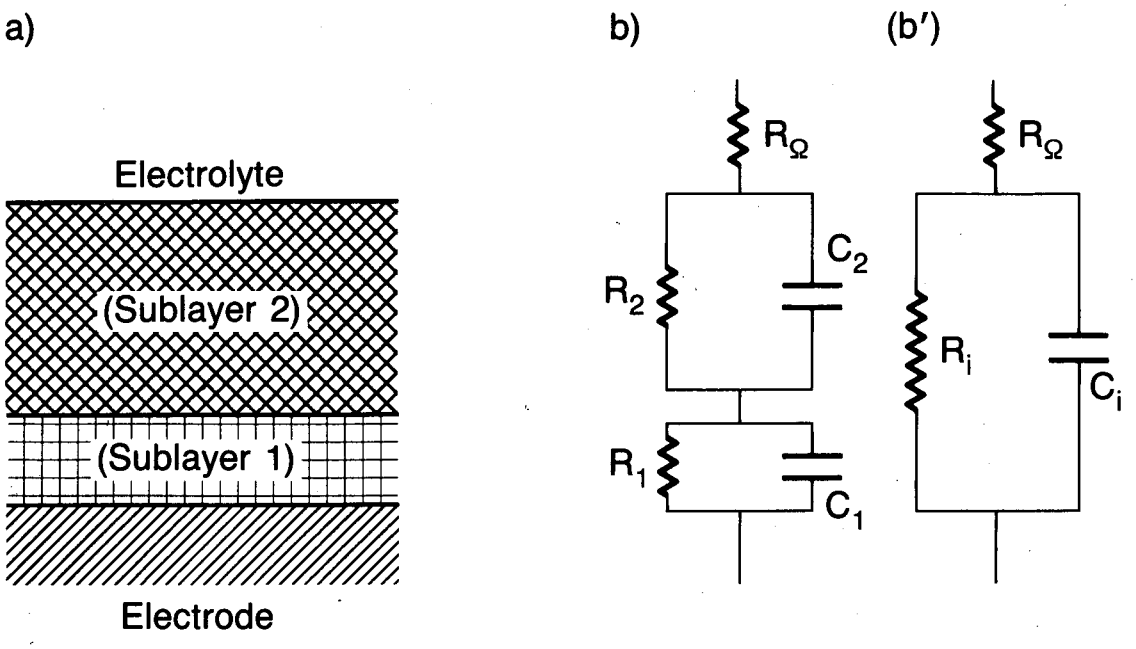

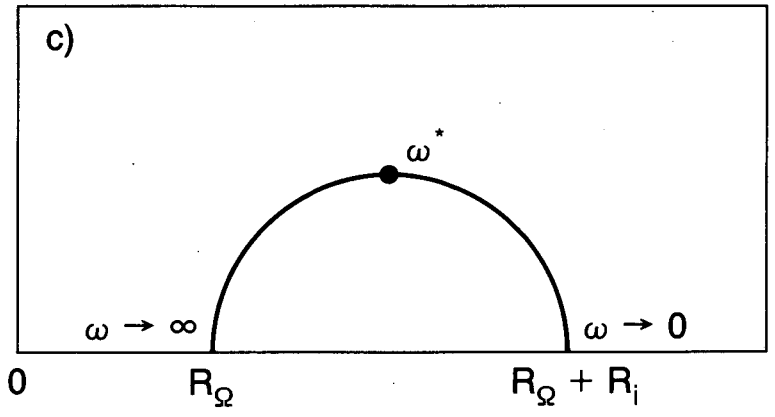

$$\omega^* = 1/R_i\, C_i$$

XBL 861-6024

Fig. A6-1

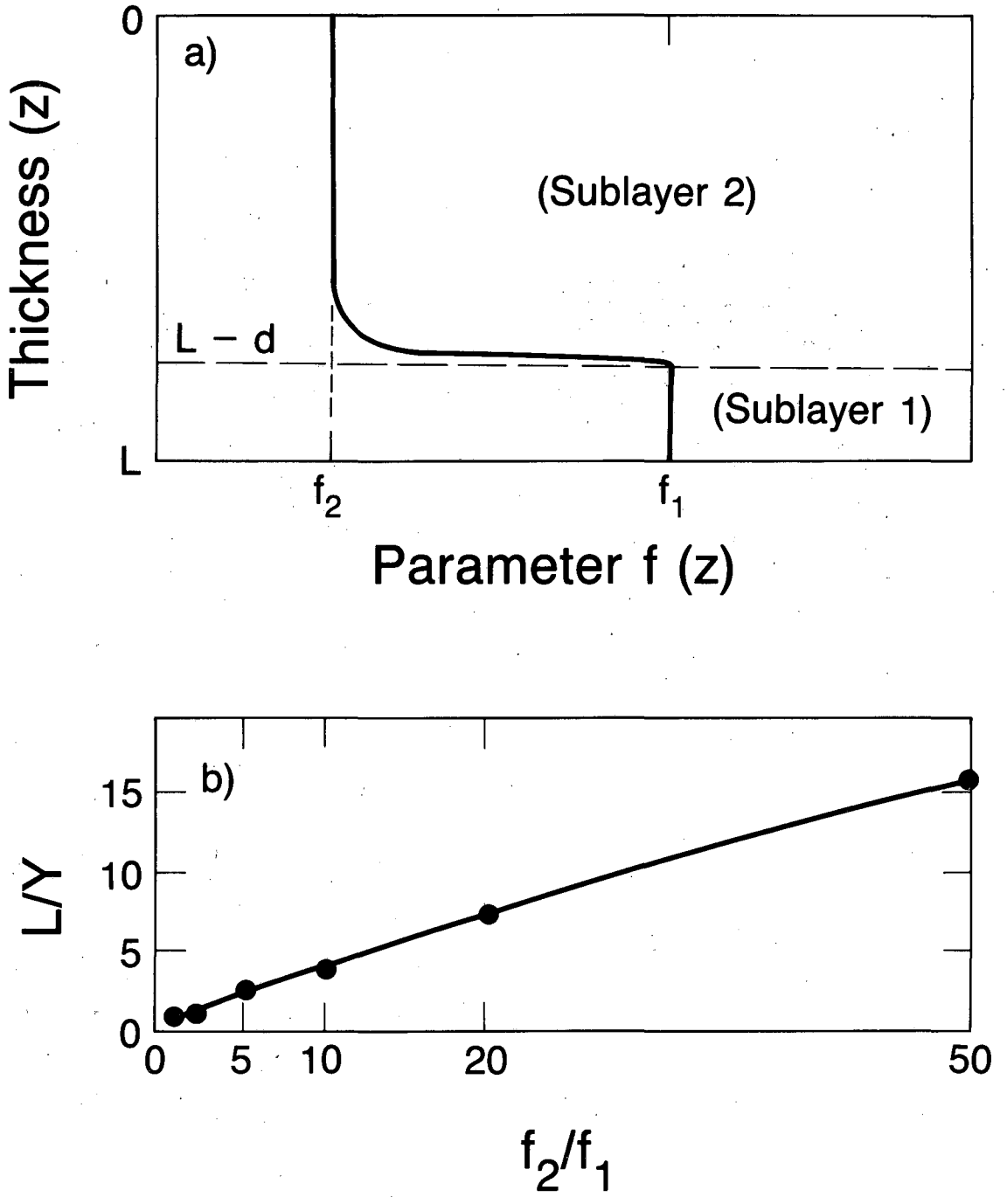
a)
0
L
Thickness (z)
(Sublayer 2)
(Sublayer 1)
L – d
f_2
f_1
Parameter f (z)
b)
L/Y
15
10
5
0
0
5
10
20
50
f_2/f_1
XBL 861-6006

Fig. A6-2

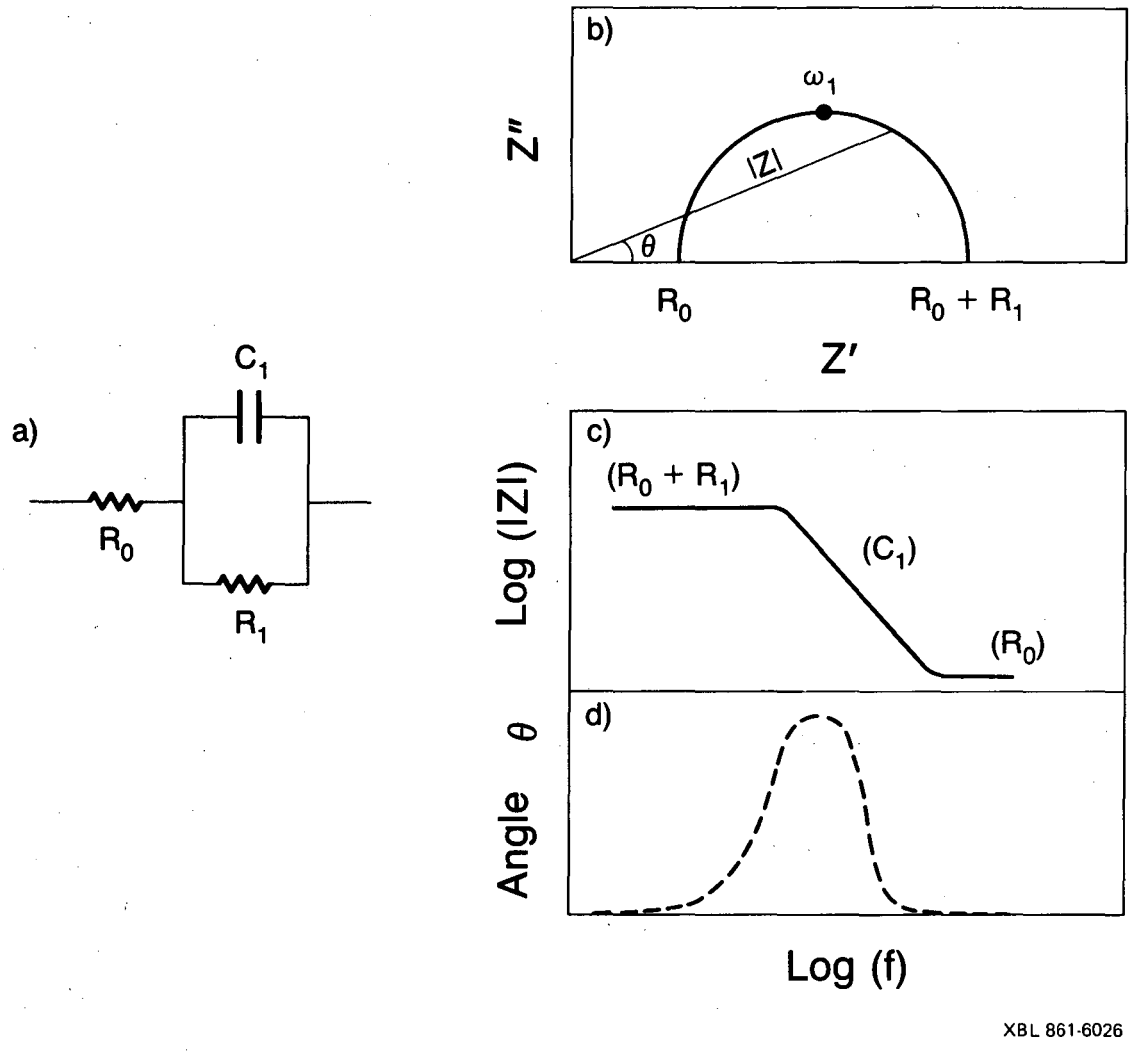
a)
C_1
R_0
R_1
b)
ω_1
Z″
|Z|
θ
R_0
$R_0 + R_1$
Z′
c)
$(R_0 + R_1)$
(C_1)
(R_0)
Log (|Z|)
d)
Angle θ
Log (f)
XBL 861-6026

Fig. A7-1

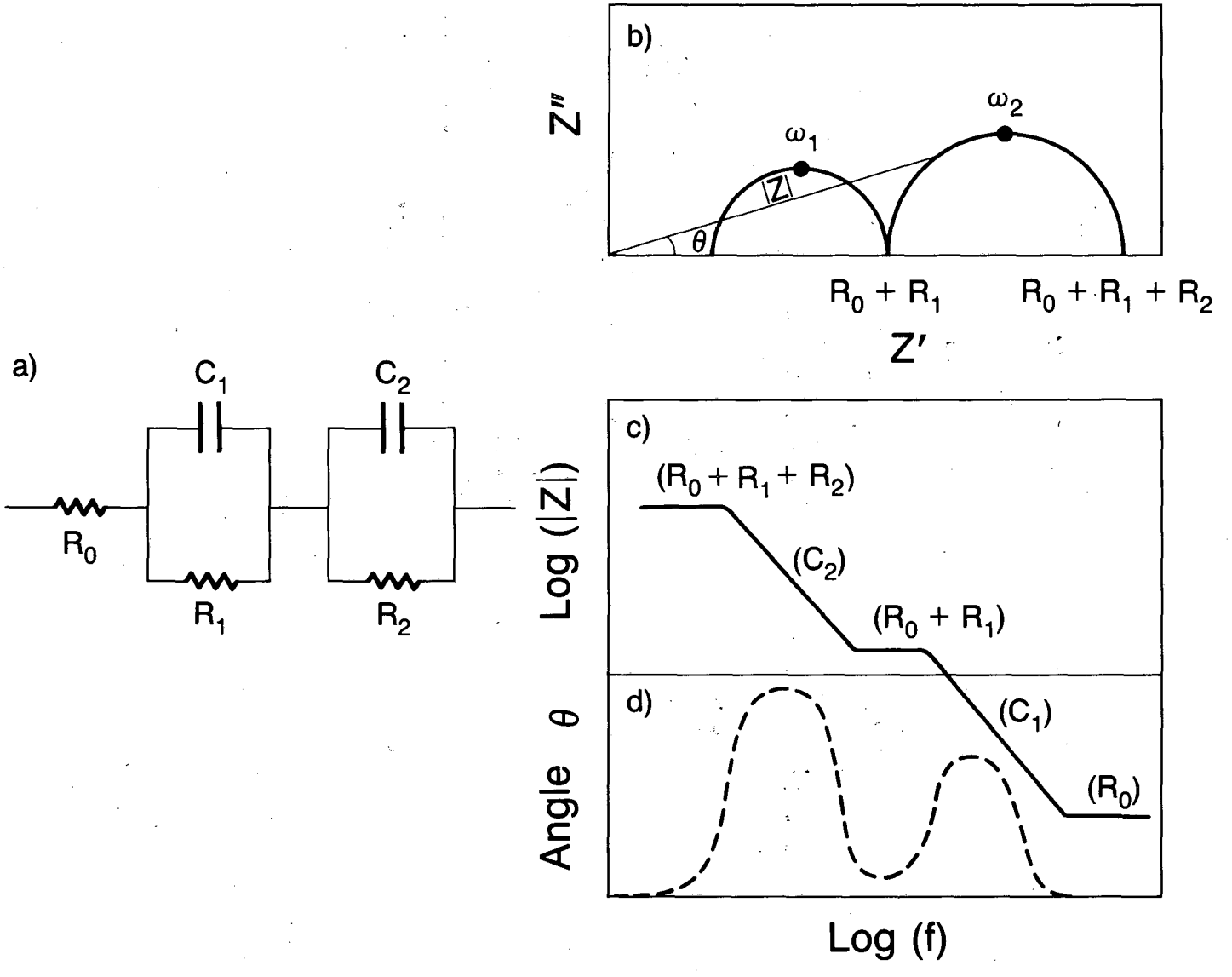

XBL 861-6039

Fig. A7-2

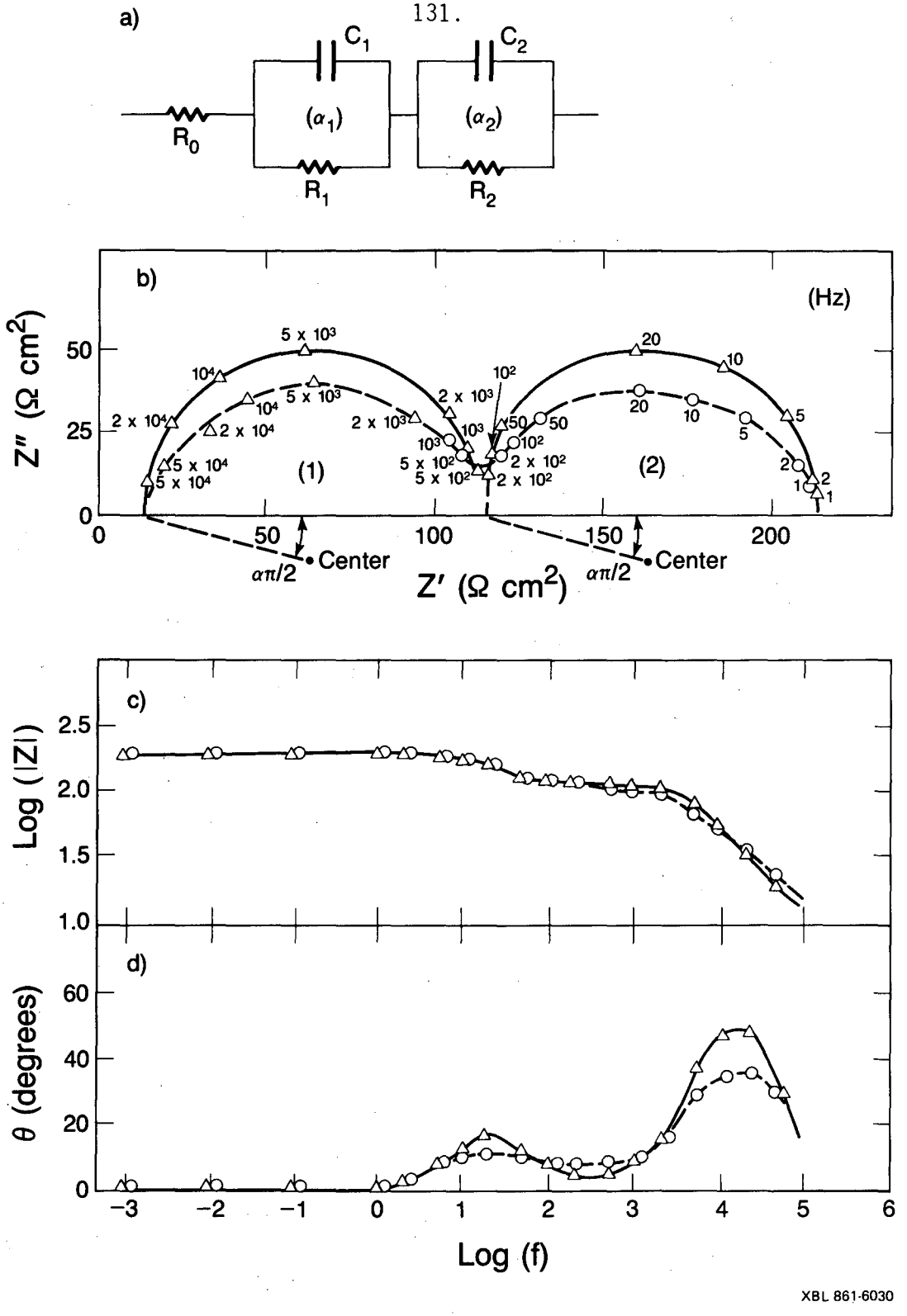
a)
C1
C2
(α1)
(α2)
R0
R1
R2
b)
(Hz)
Z″ (Ω cm2)
Z′ (Ω cm2)
(1)
(2)
Center
απ/2
c)
Log (|Z|)
d)
θ (degrees)
Log (f)
XBL 861-6030

Fig. 8-1

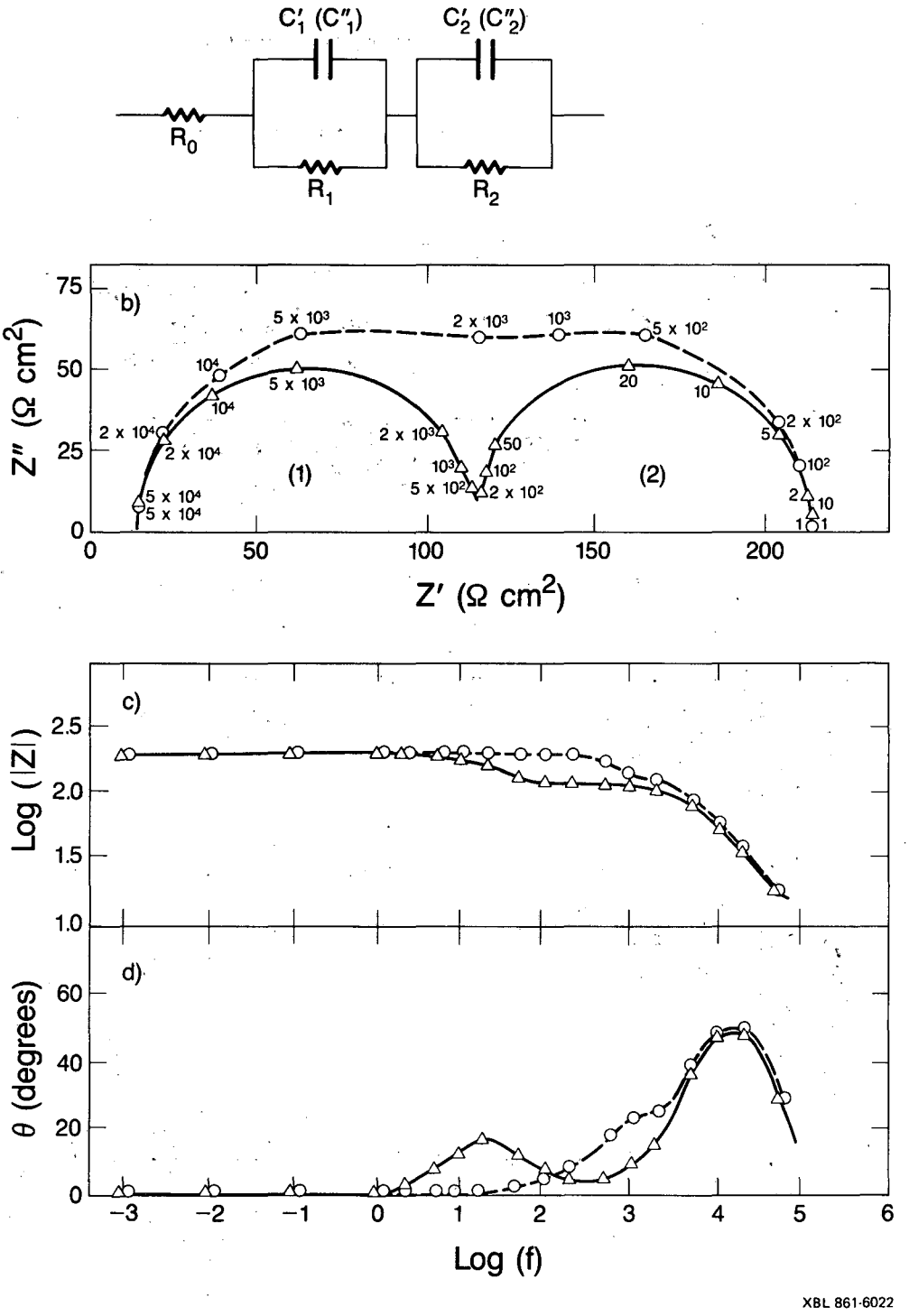
C'1 (C"1)
C'2 (C"2)
R0
R1
R2
b)
Z" (Ω cm2)
Z' (Ω cm2)
(1)
(2)
c)
Log (|Z|)
d)
θ (degrees)
Log (f)
XBL 861-6022

Fig. A9-1

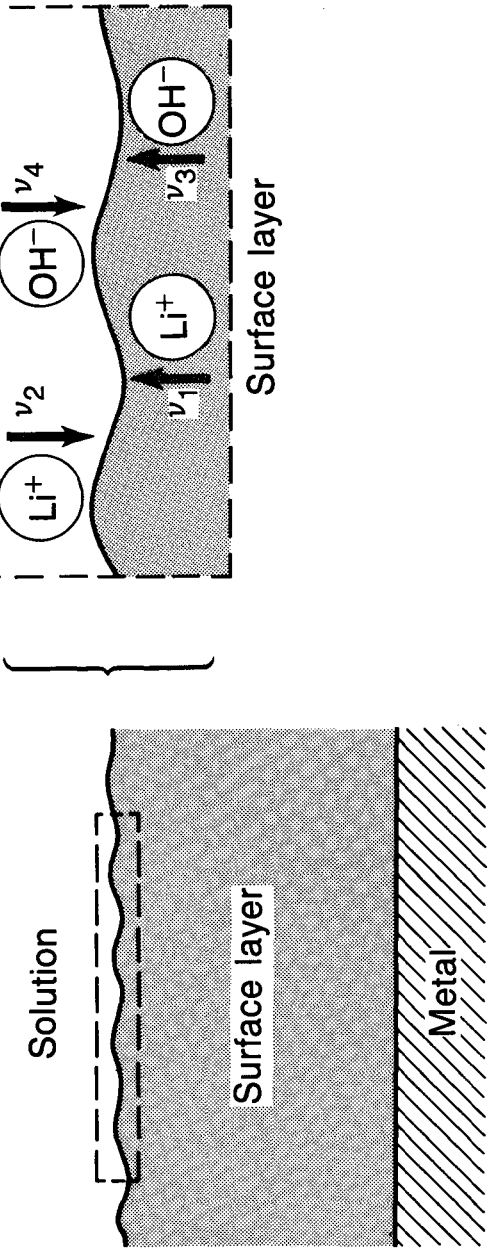

XBL 861-6014

Fig. A15-1

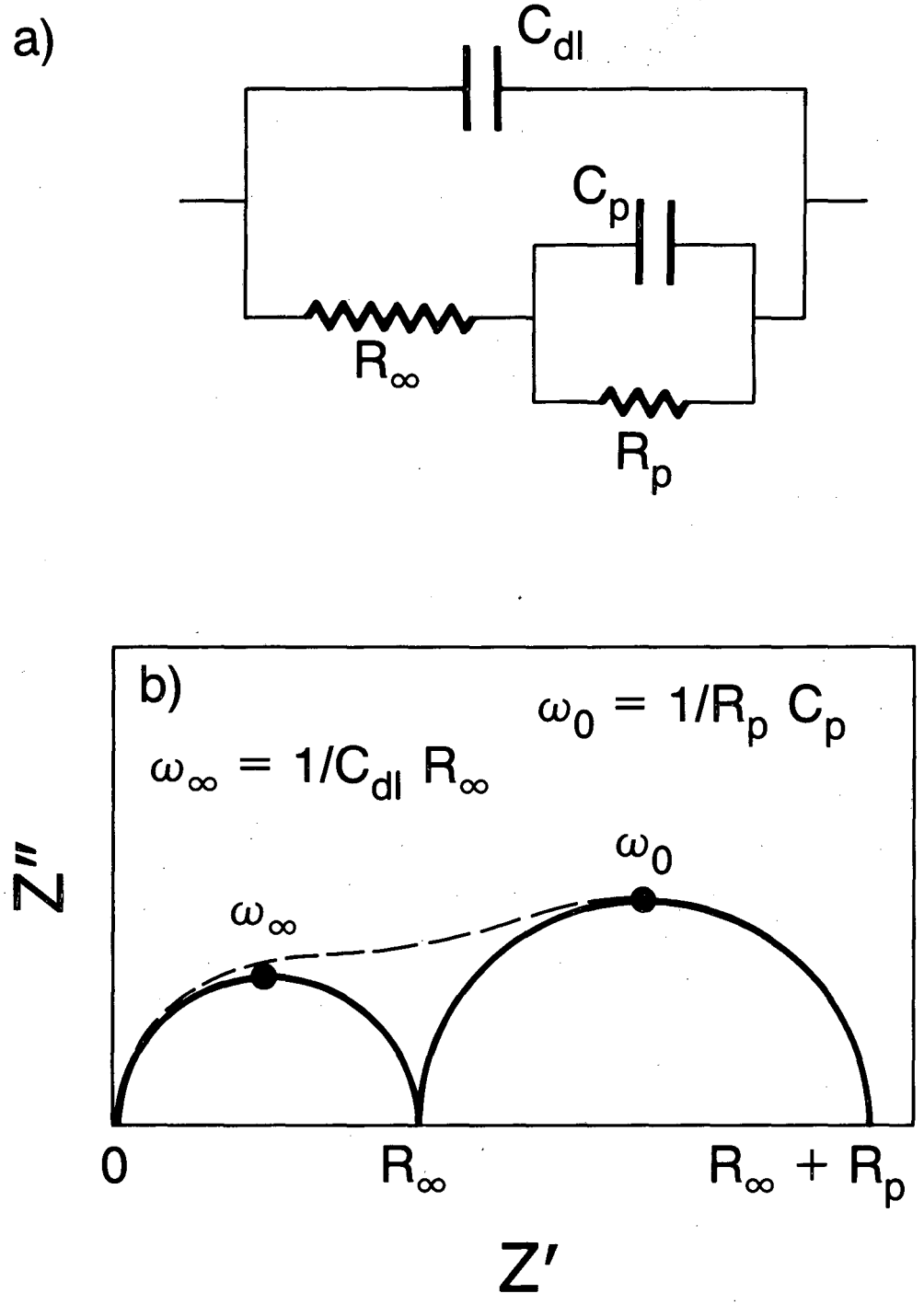
a)
C_{dl}
C_p
R_∞
R_p
b)
$\omega_0 = 1/R_p C_p$
$\omega_\infty = 1/C_{dl} R_\infty$
ω_0
ω_∞
Z″
0
R_∞
$R_\infty + R_p$
Z′
XBL 861-6015

Fig. A15-2

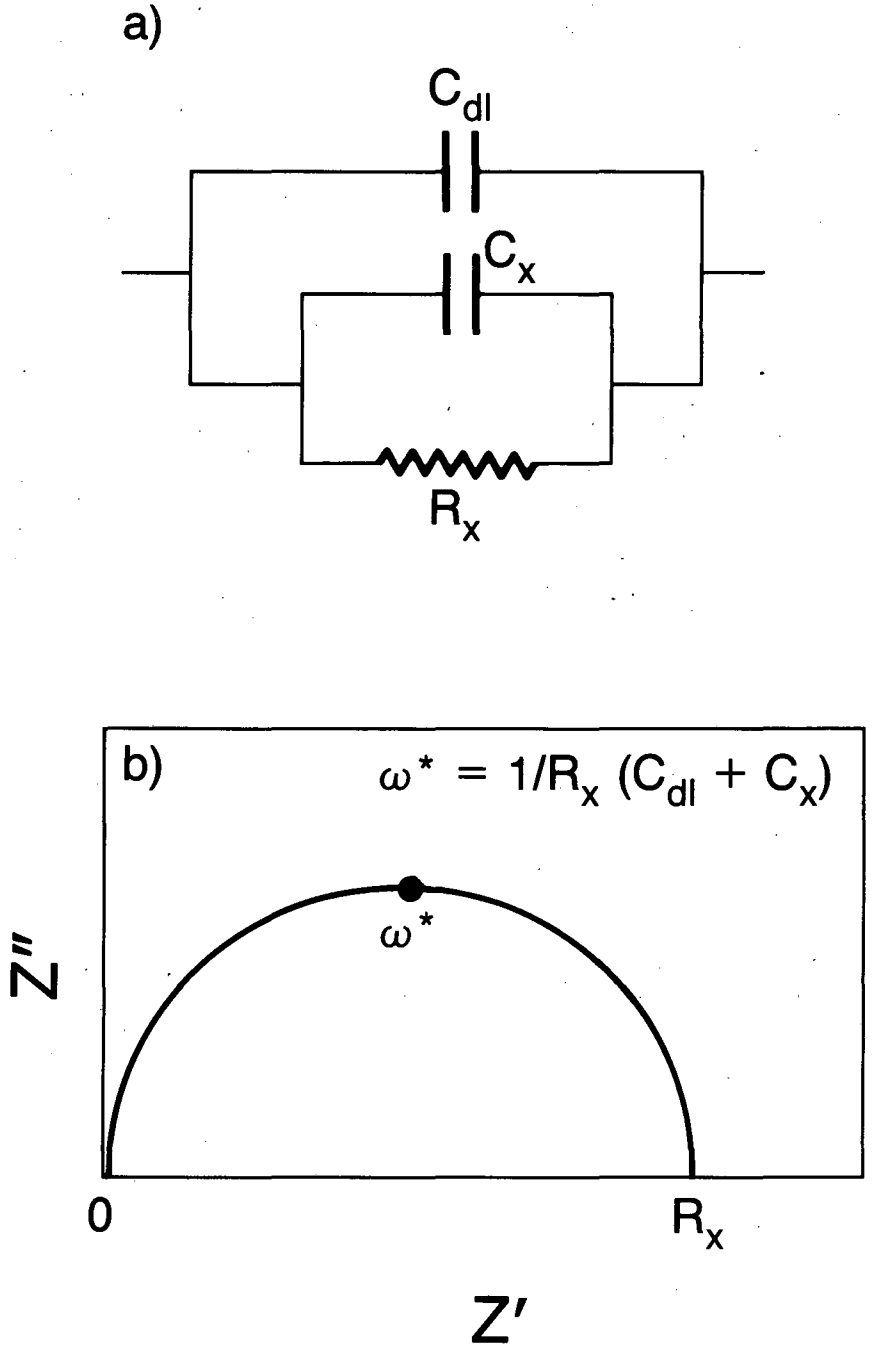

Fig. A15-3

LAWRENCE BERKELEY LABORATORY
TECHNICAL INFORMATION DEPARTMENT
UNIVERSITY OF CALIFORNIA
BERKELEY, CALIFORNIA 94720